Droplet-based Air-liquid Interface Biofilm Reactor

LIU, Songlin

A Thesis Submitted in Partial Fulfillment

of the Requirements for the Degree of

Doctor of Philosophy

in

Electronic Engineering

The Chinese University of Hong Kong

April 2015

Abstract

Abstract of thesis entitled:

Droplet-based Air-liquid Interface Biofilm Reactor

Submitted by LIU, Songlin

for the degree of Doctor of Philosophy

at The Chinese University of Hong Kong (April 2014)

Bacterial biofilms consist of communities of cells encased in self-produced extracellular polymeric substance (EPS) at the interface of different phases. While most of our understanding of biofilms to date has been obtained from submerged biofilms formed at the solid-liquid (S-L) interface, the interface between air and liquid provides a niche for the formation of biofilms with unobstructed access to both liquid and gaseous phases, which is of ecological, clinical and commercial significance. But there is a paucity of information on air-liquid (A-L) interface biofilms. Cultivation and characterization of A-L interface biofilms are still limited to traditional methods created for S-L interface biofilms, mostly based on microtiter plates and tubes. In this thesis, two bioreactors have been designed, fabricated and validated to culture A-L interface and air-liquid-solid (A-L-S) interface biofilms.

The first bioreactor, named hanging drop biofilm reactor (HDBR), has been constructed on an open microfluidic platform to hold hanging droplets culturing biofilms in a suspended fashion. Hanging droplets containing microorganisms were accessed from the topside of the microfluidic platform, whilst measurement and harvesting were performed on the underside. The system was driven by evaporating

flows. No additional electronic or mechanical actuation was needed. Biofilms were formed in hanging droplet biofilm reactors with bacterial suspensions. After 24 h of incubation under optimized conditions, biofilm-positive phenotype *Bacillus subtilis* developed A-L biofilms eliciting distinct developmental stages. Formation and dispersal of A-L interface biofilms were for the first time analytically characterized. Biofilms harvested by dripping droplets showed a spherical cap shape with porous structures. This is the first reported attempt to culture A-L interface biofilms inside a hanging droplet on an open microfluidic platform under evaporation flow.

The second bioreactor, named segmented-flow microfluidic air-liquid-solid interface biofilm reactor (SFMBR), has been implemented to grow A-L-S interface biofilms on chip. A distinct A-L-S interface was made available by introducing a gas phase into successive nutrient flows with a T-junction design, forming a segmented gas-liquid flow. Velocity fields were computed by numerical simulation, involving not only the hydrodynamic fields in the gaseous and aqueous phases, but also of the air-liquid and solid-liquid interfaces. Formation of A-L-S interface biofilms along microfluidic channels was observed and characterized by microscopy techniques non-destructively. The effect of hydrodynamics, interface topology and channel hydrophobicity on A-L-S interface biofilm formation was simulated and tested. Biofilms interacted with the shear forces introduced by the passage of A-L interfaces of an air slug with a shear stress of about 0.66 Pa and relaxed after the A-L interface passed. This device is a low-cost on-chip biofilm reactor to culture A-L-S interface biofilms and to measure *in situ* biological and mechanical properties of growing biofilm.

We have successfully constructed and validated two novel microfluidic strategies utilizing the interfacial phenomenon at the air-liquid interface and evaporating flow to culture and investigate the complex biology of A-L and A-L-S interfaces biofilms.

摘要

哲学博士毕业论文摘要:

题目：基于液滴的气-液界面生物膜反应器

提交：刘松麟

学位：哲学博士

2015 年 4 月于香港中文大学

细菌生物膜（生物膜）由生长在固、气、液相的界面上的细菌包裹于由其产生的细胞外间质聚合物内组成。固-液界面生物膜可以利用微流系统低耗材高效培养检测。但没有微流系统可研究生长在气-液界面的生物膜。为了填补这个空白，本论文设计了两种微流生物膜反应器(反应器)培养气-液和气-液-固界面生物膜。

一种反应器是培养气-液界面生物膜的基于蒸发产生的微流动和微循环的倒悬液滴反应器。我们创新的利用蒸发产生的微流和微循环增加微流系统中材料混合和供氧。我设计了两种倒悬液滴反应器：倒悬液滴气-液界面反应器微孔板和微流气-液界面反应器在静态和流动培养液条件下培养气-液界面生物膜。我们监控并分析了气-液界面生物膜形成过程。第一次报道了气-液界面生物膜生长阶段的划分。了解反应器的特性，如微流动和反应器形态等对应用反应器有至关重要的作用。我们使用粒子图像测速和数值模拟的方法研究了反应器特性。设计了滴落打印的方法收获并离线测量生物膜。这是第一种可以方便、可重复收获生物膜的方法。我们研究了收获后生物膜的抗药性和微结构，发现倒

悬液滴反应器培养的生物膜对干燥和灭菌过程有很高的抗性。 我们还首次发现了细菌由纳米管连接的气液界面细菌生物膜。

另一种反应器是基于微流分段气-液流的分段流微流反应器。这是首个培养气-液-固界面生物膜的微流反应器。我们创新性的应用了分段气-液流为生物膜滴定供养。我们的微流反应器模拟工业标准方法培养气-液-固界面生物膜的反应器。为了研究生物膜在反应器中的生长和流动对生物膜的影响，我们监测了生物膜的生长，用数值模拟的方法研究了分段流的流动。发现了单层菌落储水的现象。我们还首次报道了微流系统中，用粒子图像测速和数值模拟的方法研究生物膜的弹性松弛过程。

这里设计的基于液滴的高通量，高效率，低成本，操作简单的生物膜反应器可以加快生物膜的研究。

Acknowledgement

I owe my deepest gratitude to my supervisor, Prof. Yung, Pun To for his guidance and support. It is due to his guidance and support that made me get into this fantastic field and finish this work. I appreciate the time and attention of my committee members: Prof. Mak, Arthur Fuk-Tat, Prof. Samaranayake, Lakshman Perera, Prof. Zhang Li, and Prof. Wu Yilin. It is very kind of them to take their time from their busy schedules to give advice to my Ph.D. thesis.

I would like to express my gratitude to all members of the Yung's group. I enjoyed working with them, discussing with them and having fun together with them. They made my graduate experience enjoyable and full of passion that I will cherish forever. I would like to express thanks to Liu Sili and Wu Wenjie, who have helped a lot in my thesis work. Li Lin Kai (Leo) taught me micro fabrication technologies. I would like to thank Dr. Tao Wenyan for her helpful discussions. I appreciate help from undergraduate students: Cheong Hio Teng (Lizzie), Law Sau Kam Liliana, and Hu Dawei.

I have to express my heartfelt gratitude to my family for their continuous understanding, support and love. Particularly, I would like to thank my wife Cao Qingqing and her family. Without their support, I could not go on with my doctorial study and finished this work. I want to thank my parents Liu Xiangyang and Wang Changyong for their endless love since I was born.

Table of contents

List of figures

List of table

Abbreviations

2-D	Two dimensional
3-D	Three dimensional
A-L	Air-liquid
A-L-S	Air-liquid-solid
AFM	Atomic force microscopy
ATCC	American Type Culture Collection
ATPS	Aqueous two-phase system
B. subtilis	*Bacillus sbutilis*
B. cereus	*Bacillus cereus*
BAM	Brewster-angle microscopy
CDC	Centers for Disease Control
CDFF	Constant depth film fermenter
CLSM	Confocal laser scanning microscopy
DFBR	Drip flow biofilm reactor
E. coli	*Escherichia coli*
EHD	Electrohydrodynamic
EPS	Extracellular polymeric substance
HDBR	Hanging droplet biofilm reactor
LBL	Layer-by-layer
LPS	Lipopolysaccharide
MFC	Microbial fuel cell
MRD	Modified Robbins device
MTP	Microtiter plate

OMP	Outer membrane proteinPBF Perfused biofilm fermenter
PDMS	Polydimethylsiloxane
PIV	Particle image velocimetry
P. aeruginosa	*Pseudomonas aeruginosa*
P. fluorescens	*Pseudomonas fluorescens*
QS	Quorum sensing
S. epidermidis	*Staphylococcus epidermidis*
S-L	Solid-liquid
SALF	Segmented air-liquid flow
SEM	Scanning electron microscopy
SFMBR	Segmented air-liquid flow microfluidic air-liquid-solid interface biofilm reactor
SGLF	Segmented gas-liquid flow
SR-FTIR	Synchrotron-radiation-based Fourier transform infrared spectromicroscopy
TSA	Tryptic soy agar
TSB	Tryptic soy broth
μCP	Microcontact printing

Chapter 1 Introduction

Colonization of microorganisms on surfaces leads to phenotypic changes on the morphology, trait and mode of life. Bacteria employ a wide suite of strategies to accomplish a switch from planktonic to a biofilm-like sessile state. Adherent microorganisms do not sit idle on surfaces, but adapt to this mode of life by manifesting a series of physiological changes. They form an interactive network with the substrata and respond to environmental cues by forming resilient endospores, developing elevated fruiting bodies, entering dormancy, and burgeoning into surface-associated biofilm. Inside the biofilm matrix, microcolonies interact with others to exchange information in the form of quorum sensing, exchange genetic materials and share nutrients via the presence of voids and interspersed fluid-filled channels. These highly specialized forms are commonly found in microbiology because of a higher resistance towards inactivating agents. Formation of biofilm is one of the common strategies. Biofilms are adherent microbial aggregates on biotic or abiotic surfaces enclosed by a matrix of self-secreted proteins. Insight about the physiologies of this assemblage of surface-associated microorganisms is necessary for the understanding of infections, ecological processes and design of bioreactors. This chapter introduces the fundamentals of bacterial biofilm, with emphasis on the biofilm developmental process, biofilms formed at the air-liquid interface and the application of engineering tools on biofilm research.

History of biofilms

Biofilms, manifested in the form of adherent microorganisms covered in slimy matrices, have been omnipresent in our everyday life, notably in industrial and

medical settings, including wastewater facilities, cooling water system, piping, indwelling catheters, implants and other medical surfaces and utensils [1]. It was van Leeuwenhoek who first observed films of slimy microorganisms on the surface of teeth with his simple microscope, which was later believed to be biofilm. Until 1978, biofilms have simply been perceived as aggregations of microorganisms without much in-depth appreciation of the architecture, gene expression, and communication. Fueled by invention of tools offering higher magnification and resolving power, biofilms have been identified in soil and aquatic environments. The past few decades have seen the emergence of a nascent microbiology field on adherent biofilms. Advances in microscopy techniques have paved ways for more direct and minimally invasive visualization of cells in 3D stacks. Scientists and engineers started to appreciate the elaborate biofilm structure, form-function correlation, and the underlying gene expression for this sessile mode of life, which is completely different from the planktonic mode. Confocal laser scanning microscopy (CLSM) renders the resolution and 3D sectioning capability to image sessile microcolonies, indwelling fluid-filled channels and voids amidst a highly complex matrix of exopolymeric substances. Quantitative information on biofilms can readily be obtained by scanning electron microscopy (SEM) and CLSM.

Microorganisms exhibit a tendency to adhere to solid substrata in multiple layers in a cascade of developmental stages to form surface-attached communities enclosed in a matrix of extracellular polymeric substance (EPS), known as biofilms. Attachment is a complex process mediated by a plethora of factors, such as the substratum properties, growth medium, cell strain, and hydrodynamics. One of the defining features of biofilms is their adherence to surfaces. The solid-liquid interface,

commonly found in the environment and our body, provides an ideal substrate for the attachment and proliferation of biofilms. On the other hand, biofilms burgeon as suspended pellicles or flocs along the phase boundary between air and liquid. Biofilms amass high numbers of organisms in close proximity with a cell surface density on the order of 10^8 cells/cm^2 [2]. The proximity of microcolonies is ecologically and physiologically substantial for quorum sensing, gene transfer, exchange of nutrients, and dispersal. The development of biofilm is a dynamic process of growth and detachment of bacterial cells and aggregates. They are ubiquitous in nature contributing to nosocomial contamination and infectious diseases such as otitis media, periodontitis and cystic fibrosis.

Extensive investigations on the formation and characteristics of biofilms formed at the solid-liquid (S-L) interface have been made, one of the ways in which biofilms exist in the nature [1]. These studies have established our current understanding on the developmental stages of biofilm on the S-L interface in the bulk phase. Interactions among the extracellular polymeric matrix, protein, and substrate include electrostatic attraction and hydrophobic affinity. From the studies in the bulk phase at the S-L interface, it is apparent that the substrate would considerably affect the adherence and resistance properties of biofilms, underpinning a complex mechanism. At the A-L interface, on the other hand, microbes are much affected by oxygen availability, microcirculation of nutrients, cell matrix-surface interaction as a function of bioreactor geometry, relative concentration of solutes, and environmental parameters. Biofilms formed at the air-liquid (A-L) interface and planktonic biofilms have garnered much attention recently because of their unique properties and physiology [1]. Nevertheless, there is a paucity of work looking at A-L biofilms due

to difficulty in culture and harvest. Surface behavior and bulk solution behavior can be inferred by measuring the variation of surface tension. This thesis investigates the formation and measurement of A-L interface bacterial biofilms, which is of direct relevance to a range of applications within biomedical engineering, pharmaceutical, and food industries.

Biofilm formation

The formation of biofilm usually follows three mechanisms [3, 4]:

(1) Microbial active translocation: Adherent microorganisms are able to move to surfaces by different active translocation strategies. Biofilm forms as a result of this spatial redistribution of cells. Twitching mobility is one of the commonly employed translocation strategies in biofilm organisms, notably in *Pseudomonas aeruginosa*. Type IV pili, for example, plays a significant role in biofilm formation [5, 6].

(2) Binary fission of adherent cells: Binary fission is a multiplication process for microbes to propagate. Cell grows to twice its original size and then splits into two with an exact replica of the parent. Binary fission of surface-attached cells lead to daughter cells growing in an outward and upward direction, which is reminiscent of the colony formation mechanism on agar surfaces.

(3) Recruitment of cells from bulk fluid: This is conventionally known as the accumulation type of biofilm formation. Biofilm amass by deposition, clustering and aggregation of neighboring as-formed biofilms pellicles, planktonic cells and biogenic materials.

The relative contributions of each of these three active or passive mechanisms depend on the interaction among the microbes, substrate properties and environmental conditions. Biofilms often grow by a combination of these mechanisms. Mature biofilms consist of cells working together in a complex architecture. Biofilms take days, weeks or even months to progress through the developmental stages and finally reach structural maturity for dispersal. Once attached, bacteria in biofilms commonly express a large amount of EPS to promote the adherence and to protect themselves from desiccation [7].

Species information is one of the most important factors in determining biofilm structure and physiology. *Pseudomonas aeruginosa* is one of the most well studied species among the biofilm formation bacteria. This well-sequenced, clinical and industrial infection related species has a short biofilm formation time of 24 hours, which makes it suitable for biofilm research [8-10]. Biofilms formed by other species such as *Bacillus cereus* and *Bacillus subtilis* biofilms are also widely studied because they are implicated in many industrial and medical applications [11, 12].

Another component underlying biofilm structural distribution and determining other biofilm properties is the EPS composition [3]. In most biofilms, EPS accounts for > 90% of the total dry biomass of the biofilms [13]. EPS contains a mixture of biogenic materials such as extracellular polysaccharides, lipids, proteins, nucleic acids, humic substances, *etc*. EPS has widely been reported to contribute to the formation, differentiation and structural complexity of biofilm [14, 15], as well as susceptibility to antibiotics in many biofilm formation species, such as Gram-positive

Staphylococcus epidermidis, *Staphylococcus aureus* biofilms and Gram-negative *Escherichia coli*, *Pseudomonas fluorescens*, *Vibrio cholerae biofilms* [16-18].

Knowledge on bacterial biofilm formation is still limited. One of the widely accepted biofilm developmental processes on solid surface includes 5 stages [3, 19] (Fig. 1.1):

1. Initial attachment;
2. Inreversible attachment;
3. Development of biofilm architecture (maturation I);
4. Maturation of biofilm architecture (maturation II);
5. Detachment and dispersal.

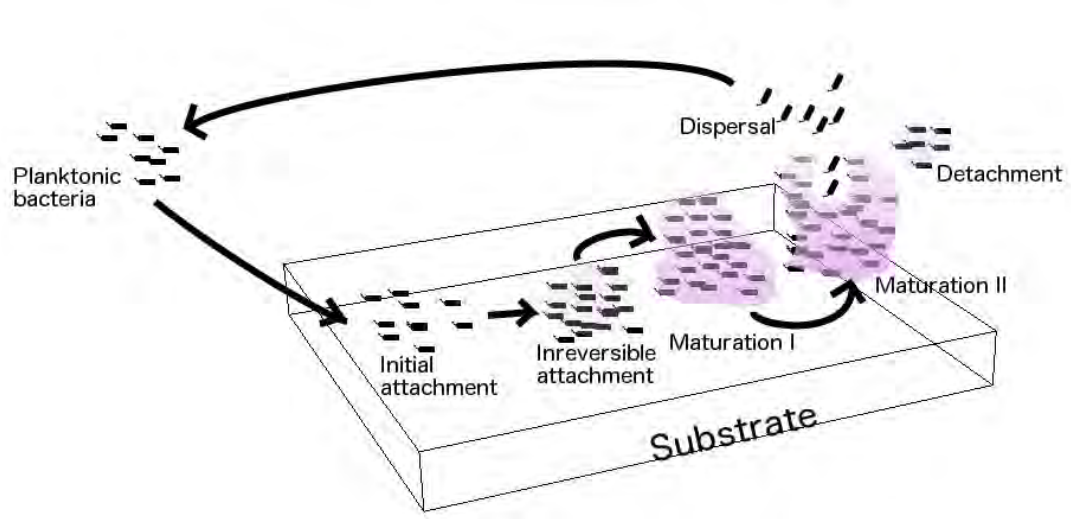

Figure 1.1 Development of a biofilm in 5 stages. Stage 1: Initial attachment of cells on surfaces. Stage 2: Reversible attachment. Production of EPS contributes to better adherence in this stage. Stage 3: Early development of biofilm architecture known as maturation I. Stage 4: Further maturation of biofilm architecture. Stage 5: Dispersal of cells from the biofilm and detachment of biofilms.

Stage one of biofilm formation is marked by the reversible adherence of individual cells on a substrate. At this stage, many of the cells are able to move to the substrate with the aid of various pili-mediated translocation strategies, such as twitching or gliding, known as translocation. Translocation of bacteria is affected by a number of factors primarily due to the interactions between the surfaces of cells and substrate

via gravity, van der Waals forces, electrostatic forces and hydrophobic interactions [20]. Flagella and other swimming organelles of bacteria also affect translocation and attachment, as suggested by earlier work on mutant *P. aeruginosa* [6, 21]. The attachment between cells and substrates remains reversible at this state. Cells can still be easily dislodged or washed into the surrounding fluid and return to a planktonic form of life [22]. A wide spectrum of behaviors has been observed in different species, such as creeping, twitching, pili-mediated movement, rolling, and formation of pellicles and aggregations. Cells exhibit logarithmic growth [23]. Presence of biofilm components such as outer membrane protein and lipopolysaccharide enhances bacterial adherence in this reversible attachment process [24].

In stage 2, the cells begin to exude exopolysaccharide and adhere irreversibly. Specific surface-associated genes were expressed within a short period of time upon attachment. As reported by Davies & Geesey, genes responsible for alginate production, a critical integral component of EPS, was up-regulated of *algC* within 15 min in *P. aeruginosa* biofilm developments [25]. Bacteria may strengthen their adherence to the substrate by producing EPS or *via* hydrogen and covalent bonds [26, 27].

In the third stage, also known as maturation I, burgeoning biofilms develop well-defined micro-colonies with a more conspicuous architecture of water channels. The overall thickness of biofilm could reach approximately 10 μm. Some of the cells may alter their metabolic mode to anaerobic as a response to a change in microenvironment [23, 28]. An oxygen concentration profile was established as

biofilms continue to mature in maturation II, which sees a complex architecture harboring voids, channels, and a translocation and redistribution of microbes inside the matrix [28]. Mature biofilms elicit a different protein profile from their planktonic counterparts. For example, a significant fraction of proteins, approximately 300, were found to exist only in mature *P. aeruginosa* biofilms, but not in planktonic cells [4]. This further substantiated the alternation in gene expression between surface-associated cells and free-swimming cells.

The final stage in biofilm formation is detachment and dispersal. Detachment is a process in which pieces of biofilms detach from the parent biofilms by various forces. During biofilm dispersal process, cells detach from biofilm and disperse in the environment. Microcolonies, individually or in clusters, may be dislodged from the substrate to revert to planktonic form by mild perturbation in the medium or naturally by processes whose mechanisms remain elusive. The detachment and dispersal process is cited as an asynchronized process [3]. There are two kinds of dispersal: active dispersal initiated by the bacteria inside the biofilm and passive dispersal caused by external forces such as fluid shear and abrasion [29]. A type of active dispersal called seeding dispersal was found in *P. aeruginosa* [30]. In seeding dispersal, a microcolony breaks from mature biofilm, develop into planktonic cells and colonize another habitat as burgeoning biofilm. Environmental conditions such as nutrition level and oxygen depletion changes also contribute to dispersal. For example, *P. aeruginosa* biofilm disperse at times of a sudden decrease or increase in nutrient level [28]. Biofilm dispersal is an evolutionary strategy to allow the bacterial population to expand and survive [31]. On the other hand, the detachment process is primarily affected by variation in hydrodynamic shears that occurs concomitantly

with changes in flow rate. For example, under low shear and static conditions, biofilms are more susceptible to detachment in times of hydrodynamic changes [32, 33].

Significance of biofilms

Biofilms have been implicated in the pathogenesis of many nosocomial diseases. Biofilm formation on inanimate surfaces and their inherent resistance to antimicrobial agents are at the root of chronic bacterial infections and hospital-acquired contamination [34, 35]. Biofilms can potentially form in medical implants and medical devices, which may lead to nosocomial infections [36-38]. *S. epidermidis* is among one of the notorious microorganisms whose biofilms are closely associated with foreign body infections [36]. Initial adherence of *S. epidermidis* cells to implants leads to the formation of confluent and multilayer biofilms, which may subsequently result in infections. Cells in biofilms are protected from human body host defense mechanisms and antibiotic therapy by the biofilm matrix and the slimy extracellular polymeric substance. In clinical settings, biofilms have been implicated in orthopaedic implants [37], intravascular catheters [39], and contact lenses [40].

One of the industrial problems caused by biofilms is microbial influenced corrosion and biofouling [11, 41, 42]. Corrosions of machines and pipes made of metal or metal alloy are directly or indirectly affected by biofilms through their metabolic end products (e.g. sulfuric acid produced by *Thiobacillus thioxidans*) [43]. Biofilms reduce heat transfer and increase flow resistance of the transfer pipes used for food production [22, 44], and cause foodborne diseases [45-47].

Many researches focus on the deleterious effects of biofilms, but beneficial biofilms are found in plenty of industrial implications [11]. For example, biofilms are used in nutrient removal in wastewater treatments [48-50]. Bioremediation utilizes biofilms to remove, detoxify or immobilize chlorinated hydrocarbons, polyaromatic hydrocarbons, heavy metals, *etc.* [51-55]. About 150 reported biocatalytic processes in the industry have exploited the use of planktonic cells [56], which could be improved by replacing with biofilms. In microbial fuel cell (MFC), low energy transfer efficiency is the main obstacle [57]. Coating the MFC anodes with biofilms can solve this problem [57-59]. At the biofilm-substrate interface, a higher enzyme concentration is recorded [60]. *Bacillus brevis* 18-3 biofilm has been reported to prevent microbial influenced corrosion of mild steel by inhibiting the growth of *Desulfosporosinus orientis* and *Leptothrix discophora* SP-6 [11]. Benign *B. subtilis* biofilms have been reported to disrupt the growth of pathogenic *S. aureus* and *P. aeruginosa* biofilms on the roots of plants [61-64].

Biofilm research areas

Biofilm was discovered in the 1980s to be highly differentiated surface-associated communities of microorganisms encased in EPS. Genetic researches of biofilm are of great interests [65] because biofilm dynamics are ultimately genetic processes differentially controlled by hundreds of genes [31, 66]. Genes determine the high resistance of biofilm to antibiotics as well [9]. Biofilm positive species such as *E. coli* [67, 68], *S. enteritidis* [69], and *B. subtilis* [70] are widely studied from genetic and molecular biology perspectives.

Quorum sensing (QS), bacterial gene regulation in response to cell population density, garners much attention recently in biofilm researches. Quorum sensing is mediated by the production, secretion and subsequent detection of designated extracellular signal molecules, known as autoinducers. Gene expressions are altered when autoinducers reach a critical concentration in response to changing cell population and density in the local vicinity [71]. Quorum sensing underpins the entire process of biofilm formation, growth and dispersal [71-76].

Resistance is one of the most significant characteristics of biofilms. The resistance of biofilms could be 1000-fold higher than that of planktonic cells [8]. The mechanism of biofilm resistance is widely studied. Some reasons for the high antibiotic resistance of biofilm include: (1) hindered penetration of antimicrobial substances into the biofilm matrix; (2) slow growth of the bacteria in biofilms; and (3) heterogeneity of biofilms. The level of biofilm resistance against antibiotics varies from species to species with the underlying mechanism remaining elusive [8, 77].

Biofilm architecture including the porous structure of biofilm composed of microchannels and colonies and the surface shape of the biofilms is of great interests to the biofilm researchers [78]. The microchannels separating the colonies in the porous structure are formed to exchange nutrients, oxygen and bacteria inside the biofilm. The surface shapes of biofilms including microstructures such as micro-niches, microchannels and spatial distributions of substance greatly affect biofilm activities and solute transport rate into the biofilms [79]. Biofilm structures are affected by many factors such as biomass changes caused by bacteria growth and EPS production [80], nutrients concentration, hydrodynamics of environments [32],

etc. Biofilms are found to exhibit some level of heterogeneity resulting in the structural complexity of the biofilm [81].

Air-liquid interface biofilm

In the laboratory, biofilm cultures are conventionally grown on artificial substrates immersed in culture medium. To render the culture of these cells closer to one of their native environment, it seems legitimate to raise the biofilms to the air-medium interface. A-L interface biofilm are biofilms formed at the interface between air and liquid. Some clinical and industrial bacterial strains such as *B. subtilis*, *B. cereus* [82, 83], *P. fluorescens* [84, 85], *P. aeruginosa* [86, 87], *E. coli* [88, 89] and so on, possess the ability to form A-L interface biofilms. Not all S-L biofilm forming species can form A-L interface biofilms because the biofilm develop process is complex processes, which cannot be simply describe by the bacteria species or EPS production [90]. A-L interface biofilm usually grows faster than the S-L interface counterpart because of easier access to nutrients and oxygen.

There is a lack of consistency on the experimental observations and a general explanation of the findings in S-L interface biofilm studies due to the design differences in experiments, such as the nature of bacterial colonizing surfaces, the bacterial species, and other experimental conditions [91]. A-L interfaces may provide a solution to setup a consistent experimental environment for biofilms to grow.

Studies on *B. subtilis*, *P. fluorescens* SBW25 wrinkly spreader and *Salmonella enteritidis* indicated the importance of biofilm genes in the resistance, physical properties and formation of A-L interface biofilm [69, 85, 92, 93]. Genetic analysis

can readily be carried out on A-L interface biofilm than the S-L interface counterpart because the former is easier to harvest. Interactions of multispecies bacterial cells in A-L interface biofilms were studied easily by measuring the dry mass of the single species and multi-species biofilms [82]. Study of the species-to-species interaction of multi-species biofilms enjoyed advantages such as fast proliferation of biofilms and ease of harvesting.

Resistance screening of antibiotics, heat and pH were also conducted on A-L interface biofilms. For example, resistance to chlorine and sodium hypochlorite of *Salmonella enterica* serovar Typhimurium A-L interface biofilm was higher than planktonic cells but resistance to heat or low pH was similar to planktonic cells [94]. A-L interface biofilms were easily harvested with tweezers for further analysis. High-throughput measurements on A-L interface biofilms, however, remain challenging.

Objective

The objective of this thesis is to culture air-liquid interface and air-liquid-solid interface biofilms on-chip by mimicking the natural microenvironment.

Outline

This thesis is organized as follows:

Chapter 1 introduces the background, formation, and uniqueness of biofilm with a focus on the air-liquid interface biofilm, as well as the motivation of this thesis work.

Chapter 2 reviews biofilm cultivation methods, microfluidic technology developed for culturing and measuring biofilm, and the droplet physics.

In Chapter 3, the hanging droplet biofilm reactor (HDBR) was constructed on an open microfluidic platform to hold hanging droplets for culturing biofilms in a suspended fashion. This technology enjoys a number of novel advantages in the research of biofilm. First, surface area to volume ratio is high as compared with bulk cultivation methods, resulting in a higher efficiency of oxygen exchange at the interface to promote growth and biofilm formation. Second, Marangoni effect and evaporating flows enhance the mixing and aeration of bacteria in the hanging droplet resulting in a microenvironment favored by A-L interface biofilms. Third, evaporation flows are laminar flows, which are commonly found in microfluidics. Therefore, the reactor can be easily implemented with most advanced microfluidic technologies. Fourth, freely standing biofilms on surfaces of droplets can be harvested easily by dripping the droplets.

Chapter 4 introduces the design and implementation of the segmented-flow microfluidic air-liquid-solid interface biofilm reactor (SFMBR) to culture air-liquid-solid (A-L-S) interface biofilms on chip. A distinct A-L-S interface was made available by introducing a gas phase into successive nutrient flows with a T-junction design, forming a segmented gas-liquid flow. By studying the standard method to culture A-L-S interface biofilms using drip flow biofilm reactor, we found that the main challenge in microfluidics was to guarantee the repeated and reproducible contact of biofilms with nutrient and air in a controllable fashion. Segmented air-liquid flow (SALF) in microfluidics is an ideal candidate to address this challenge

thanks to following advantages. First, liquid and gas filled the whole cross section of the channel resulting in ample amount of contact between biofilms on the microfluidic walls with nutrients and air. Second, the relative amount of air and liquid can be controlled independently. Third, mixing of nutrients and biomaterials in the droplets of the SALF can be customized. Fourth, movements of the A-L interface on the bubbles intercepted in the liquid can be controlled to exert different degree of mechanical shear forces on the formation of biofilm.

Chapter 5 concludes the thesis and projects future work on the development of a biofilm printing technique as the next-generation revolutionary biofabrication strategy.

Chapter 2 Literature review

Microorganisms in nature often exist in surface-associated sessile communities known as biofilms. Biofilms are aggregates of microorganisms where the indwelling cells are encased within a self-secreted matrix of EPS, colloquially known as a slime, adhered to each other and/or to a substrate or phase boundary. Microbial biofilms have been the subject for lots of studies during the last decade mainly for two reasons. First, it is of basic scientific interest to understand how bacteria form and live in multicellular communities. Second, bacteria in the form of biofilms are difficult to eradicate *via* biocide, antibiotic treatment or host immune responses. The notorious formation of biofilm is often associated with contamination in industrial and medical settings. Knowledge about the effect of environmental cues, contribution of gene expression, and delineation of molecular mechanisms are instrumental for a holistic understanding of biofilms, as well as forming the basis for the development technologies for biofilm monitoring.

A substantial part of the studies of microbial biofilms carried out during last few decades involved laboratory setups such as microtiter plates and flow chambers. With the use of model biofilm strains, such as *Lactobacillus plantarum*, *Lactococcus lactis*, *Escherichia coli*, *Pseudomonas aeruginosa*, *Listeria monocytogenes*, *Staphylococcus* spp., and *Bacillus* spp., it is known that biofilm formation and properties depend much on the choice of substrates and environmental factors. The underlying mechanisms remain elusive to a large extent. For instance, adherence, surface-associated spreading, cell-to-cell communication, maturation, and dispersal are some of the biofilm properties that are still not well understood. In this chapter, biofilm cultivation methods in the literature will be reviewed in a systematic way

from biofilm reactors, microfluidics, droplet physics and evaporating flow-induced microcirculation.

Biofilm cultivation

Biofilm is broadly defined as communities of microorganisms attached to and associated with a surface. Henrici, one of the pioneer scientists, stated in his paper in 1933 that "… it is quite evident that for the most part water bacteria are not free floating organisms, but grow upon submerged surfaces." [95]. Since then, biofilms found at the interface of various substrates and phase boundaries have been characterized. Biofilm formation on the solid-liquid interface is a relatively well-characterized process with a progression from initial attachment, further development and finally formation and dispersal of micro-colonies eliciting micropillars and mushroom-like structures with a network of water channels amidst the EPS matrix. These phenotypic changes are coupled with corresponding changes in gene expression, which underpins the vast differences observed between the planktonic and sessile forms of life in bacterial. While biofilms in the nature are often composed of multiple species, single-species biofilms cultivation methods are the focus of this thesis and will primarily be reviewed in this chapter.

There are three conventional mechanisms to form biofilms in the literature [3]. The first method hinges on the surface motility of adhered microbes on a surface. O'Toole & Kolter have illustrated the role of type IV pili-mediated twitching motility in aggregation and surface mobility of the mutants of *P. aeruginosa* [6]. The second approach is simply the proliferation of daughter cells outward and upward to form 3D cell aggregates. This mechanism is reminiscent of colony formation in Petri

dishes. The third mechanism involves the recruitment of planktonic cells in the local fluid vicinity by a growing biofilm. These three mechanisms often work in a concerted effort in the development and maturation of biofilms, with the relative contribution dependent on the physical and chemical microenvironment. Biofilms are conventionally cultured in laboratory-controlled conditions mimicking the natural environment. Biofilm cultivation methods broadly fall into two categories: batch cultivation methods and continuous cultivation methods [96].

Batch biofilm cultivation

Batch biofilm cultivation is based on a basic assumption that microorganisms will adapt to defined process conditions in a batch fed system. Batch biofilm cultivation often entails submerging metal and plastic coupons in nutrient broth or directly on solid culture media, which served as substrata for biofilm adherence [1]. Microtiter plates (MTP) are commonly used in biofilm cultivation [10], where A-L and S-L biofilms grow on the broth surfaces [97], inserted coupons [83], pegs [98], walls and bottom of the plates [99]. A microtiter plate is a flat plate with multiple wells (typically with 6, 24, 96, 384 or 1536 wells) for compartmentalized analytical chemistry or clinical diagnostic use. Crystal violet staining has become a standard in quantifying the mass of S-L interface biofilms cultured using MTP-based methods [100], but it is fundamentally challenging for A-L interface biofilms because this method entails the biomass of A-L interface biofilms to adhere to the wall of MTP wells before staining. While MTP-based assays provide a high-throughout and rapid way for analytical characterization of biofilms, the multi-array structure is inconvenient for culture and harvesting outside of a laboratory setting. The choice of

materials for microwells is often limited to a few types of plastics, such as polystyrene, polypropylene and polycarbonate.

Colony biofilms have conventionally been cultured on nutrients agar [101] or on membranes placed on agar plates [102]. For example, wrinkly patterns of colony biofilm on agar were used to study biofilm structures [103]. Agar plate biofilm cultivation and harvesting are straightforward to conduct, but it is of a low throughput and not adaptable to culture A-L interface biofilms. Alternatively, growing biofilms in broth media inside glass tubes and beakers are also easy to set up [83, 99]. Yet, they suffer similar limitations as the solid agar cultivation method. An unnecessarily excessive amount of materials is needed to grow biofilms at the interface while cells in the bulk of the media are to be discarded afterwards. Replacement and replenishment of the culture media are not only time-consuming and labor-intensive, but also susceptible to contamination. However, many A-L interface biofilms are still cultured using these methods [104, 105].

Another appealing biofilm cultivation approach widely used in medical and industrial applications is rotating bioreactors such as concentric cylinder reactors and rotating disk biofilm reactors [106]. In a rotating disk biofilm reactor, a disk coupon holder rotates at specific speeds to generate low shear stresses across the surfaces of biofilms on the coupons [101]. Instead of using coupon holders, a concentric cylinder reactor has a stainless steel cylinder that provides a surface for biofilm to adhere. The Center for Disease Control (CDC) biofilm reactor contains rotating vanes, which generate nutrient flows for biofilms to grow on coupons around the vanes [39]. Though these biofilm reactors can be used to simulate various flow situations to

customize biofilm properties under different microenvironments, these setups entails dedicated devices and power and material consuming. Scalability is another issue of these settings. Furthermore, they cannot be used to culture A-L interface biofilms.

Continuous biofilm cultivation

Continuous biofilm culturing methods are considered better than the aforementioned batch biofilm cultivation methods because of a better control of nutrients and environmental conditions in the course of biofilm formation. Different stages of biofilm formation entail different nutrient levels and shear forces, which can all be adjusted accordingly in the continuous cultivation techniques [101]. In nature, biofilm ecosystems are fed continuously or at regular intervals, which resemble more closely to the continuous biofilm culturing methods. Flow cell biofilm reactor is a widely used technique in continuous biofilm cultivation studies [107, 108]. Through an elaborate network of tubes and chambers, culture media is continuously fed while waste materials are being removed in a controllable fashion. Operations of these reactors are very much similar to convention bioreactors with precisely controlled inputs, outputs and biological reaction environments. Specific for biofilm culture, mechanical perturbation in the form of shear stresses along interfacial surfaces is another critical consideration that affects initial adhesion and subsequently affects biofilm properties. Shear forces on biofilms can be adjusted by controlling the nutrient flow rates along the tubing walls or chamber surfaces. For example, the modified Robbins device (MRD) is widely found in industrial pipe systems and medical lines for biofilm monitoring [101]. Replaceable pegs inserted into the walls of tubes or pipes are used in MRD to monitor the biofilms [109]. Recently, there arises a surge of microfluidic biofilm reactors based on the flow cell principle. In a

nutshell, the flow cell operation is miniaturized and realized within microchannels, taking advantage of the flexibility of microfluidics for a seamless integration of input, output and detection. With the use of transparent material such as PDMS and indium tin oxide, microscopic and electrochemical detection techniques are made feasible for online monitoring of biofilm physiology. More details on the microfluidic implementation of biofilm reactors will be reviewed in later sections of this chapter.

Continuous dripping is another technique widely used in continuous biofilm reactors. Liquid nutrients are made to drip continuously along a slanted substrate for the growth of biofilms. For example, drip flow biofilm reactor is used to simulate the biofilm-growing environment of food-processing conveyor belts, catheters, lungs with cystic fibrosis and the oral cavity [86, 110]. A-L interface biofilms can be cultured on solid surface with continuous culture media dripping reactors. While this technique confers controls on the nutrient level and shear stress over time, the entire system are often large, material intensive and of a low throughput. A novel microfluidic version of drip flow biofilm reactor is introduced later in this thesis to address some of the current limitations. There are many other biofilm reactors for niche applications such as biofilm reactors in wastewater processing [50, 111] which are not discussed here.

Microfluidic methods in studying biofilms

Droplet-based open microfluidics

Microfluidics deals with minute volumes of fluid with microscale flow components such as channels, chambers and valves [112, 113]. Many applications of microfluidics can be found in material science, chemistry, biochemistry and biology

researches [114, 115]. Microfluidics is a promising tool for microbiology because both of them work on micrometer scale subjects [116, 117]. Advantages of using microfluidics include fast detection, low cost, ease of fabrication, precise concentration gradient control, high-throughput operation, *etc.* [118].

Droplets are utilized in microfluidics as individual compartmentalized micro-reactors [119-121]. Droplets can be generated by electrohydrodynamic (EHD) methods such as dielectrophoresis and electrowetting [122], and alternatively by methods based on channel geometries such as T-junction and right angle cross channels [121-123]. Droplet generation methods based on EHD do not entail the use of pumps, which significantly cut down the clutters associated with the overall setup. But the complexity of system setup limits the applications of EHD-based droplet generation methods. Geometry-based droplet generating devices are easy to fabricate and operate, which has been the technology selected in this thesis for the generation of droplets or bubbles in microchannels for the interfacial formation of biofilm.

In open microfluidics, samples are made exposed to air on one hand and still cling to the actuation and sensing substrate on the other hand, often in the form of droplets on a plane and channels without overhead roofs [124-127]. Open microfluidics are often desirable for online monitoring for biological processes with sensors placed in contact or in close proximity with the samples. There is a wide range of electrochemical, optical and mechanical characterization technique available, with atomic force microscope (AFM) as one of the prime examples reported in the literature [128, 129]. Open microfluidics enjoys ease of sample introduction and withdrawal [125] and direct gas diffusion, which matches the cultural conditions and

requirements of A-L interface biofilms. However, evaporation in open microfluidic devices presents a grand challenge due to the high surface area to volume ratio of the liquids [130]. Utilizing open microfluidic devices for long-term biofilm culture have a lots of challenges to be resolved.

To take advantage of droplet-based microfluidics and open microfluidics, a droplet based open microfluidic system is designed in this thesis for long-term biofilm cultivation. Minute volume of nutrient can be precisely controlled to compensate for evaporation with the fluidic control conferred by microfluidics. Open microfluidics allows direct gas diffusion, which benefits the growth of A-L interface biofilms. Evaporation, rather than regarded as a disadvantage against the overall design of open microfluidics, is utilized to induce a gradient of surface tension and thermal distribution along the droplet surface in order to generate evaporation flows for effective mixing inside the droplet.

Biofilm cultivation and analysis on chip

Biofilm reactors built on a microfluidic platform are used to mimic the biofilm growing environments in the nature, and to generate precise hydrodynamic conditions for biofilm formation screening [131]. Microfluidic biofilm reactors mostly grow S-L interface biofilms in channels or chambers with a continuous input of nutrients [132]. For example, *Micrococcus luteus* biofilms have been reported to be cultured and analyzed on an 80-channel chip with small amount of bacterial suspension (1.6 mL) [133]. *P. aeruginosa* PAO1 biofilms were also cultured and analyzed in a 96-channel microfluidic plate based on a MTP [134]. Microfluidic devices can also be used to generate precise concentration gradients of antibiotics,

cell communication signals [131] and oxygen [135] to study the concentration-dependent effects on biofilm formation and biofilm properties [136]. The Young's modulus of biofilms can also be measured by using a microfluidic device with a flexible PDMS membrane [137]. Hydrodynamics, which affects biofilm formation, can easily be controlled in microfluidics by adjusting the flow rate of nutrients [138]. Shapes of channels and micro-patterns in microfluidic chambers [139, 140] that affect hydrodynamics of the microflows are easy to fabricate to study the effects of hydrodynamics on biofilm formation.

Many real-time monitoring methods of microfluidics can be integrated in biofilm research. For instance, it was reported that a modified confocal reflection microscopy was used to monitor biofilm growth in a PDMS microfluidic device [141, 142]. Impedance and electrochemical methods were used to track biofilm formation by monitoring the impedance measured across electrodes in the microfluidic channels [143, 144]. Optical density measurement was one of the commonly used techniques for biofilm monitoring [142]. An interesting biofilm monitoring method based on open microfluidics using synchrotron-radiation-based Fourier transform infrared spectromicroscopy (SR-FTIR) was reported, which imaged real-time chemical activities in biofilm formation process [127].

Though microfluidics is an ideal tool for biofilm researches, current implementation and bioreactors are mainly geared towards the study of S-L interface biofilms. A microfluidic device to culture and analyze A-L interface biofilms is in demand. Some commonly used biofilm cultivation methods are summarized in Table 2.1.

Table 2.1 Comparison of biofilm cultivation methods.

Biofilm Cultivation methods	Batch (B) or continuous (C) methods	Biofilms on interfaces	Material cost	Throughput	Monitoring difficulty	Harvesting difficulty	Fabrication difficulty	Labor costs	Automatic culture and detection	References
MTP based	B	S-L / A-L	High	Medium/ High	High	High/Medium	Low	High	N	[10], [99] [83], [98].
Agar based	B	S-L	High	Low	High	High	Low	High	N	[101], [102], [103].
Cell culture (glass-ware) based	B/C	S-L / A-L	High	Low	High	High	Low	High	N	[99], [104, 105].
Rotating disk	B/C	S-L	High	Low	High	High	High	High	Y	[106], [39].
Flow cell	C	S-L	High/ Medium	Low	Low	High	Low-High	Medium	N	[107, 109].
Dripping culture media	C	A-L-S	High	Low	High	High	High	High	Y/N	[86, 110].
Microfluidics	B/C	S-L	Low-High	High	Low	High	Low-High	Low	Y	[131], [133], [134-136].
Hanging droplet biofilm reactor	B/C	A-L	Low	Very High	Low	Low	Low	Low	Y	
Segmented flow microfluidic air-liquid-solid interface biofilm reactor	C	A-L-S	Low	High	Low	High	Low	Low	Y	

Droplet properties and droplet evaporation

Motivation of using droplet in microfluidics is to provide compartmentalized micro-reactors for chemical reactions and physiological processes [122]. In this thesis, evaporating hanging droplets were utilized to culture biofilms. The following sections elucidate the foundation of droplet-based bioreactors.

Droplet properties

Surface tension

A droplet is confined by interfaces, which is defined to be the geometrical surface delimiting fluid-fluid or solid-fluid domains [124]. Biologically found phase boundaries include solid-liquid, air-solid and air-liquid interfaces. For example, a hanging droplet is confined by an air-liquid interface and a solid-liquid interface. From an engineering point of view, all interfaces associated with biofilms in this thesis are assumed to be smooth with negligible thickness [124].

Surface tension is a phenomenon resulted from surface energy difference across an interface. Molecules in liquid are much denser than that in gas. In Fig. 2.1, different intermolecular forces between the molecules on the surface and molecules inside the liquid contribute to an imbalance of surface energy across the interface, thereby resulting in a gradient of surface tension. Surface tension is characterized by the cohesive energy of molecules exerted on a unit area at an interface. If U is the total cohesive energy per molecule, the energy of a molecule at the interface is roughly $U/2$. δ is the characteristic molecular dimension. δ^2 is the associated molecular surface area. Surface tension is defined as

$$\gamma \approx \frac{U}{\delta^2} \qquad 2.1$$

Where γ is the measured surface tension, which is a property of the liquid material. For example, water has a surface tension of $\gamma \approx 70$ mN/m.

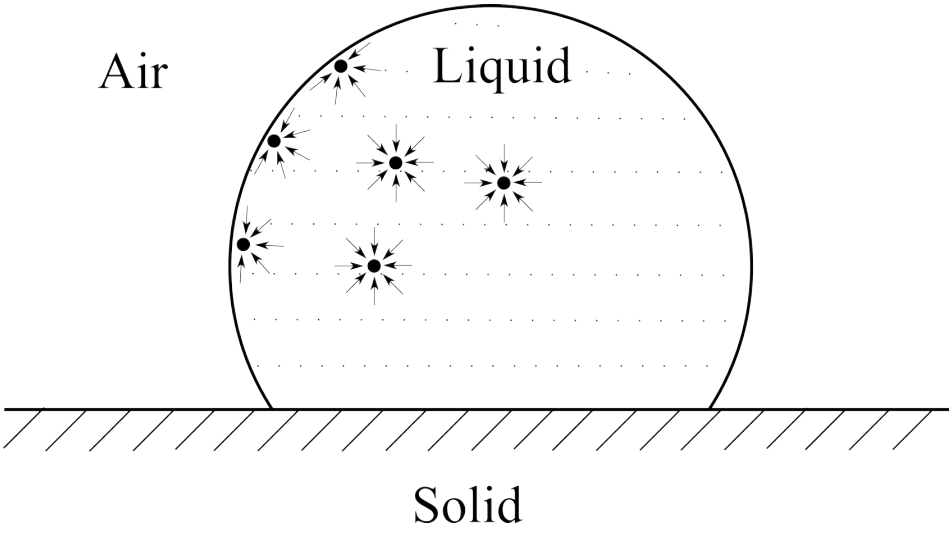

Figure 2.1 Schematic showing forces on molecules along the air-liquid phase boundary of a sessile droplet placed on an ideal smooth horizontal surface. The arrows stand for force direction. Surface tension is defined to be the attractive cohesive force of molecules along the droplet surface. The three-phase contact line is assumed to be circular with a uniform distribution of contact angle along the contact line.

Surface tension is related to the shape and curvature of droplets. The planar curvature κ is defined by the radius of the osculating circle at a given point on the curve (Fig 2.2). It is defined as

$$\kappa = \frac{1}{r} \qquad 2.2$$

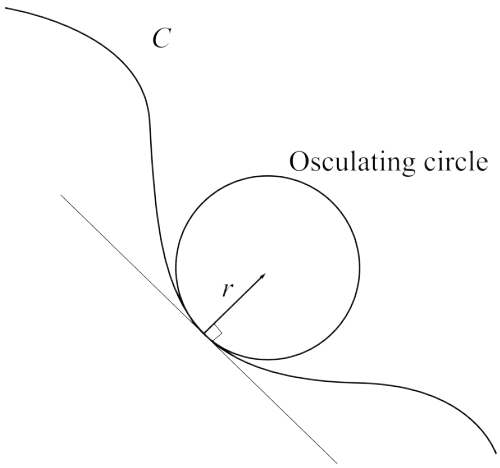

Figure 2.2 Planar curvature. Curvature of a 2D curve *C* is defined by radius *r* of an osculating circle.

Mean curvature is used to characterize a surface. Mean curvature of a surface is the mean of the maximum and minimum curvatures κ_1 and κ_2.

$$H = \frac{1}{2}(\kappa_1 + \kappa_2) \quad 2.3$$

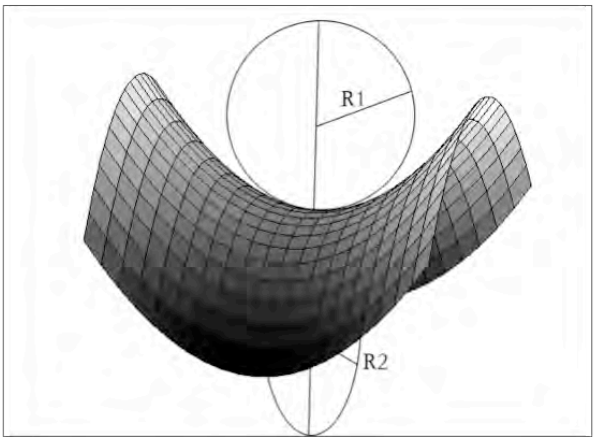

Figure 2.3 Surface curvature. The curvature of a surface is defined by mean of the maximum curvature and minimum curvature. The mean of maximum osculating circle radius R_1 and the minimum osculating circle radius R_2 define the curvature.

Contact angle

Contact angle is the angle at the triple line between solid, liquid and gas (Fig. 2.4). Surface tension is deemed as a force here. At the triple line, all forces should be at equilibrium, as shown in Fig 2.4 along the *x* direction:

$$\gamma_{LG} \cos\theta = \gamma_{SG} - \gamma_{SL} \quad 2.4$$

Equation 2.4 is derived from the Young's Law. The surface tension, γ_{LG}, γ_{SG}, and γ_{SL} are liquid-gas, solid-gas, and solid-liquid interface surface tensions, respectively. θ is the contact angle, which is related to surface tensions given by the following relationship:

$$\theta = \cos^{-1}\left(\frac{\gamma_{SG} - \gamma_{SL}}{\gamma_{LG}}\right) \quad 2.5$$

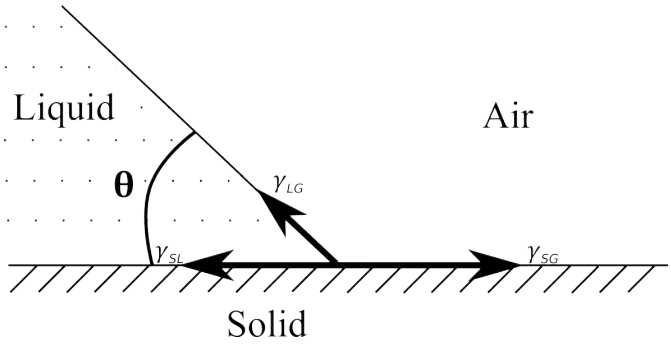

Figure 2.4 Contact angle of a sessile liquid drop on a solid surface. Contact angle is defined as the angle between a tangent line of the drop and the solid surface at the three phase contact line. $\boldsymbol{\gamma_{LG}}$, $\boldsymbol{\gamma_{SG}}$, and $\boldsymbol{\gamma_{SL}}$ are the surface tensions of liquid-gas, solid-gas and solid-liquid interfaces.

Bond number

Bond number describes the ratio of gravitational force and surface tension forces of a droplet. Bond number is defined by

$$\mathcal{B}_o = \frac{\Delta\rho g \mathcal{R}^2}{\gamma} \tag{2.6}$$

where $\Delta\rho$ is the density difference between the liquid and the surrounding fluid, g is the gravitational constant, γ is the surface tension and $\mathcal{R}$ is a typical dimension (usually the droplet radius or the droplet height) of the droplet. For a suspending droplet, gravity tends to elongate the droplet vertically to make it elliptical while surface tension tends to minimize the droplet surface area by making it spherical. When $\mathcal{B}_o \ll 1$, surface tension determines the shape of a droplet. In this case, the shape of the droplet will usually be of spherical. Otherwise, the droplet will elongate vertically to form an ellipse. When a droplet in air is about 1 mm in dimension, the Bond number is 0.03 to 0.04. Therefore, gravity is ignored and the droplet shape principally depends on surface tension [145-147].

Surface area

An advantage of tiny droplet is the large surface area to volume ratio, which increases while droplet volume decreases. When droplet is of a spherical cap shape, the surface area can be calculated from the equation [124]

$$S = 2\pi \int f(x)\sqrt{1 + f'(x)}\, dx \qquad 2.7$$

where the surface of droplet is obtained by rotating the curve $y = f(x)$. Define $r = f(z)$ and rotate about the *z* axis, the formula becomes:

$$S = 2\pi \int r\sqrt{1 + r'^2}\, dz \qquad 2.8$$

Surface area between $\mathcal{R} - h$ and $\mathcal{R}$ (h is the height of the droplet) can be calculated by:

$$S = 2\pi\mathcal{R}h \qquad 2.9$$

Microscale droplets greatly increase the reaction area at the air-liquid interface, thereby resulting in a larger exchange area for oxygen diffusion in aerobic microbiology. Take an example to compare the surface area to volume ratio of a traditional microtiter plate based biofilm reactor and hanging droplet biofilm reactor. Diameter of a well of a 24-well microtiter plate is 16 mm. The A-L interface area is calculated to be 200.96 mm^2. A-L interface area of a 25-μL hanging droplet is 33 mm^2. The surface area to volume ratio of a droplet is therefore 6.6 times higher than that of a microtiter plate with a 1-mL working volume. When the volume is further brought down to 7 μL using a microfluidic hanging droplet bioreactor, the A-L interface area of the hemisphere increases to 40.7 mm^2, which brings the surface area to volume ratio up to 29 times than the surface area in a 24-well microtiter plate.

Droplet evaporating flow

Evaporation is a proportionately huge problem when working with tiny droplets [130]. Evaporation of a tiny droplet is very fast because of the high surface area to volume ratio. Evaporating flows are generated as a result of evaporative cooling and nonuniform evaporation along the droplet surface in a sessile droplet.

Droplet evaporation

Evaporation is a significant factor affecting droplet behavior because of the high surface area to volume ratio of the droplets. It is often a problem to work with a small amount of liquid such as droplets [125, 130, 148] due to the undesirable increase in solute concentrations when droplet evaporates. On the other hand, evaporation can sometimes be exploited as an alternative means for pumping liquids, patterning and separating particles [126, 149, 150].

Disregarding the flow of surrounding air and Marangoni type convection (to be discussed later) inside a droplet, evaporation rate can be derived by Fick's Law [151]:

$$\frac{dm}{dt} = \rho \frac{dV}{dt} = -D \int \nabla c \cdot dS = -D \int \frac{\delta c}{\delta n} dS \qquad 2.10$$

where m is the liquid mass, V is the volume, ρ is the density of liquid, D is the diffusion coefficient of vapor and c is its concentration. The concentration gradient is approximately

$$\frac{\delta c}{\delta n} \approx \frac{c_0 - c_\infty}{R} \qquad 2.11$$

where R is the radius of the droplet, c_0 and c_∞ are the vapor concentrations at the interface and at infinity, respectively. The evaporation rate becomes:

$$\frac{dm}{dt} = \rho \frac{dV}{dt} = 4\pi R D (c_0 - c_\infty) \qquad 2.12$$

The evaporation rate is proportional to the radius of the droplet.

Droplet evaporation flow

Droplet evaporation is characterized into two stages [152-155]. The contact line pins and contact angle decreases till a critical value ($2° - 4°$ for water on glass) is reached in the first stage. Evaporation flux at the edge is much higher than that in the center, which causes more liquid loss at the edge. Liquid flows to the edge to compensate for the loss resulting in a flow from the center to the edge. In the second stage, the contact line recedes.

With regard to a tiny droplet, capillary force may also affect the shape and contact angle of the droplet. Capillary force is characterized by a capillary number, defined as $Ca = \frac{\mu \overline{U}_r}{\gamma}$ where μ is liquid viscosity, $\overline{U}_r$ is average radial velocity, and γ is surface tension. When the flow is 1 $\mu m/s$, Ca is on the order of 10^{-8}. So the capillary force can be ignored.

Flows are generated because of nonuniform evaporation along the droplet surface [156]. Reynolds number, $Re \equiv \frac{\rho \overline{U}_r}{\mu}$, measures the ratio of inertial force to viscous force. Evaporation flow is a type of laminar flow because of the low Reynolds number which has been reported to be about 0.003 for a evaporating droplet from the literature [157]. The Navier-Stokes equation is used to describe the velocity field of a laminar flow. By solving a set of equations, the circulation flow inside an evaporation droplet can be described [152].

Surface tension gradient along the droplet surface usually generates convective flows named Marangoni flow [158]. Marangoni effects were observed as early as 1800s,

which is also known as tears of wine [157, 159]. In an evaporating droplet, surface tension gradient generate by nonuniform evaporation induce temperature gradient or composition gradient on the A-L interface of the droplet causes the Marangoni flow. Utilizing the Marangoni flow and the evaporation flow, which is the flow from the center to the edge to compensate the nonuniform evaporation, the full flow field inside an evaporating droplet can be mapped show in Fig. 2.5.

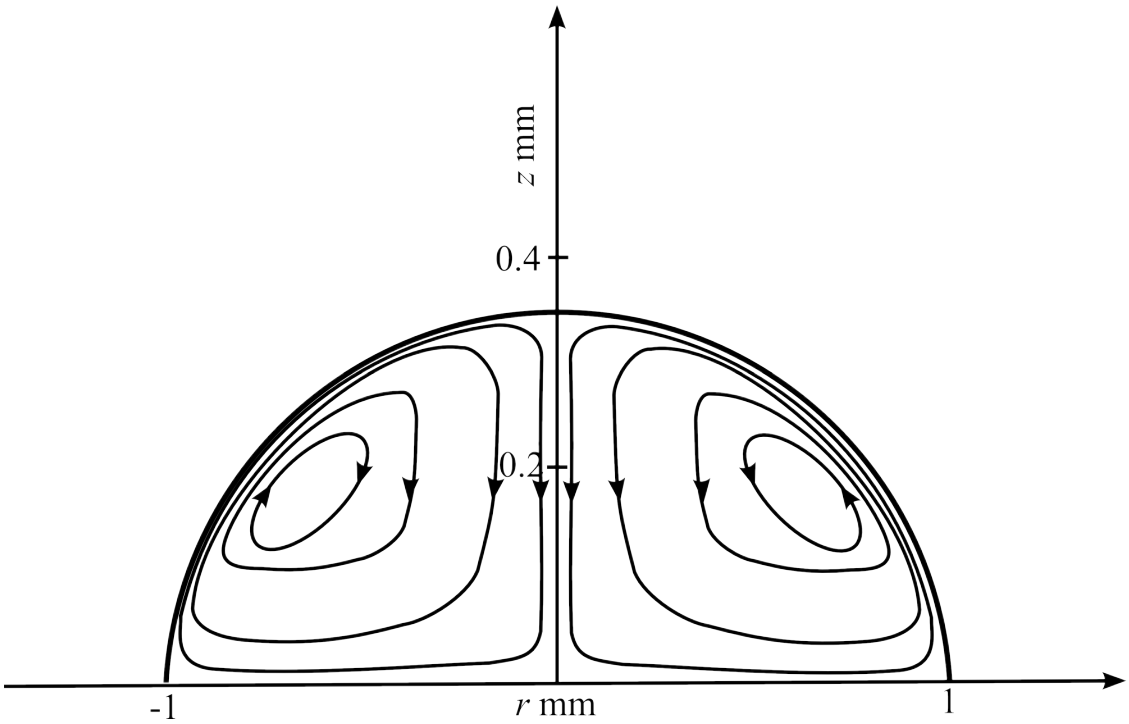

Figure 2.5 Flows in a droplet on a solid surface with a contact angle of 80 °. A water drop on a solid surface is evaporating. Marangoni stress on the droplet surface generates flows on the surface. Circulations were generated by the evaporation flows and Marangoni flows. Revised from [157].

Marangoni flow is related to the contact angle of the evaporation droplet [157]. At the first stage of evaporation, the edge of the droplet is pinned as discussed above. The temperature gradient on the droplet surface attenuates when the contact angle decreases leading to decreases of Marangoni stress [157]. At the critical contact angle of 14°, circulations disappear due to the sign of Marangoni flow changes to the same as evaporation flow (Fig. 2.6) [157].

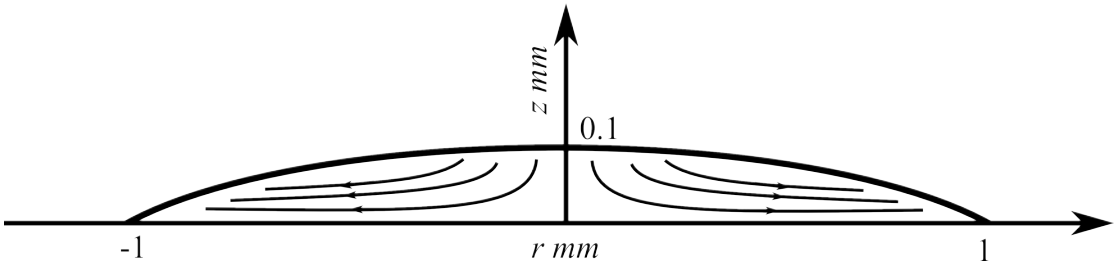

Figure 2.6 Flows in a droplet while Marangoni flow has the same sign with evaporation flow. Marangoni flow has the same direction as evaporation flow when the contact angle is smaller than a critical angle. Revised from [157].

Particles inside an evaporating droplet in this flow condition tend to move to the edge of the droplet resulting in a “coffee ring” pattern after evaporation [160-162].

It should be noticed that the flow field was simplified by assuming a pure liquid droplet sitting on a surface in an ideal symmetrical state. Flows in an evaporating hanging droplet biofilm reactor discussed in this thesis are more complex than in an evaporating water droplet, compounded by the continuously added nutrients and the blockage of droplet interface by A-L interface biofilm formation. The distribution of surface tension and thermal profile across the droplet surface will invariably change in a non-linear fashion over time.

Chapter 3 Formation of air-liquid interface biofilm under evaporating flow in an open microfluidic hanging droplet biofilm reactor

Abstract

Bacterial biofilms consist of bacterial communities encased in self-produced extracellular polymeric substance (EPS) at the interface of different phases. While most of our understanding of biofilms to date has been obtained from submerged biofilms formed at the solid-liquid (S-L) interface, the interface between air and liquid (A-L) provides a niche for the formation of biofilms with unobstructed access to both liquid and gaseous phases, which is of ecological, clinical and commercial significance. But there is only limited information on A-L interface biofilms. Cultivation and characterization of A-L interface biofilms are still limited to traditional methods designed for S-L interface biofilms, mostly based on microtiter plates and tubes. In this chapter, we describe the design, implementation and validation of an open microfluidic platform to hold hanging droplets to create an A-L interface culturing biofilms in a suspended fashion. Hanging droplets containing the microorganisms were accessed from the topside of the microfluidic platform, whilst measurement and harvesting were performed on the underside. The system was driven by evaporating flow. A flow pattern map was observed from particle velocimetry. No additional electronic or mechanical actuation was needed. Biofilm was formed in a 384-well hanging droplet plate and a PDMS microfluidic device with 15-μL bacterial suspension droplets. After 24 h of incubation under optimized conditions, biofilm-positive phenotype *Bacillus subtilis* developed A-L biofilms eliciting several distinct stages under microscopy observation. Over the course of

biofilm formation, evaporation rate kept decreasing due to a higher coverage of cells at the A-L interface, thereby changing the interfacial forces and tensional forces at the interface. Observations of biofilm formation and dispersal in A-L interface biofilms were illustrated for the first time. At 24 h, while the planktonic cell viability decreased by 2 orders of magnitude upon disinfection with 70% ethanol, more than 20% of the biofilm cells remained viable as revealed by fluorescence staining. From transmission electron microscopy, ultrastructure of the biofilms was observed with interconnecting nanotubes. Biofilms produced by dripping droplets harvested on substrates showed spherical cap shape with porous structures. This is the first attempt to culture A-L interface biofilms inside a hanging droplet on an open microfluidic platform under evaporation flow. Specifically, in the context of biofilm study, open microfluidic methods allow the creation of platforms that are readily treated for high-throughput biofilm cultivation and harvest, patterning, real-time measurement, and alternation of the microenvironment condition.

Introduction

Biofilm is a community of microorganisms in close association with surfaces and phase boundaries with self-secreted EPS [1, 163]. Inside this highly complex matrix is an elaborate network of interstitial water channels for the transportation of nutrients, oxygen and biomolecules. Formation of biofilm involves a whole new suite of gene expression and step-by-step formation of an intricate architecture harboring physical, chemical and biological environmental signals. Conventional microbiological techniques fall short to provide a robust high-throughput cultivation method, real-time in vitro measurement, and efficient cell harvest and subculture method. Most of the protocols widely practiced involve immersing inanimate

substrates into growth media to form solid-liquid biofilms over the span of days to weeks [98]. Harvesting S-L interface biofilms is a complex, time and labor-consuming process for subsequent measurements. S-L interface, also known as substrate-associated, biofilms are under the influence of substrate properties such as material, roughness and hydrophobicity [164, 165]. This hinders an objective comparison across biofilms formed on different substrates [166, 167]. Biofilms floating on the air-liquid interface have recently garnered much attention because of their unique characteristics and ecological significance [82, 83]. A-L interface biofilms practice a whole new set of self-organization strategies to form cell aggregates with highly specialized structures at the A-L phase boundary without the support of a robust solid substrate for initial cell adherence. A-L interface biofilms can be cultured with a faster rate than their S-L interface counterparts because of more efficient exchange of nutrients and oxygen at the phase boundary [85, 94]. Król *et al*. have reported that a higher plasma transfer efficiency in A-L interface biofilms than S-L interface biofilms [88]. This transfer efficiency was measured to rapidly drop off farther away from the air-liquid interface, suggesting the importance of oxygen availability for gene transfer.

Many biofilm cultivation and monitoring methods have been developed to mimic biofilm growing in the natural environment [96]. S-L interface biofilms submerged in culture media have long been studied either in batch condition or inside flow cells. Common batch culture techniques for S-L interface biofilms include the use of microtiter plates and crystal violet for rapid screening and quantification [100]. As for flow cells, microscopy is readily employed alongside with flow cell setup for visualization and monitoring. While most of our up-to-date knowledge on biofilms

centers on substrate-associated biofilms at S-L interface, the biofilms floating at the A-L interface are of ecological, industrial and clinical significance. A-L interface biofilms are commonly found naturally in aquatic niches. Some of the well-known bacteria include *Escherichia coli*, *Vibrio cholerae*, *Pseudomonas fluorescens*, and *Salmonella* spp. form A-L interface biofilms. Current techniques are, however, difficult to be applied on A-L interface biofilms. Biofilms grown inside microwells are inherently adhered to the walls of the microwells, forming air-liquid-solid interface biofilms rather than purely at the A-L interface [100]. The microtiter plate format poses difficulty in biofilm harvest and subculture. In addition, A-L interface biofilms have long been cultured using static cultivation methods whilst most biofilms in nature grow under continuous or semi-continuous environments [101]. There is a genuine need to devise a new method to rapidly culture A-L interface biofilms with novel bioreactor designs and integration state-of-the-art measurement technology.

Innovation in bioreactors built on microfluidic platforms has introduced lots of possibilities in the cultivation of microorganisms that would have been difficult or impossible in the past [131, 168]. Microfluidics handles minute volumes of fluid with micro scale components of a few micrometers to sub-millimeters, controlling the microenvironments experienced by each cell in the local vicinity [112, 113]. Microfluidics matches microbiology research because they both operate at the same length scale and can thus provide reproducible culture conditions to better mimic the natural physiological environment in terms of fluid dynamics, nutrient concentration and geometry [116, 117]. Microfluidic systems can readily be employed to construct highly controlled microenvironment for cell culture and metabolism in a high-

throughput, low-cost, and analytical fashion. Soft lithography based on biocompatible, transparent and easy-to-mold PDMS provides a robust yet adaptable way for devices fabrication. Characterization of biofilms were made either on-chip or off-chip by light microscopy, atomic force microscopy and electrochemical methods [131, 132, 141-144, 168]. For example, chemicals of varying concentrations were generated on chip flowing at a rate of 2 $\mu L/min$ for screening the effects of the chemicals on biofilm formation [131]. Biofilm morphology were reported to be different depending on the flow velocity and fluid shear profile of the microfluidic flow cells [169].

In this work, A-L interface biofilms were cultured inside a hanging droplet by combining droplet-based microfluidics and open microfluidics. Droplet-based microfluidics, which precisely and repeatedly generates droplets as micro-reactors, is a potentially high-throughput platform for biomedical research and applications [119-121]. The microfluidics in open space, which is called open microfluidics, has droplets or channels with one or more surfaces in direct contact with an open space [124-127]. Open microfluidics is a nascent field in microbiology. Recently, open channels haven been developed for chemical imaging in *Escherichia coli* biofilm formation process by synchrotron-radiation-based Fourier transform infrared spectromicroscopy [127]. But the biofilms were still cultured on S-L interface. The use of droplets and open microfluidics has not been reported in the long-term culture of biofilm. In the open channels as well as other popular open microfluidics systems, for example digital microfluidics, evaporation is a huge problem, which directly affects the effective volume and concentration of the culture [125, 148]. Evaporation has also been used in other ways in driving fluids inside microfluidics and separating

particles by size [126, 149, 150]. Microflows in an evaporating droplet are potentially useful but under utilized in the context of microbiology and microfluidics [157].

A microfluidic device has been fabricated to generate and manipulate hanging droplets to allow mixing, culture and coalescence of cells under well-controlled conditions. The hanging drop method is widely used in protein crystallization and tissue engineering [170, 171]. For example, spheroids were formed in a traditional way by culturing suspended cells in drops hanging on the underside of a Petri dish [172]. The drops are, however, unstable and susceptible to falling or merging with other drops. Although inexpensive, this method is labor-intensive and does not permit scalable production. An alternative method is to produce spheroids using 3D microwell [170, 171]. It enjoys a large surface area for oxygen perfusion and initial cell adherence, as well as a good supply of nutrients for tissue. However, these tissue engineering methods have not been used to culture bacterial biofilms.

In this work, we have developed a hanging droplet biofilm reactor (HDBR) for A-L interface biofilm cultivation under evaporating flows. A-L interface biofilm consisting of a single species, *B. subtilis* or *P. aeruginosa*, has been prepared at the hanging droplet surface. Biofilm physiology and droplet profile were monitored online by microscopy. Upon harvesting on glass slides and in wells of a 96-well microtiter plate, the deposited biofilms were further characterized by light microscopy, optical density measurement, confocal laser scanning microscopy (CLSM) and scanning electron microscopy (SEM). Evaporating flows and surface tension changes were characterized by image processing and finite element

simulation methods.

Materials and methods

Chemicals

All chemicals were purchased from Sigma-Aldrich (St. Louis, MO, USA), and all biological supplies were purchased from Difco Laboratories (Detroit, MI, USA) unless otherwise stated. Propidium iodide and SYTO 9 were purchased from Molecular Probes (Invitrogen, Eugene, OR, USA).

Cell culture

Bacillus subtilis ATCC 6051 and *Pseudomonas aeruginosa* ATCC 15692 were obtained from American Type Culture Collection. *B. subtilis* culture was maintained in cell buffer composed of 50 mM Tris-HCl, 1 mM $MgSO_4$, 4 mM $CaCl_2$, and 0.1 M NaCl at pH 7.2. Cultures were stored at 4 °C and transferred to fresh tryptic soy agar (TSA) or tryptic soy broth (TSB) incubated for 24 h at 37 °C in an orbital shaker at 160 rpm. *P. aeruginosa* culture was hydrated in nutrient broth and inoculated onto separate nutrient agar plates and incubated at 37 °C for 24 h. After incubation, stocks of the strains were stored at -80 °C in Luria–Bertani broth supplemented with 30% glycerol. Working cultures of *P. aeruginosa* were routinely grown in TSB at 37 °C under aerobic conditions with shaking for 24 h.

Device design and fabrication

A 3D tissue cultivation 384-well hanging drop plate (3D Biomatrix, MI, USA) [171] was used as the hanging droplet biofilm reactor (HDBR). The plate has a standard 384-well plate format with 16 rows and 24 columns. Each well of the HDBR has an

access hole through the plate. Samples could be pipetted though the access hole from the upside to form a droplet hanging underneath the plate, as illustrated in Fig. 3.1 (a). The plate was sandwiched between a lid and a tray during incubation. Reservoirs at the edge of the plate and the tray were filled with 4 mL sterile DI water to reduce evaporation. Droplets of 25-μL bacterial suspensions were formed.

Another HDBR device was made of PDMS and fabricated by soft lithography [75, 140]. A film mask was designed with AutoCAD (Autodesk Inc.) and printed on a transparent film. Four reservoirs ($\Phi 3$ *mm*) for inputs and a feeding reservoir ($\Phi 3$ *mm*) were designed. The channels were 100 μm wide. The relief features were made of SU-8 2035 photoresist (Microchem Corporation, MA, USA) spin coated on a silicon wafer with a thickness of 60 μm and developed by photolithography. Negative PDMS replicas were cast from a classical cross-type silicon positive relief master using Sylgard 184 silicone elastomer and curing agent (Dow Corning Corporation, Midland, MI, USA) at a 1:10 curing agent-to-base weight ratio. The PDMS was cured on a hot plate at 75 °C for 3 h. The PDMS was then peeled from the mold, and the inlets for cell inoculation and nutrient feeding were punched with a 27-gauge blunt needle. Another piece of PDMS without pattern was made and a hole was punched aligning with the feeding reservoir with a 27-gauge blunt needle. Hanging droplet and feeding reservoir were connected through the hole. PDMS layers were bounded with oxygen plasma (Fig. 3.1 (d)).

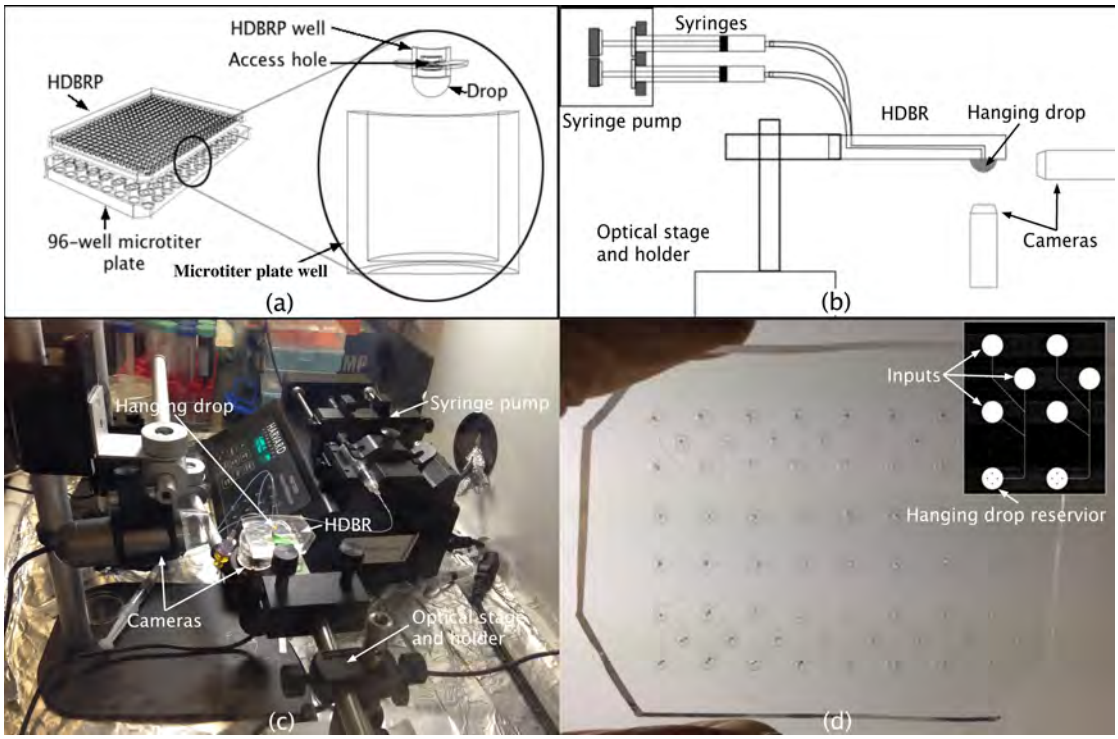

Figure 3.1 Experimental configuration of the hanging droplet air-liquid interface biofilm reactor. (a) The bioreactor was placed on top of a 96-well microtiter plate. Biofilms formed inside the droplets hanging underside of the bioreactor. Harvesting of biofilm could be realized by a pinch-off mechanism to be dripped and deposited onto a 96-well microtiter plate. The experiment was carried out in a well-controlled environment to minimize air turbulence lest the hanging droplet would be affected. (b, c) A microfluidic version of the hanging droplet biofilm reactor was shown with a full suite of equipment, such as a syringe pump, two cameras and optical mounts, all housed inside a laminar flow hood. A layout of the microfluidic chip was shown. All equipment was mounted on an optical breadboard for better precision. Automated operation was achieved with the auto-replenishment of nutrient in the droplet by the syringe pumps. Cameras were set up, one focusing sideways and one focusing from the bottom, to monitor the biofilm formation continuously for a better characterization of A-L interface biofilm formation. (d) Layout and mask design of the multiplexed microfluidic hanging droplet biofilm reactor. Nutrients, buffer, cells were fed into the hanging droplet reservoir precisely on a timely manner with the use of a set of syringe pumps. The microfluidic hanging droplet biofilm reactor provides an open microfluidic platform to generate a hanging droplet suspended on the underside of a glass/PDMS platform. Droplets of a uniform size could reproducibly be created and maintained. In this study, biofilms were cultured inside droplets. The microfluidic bioreactor was operated at a nutrient flow rate of 0.2 $\mu L/min$.

Experimental configuration

After hanging droplets inoculation, the HDBR plate was incubated at 37 °C with evaporation controlling reservoirs filled with DI water. The HDBR microfluidic device was mounted on standard optical mounting posts on an optical breadboard placed inside a non-operating laminar flow chamber (CaptairFlow 391, Erlab, USA) at room temperature (24 °C). The droplet dimension, shape and profile were

measured using two Dino-lite digital microscopes (AM413T, AnMo Electronics Corporation, Taiwan), one sideways and one capturing the bottom plane. Image analysis was done using Dino-Capture, software that came with the microscope. 100× diluted TSB were fed at a flow rate of 0.2 – 0.3 $\mu L/min$ with a syringe pump (Harvard 2000, Holliston, MA, USA) through sterile silicone tubing. Cultures prepared as mentioned above were diluted to a concentration of approximately 10^5 cells/mL and injected into the microfluidic device using a syringe. The device was incubated at room temperature under atmospheric conditions without control of relative humidity. To investigate the performance of reactors affected by A-L biofilms, 5% (v/v) penicillin/streptomycin (500 U/mL, Invitrogen, Carlsbad, CA) was added into the droplet as a control experiment. The system setup is shown in Fig. 3.1 (b, c).

Biofilm harvesting

Apart from cell seeding and culture medium supply, this culture system also enables biofilm harvesting and sub-culture. A fraction of the biofilm can be seeded on a fresh surface by dispensing. Biofilms formed at the interface of hanging droplets were harvested into individual wells of a 96-well microtiter plate (Corning, NY, USA) or glass as shown in Fig. 3.1 (a). 60-μL DI water were added to each drop hanging under the plate to dispense the droplet out into the microplate positioned underneath. The deposited biofilm was rinsed with 60-μL DI water twice to remove non-adherent cells.

Microscopy

Biofilms were observed using a Nikon Eclipse Ti-U phase contrast microscope

(Nikon, Japan). A Spot Xplorer camera and Spot software (SPOT Imaging Solutions, MI, USA) were used to capture images. Time-lapse images were taken at the same illumination intensity. The biofilms were also observed with a Nikon AZ100 stereoscopic microscope (Nikon, Japan). The images were captured with a DS-Fi1C camera controlled by a standalone control unit DS-L2 (Nikon, Tokyo Japan). Droplet profiles and biofilms formed using the HDBR were captured with Dino-lite digital microscopes (AM413T, AnMo Electronics Corporation, Taiwan).

Optical density measurement

The optical density at 600 nm of air-dried harvested biofilms was measured with an ELx800 automated absorbance microplate reader (Bio-Tek Instruments, VT, USA) at room temperature operated at a scanning mode. Each scan consisted of 31×31 points covering a circular area of 6.15 mm^2. Triplicate measurements were made. Biofilm thickness was represented in an optical density map, which was generated by Gen5 software (BioTek Instruments, VT, USA).

Live dead assay

Biofilms were formed as described above but harvested on glass coverslips. To study the viability of bacteria in the harvested biofilm after drying and disinfection with ethanol, CLSM was used. Biofilms before and after drying and disinfection with 75% ethanol were labeled with fluorescence probes: propidium iodide (PI) and SYTO 9 (Live/Dead BacLight bacterial viability kit, Molecular Probes, USA). Stained biofilms were washed with PBS and observed with an Olympus FV-500 CLSM, using a 488 nm argon ion laser. Serial sections in the x-y plane were obtained at 5-μm intervals along the z axis. Live to dead (green to red) ratio was

calculated to indicate the degree of biofilm resistance to the disinfection process.

Scanning electron microscopy

B. subtilis and *P. aeruginosa* biofilms were harvested on filter papers (5*mm*×5*mm*) with aforementioned method. Filter paper-collected biofilms were firstly fixed with 2.5% (w/v) gluteraldehyde (Sigma, USA) in PBS buffer (pH 7.4) for 2.5 h and then treated with 2% (w/v) osmium tetroxide for 2 h at room temperature (25℃). The samples were subsequently dehydrated in a series of ethanol washes (70% for 10 min, 95% for 10 min, 100% for 20 min), and dried in a critical point dryer (Ladd, Burlington, VT, USA). The specimens were coated with gold (Edwards, Sputter Coater S150B, Edwards, West Sussex, UK). After processing, samples were observed in a scanning electron microscope (Hitachi SU8010, Hitachi High Technologies Corporation, Tokyo, Japan) in high vacuum mode at 5 kV.

Image processing

The measured grayscale intensity of the microtiter biofilms should effectively represented the thickness of biofilms given the same illumination. Image analysis was carried out in ImageJ and results were plotted with customized R-scripts. The images were spatially calibrated and segmented by interactive thresholding. To measure the profile of the hanging droplet, each hanging droplet was assumed to be symmetric (Fig. 3.4 (e)) translated onto a two-dimensional coordinate system. Profile curves of each droplet were fitted into two circles by a three-point fitting to obtain radius of the curvatures at the apex and a virtual apex of the hanging droplet with the help of an ImageJ plugin (Fig. 3.4 (e)). The points selected for fitting were located

around the apex of the hanging droplet for R_1 and near the three phases (A-L-S) contact line for R_2 separately.

Red and green channels images of biofilm were captured by CLSM and subsequently processed with COMSTAT [173] to quantify the biomass of the dead cells and live cells in biofilms. Three images were measured for each sample. Red-to-green ratio of the images were calculated and plotted with custom R-scripts.

Numerical simulation

The profile of a hanging droplet can be simulated by considering the surface tension exerted on the interface in a two-dimensional (2-D) sense. Finite-element modeling was performed using the microfluidic multiphase flow 2-D symmetric module in COMSOL Multiphysics software to compute the boundary profile of the droplet and velocity field in the droplet. The focus of this study was the surface tension gradient governing boundary profile and the Marangoni flow generated by the surface tension gradient. Gravitational force was negligible in this modeling owing to similarity between the droplet dimension and the capillary length. Volume of the droplet was fixed. Only surface tension was applied on the droplet. A semi-sphere with the radius of 2mm was assumed at the beginning. The changes in liquid profile were governed by surface tension. The stationary states of the droplets reshaped by surface tension gradient generated by the A-L interface biofilms were simulated. Parameters of the liquid were chosen as follows: density, 1×10^3 *kg/m*^{3}, viscosity, 1×10^{-3} *Pa·s*, surface tension coefficient σ = 0.07 *N/m* and contact angle of the liquid with PDMS, $\pi/2$. The droplet contact with PDMS at z = 0 *mm*. Axial of the droplet was at x = 0 *mm*. The surface tension difference was set at z = -1 *mm* and with the surface tensions of

σ and 0.85 σ for the biofilm-free droplet surface area near the PDMS and biofilm-covered droplet surface area near the droplet apex respectively.

Statistical analysis

Results are presented as mean ± standard deviation for morphology and cell number of three independent experiments. Studies were replicated to ensure experimental reproducibility of trends. Statistical significance was determined by one-way analysis of variance ($p < 0.001$).

Results and discussion

The biofilm-forming *B. subtilis* and *P. aeruginosa* strains used in this study were tested for their ability to form A-L interface biofilms in HDBR. Biologists and engineers have long been mimicking Mother Nature in compartmentalizing biological reactions on length scales commensurate with tissues and cells. Not much success has been achieved because tailoring microenvironments for cells is still the bottleneck. In this work, each hanging droplet provides an individual compartment for biofilm culture without physical contact as in the solid-liquid submerged biofilm case or any constraints as in traditional close-channel microfluidics and bioreactors.

The advent of microfluidic bioreactor has brought cell culture into an increased focus with a potential to culture a myriad of once difficult to grow biological structures. A complex physical, chemical and mechanical microenvironment forms during the biofilm formation process. However, conventional technologies used to culture biofilms suffer from low throughput, labor-intensive, material-consuming and lack of reproducibility and precise control, which can only poorly mimic the complex

biofilm microenvironment in nature. On the other hand, microfluidic bioreactors can mimic the complexity of biofilm microenvironment by the aid of better control of the physical, chemical, and mechanical parameters in a high throughput way in microfluidics. Therefore, using microfluidic biofilm reactors may help to understand the biology and cement the clinical and industrial potentials of biofilms. Here we introduce a novel open microfluidic hanging droplet biofilm reactor forming biofilm at the air-liquid interface under evaporating flow to investigate the complex biology of biofilm in response to changes in local microenvironments.

Hanging droplet

The bioreactor could be operated in a 384-well plate format with pipetting or in a microfluidic format with syringe pump in Fig 3.1 (b, c). Flows, known as evaporating flow and Marangoni flow, were generated during the course of evaporation due to the nonuniform evaporation and the therefor induced surface tension gradient.

The microfluidic hanging droplet biofilm reactor provides an open microfluidic platform to generate a hanging droplet suspended on the underside of a plastic/PDMS platform. Droplets of a uniform size could reproducibly be created and maintained without a wall and floor. In this study, biofilms were cultured inside droplets of spherical-cap shape with a radius of 2 *mm*. The microfluidic bioreactor was operated at a nutrient flow rate of 0.2 $\mu L/min$. The size of the droplets and microcirculation can be varied by changing the flow rate of the feeding and environmental atmospheric conditions. The system provides flexibility of configuration for generating a diverse range of droplets with various sizes, inside

different media and culture conditions, ideal for the study of biofilms and multicellularity in a broader context.

Microfluidic channels were designed for feeding the suspended droplets through fluid flows inside PDMS. Droplets were connected to the microfluidic channels with nozzles through the under layer of the PDMS device. An array of nozzles was connected with channels in the microfluidic device. No additional valve or pneumatic controls was needed as each droplet nozzle could be manipulated individually. Choice of media, addition of antibiotics, and cell inoculation could all be easily implemented. Efficient harvesting and sampling could be realized because the design followed the format of conventional 96-well microtiter plates.

Biofilm development

The following analysis on A-L interface biofilm formation has largely been based on our customary understanding and terminology associated with S-L biofilms. Caution has to be taken because S-L and A-L interface biofilms are phenotypically diverse and would likely entail a different set of genetic circuits. Biofilm development by *B. subtilis* in the hanging droplet biofilm reactor was monitored by phase contrast microscopy as shown in Fig. 3.2. *B. subtilis* prefers aerobic growth and forms biofilms at the phase boundary between the air and medium. Phase contrast microscopy is a non-invasive imaging technique to allow real-time visualization of biofilms at the focal plane. A-L interface biofilm formation commences with preferential adherence of planktonic bacterial cells to the phase boundary during the initial stage (0 to 2 h) in Fig. 3.2 (a). Microbes began to aggregate in a monolayer along the phase boundary. Analogous to the S-L interface biofilm counterpart,

organic and inorganic molecules were concentrated along the interface to assist in the formation of a thin film of cells.

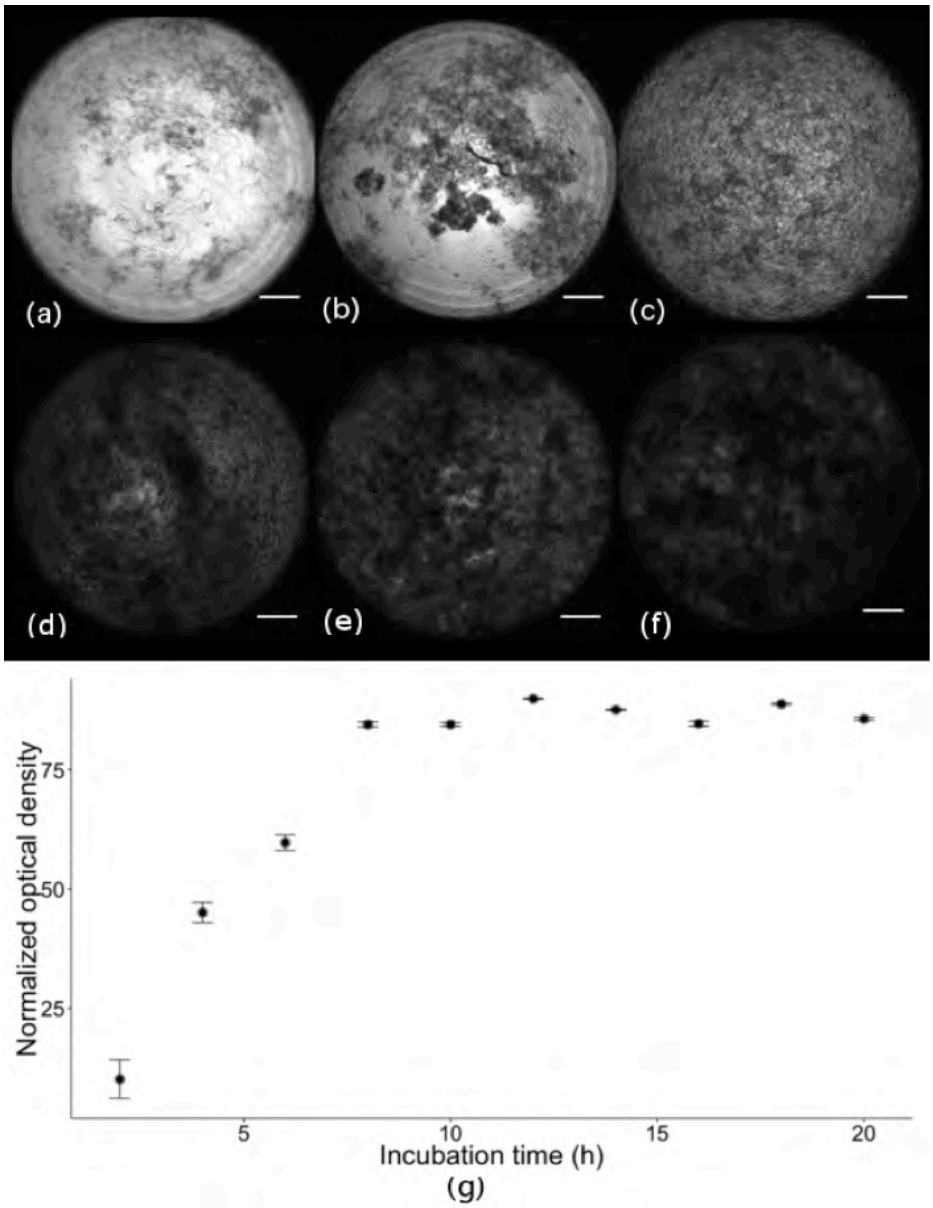

Figure 3.2 Time-lapse phase contrast micrographs showing the *B. subtilis* cell aggregation and biofilm formation process (scale bar, 200 μm). Images were taken on the hanging droplet with an interval of 2 h from 2 to 12 h as shown in (a) to (f). (a) A-L interface biofilm formation commences with preferential adherence of planktonic bacterial cells to the phase boundary during the initial stage (0 to 2 h). Microbes began to aggregate in a monolayer along the phase boundary. (b) Further adhesion and colonization of planktonic cells was observed in the elapsed 2 h. (c) The entire focal plane was colonized by biofilms. (d) A thin layer of condensation of cells with vein-like appearance was observed. (e) Coadhesion and coaggregation were observed. (f) Further biofilm growth and expansion took place. (g) Normalized optical density vs. incubation time. Biofilm continued to grow to full maturity until 12 h of incubation when the optical density measurement leveled off. The error bars represent standard deviation (n = 3).

Denser colonies with a higher extent of coverage could be observed in Fig. 3.2 (b) indicating cells were actively growing in the elapsed 2 hours. Further adhesion and colonization of planktonic cells were observed. The entire surface focal plane was colonized by biofilms in Fig. 3.2 (c). Electrostatic attraction, hydrogen and covalent bonding, hydrophobic interaction and dipole-dipole interactions all may contribute to the adherence of microbes to the A-L interface. At this stage, the cells at the interface elicited themselves as a thin layer of fragile and structure-less pellicles. Not much macroscopic architecture could be observed. Bonding and association of cells was still weak.

Over the course of biofilm formation, the network of cell aggregates became denser, darker and had more coverage. A thin layer of condensation of cells with vein-like appearance was observed in Fig 3.2 (d). The initial monolayer of cells attracted secondary colonizers to form lateral and vertical microcolonies. Coadhesion and coaggregation were observed. Further biofilm growth and expansion took place in Fig. 3.2 (e). Biofilm further grew and expanded in the following 2 hours (Fig. 3.2 (f)). By 24 h, biofilms were observed to be approximately 50 μm farther from the air-liquid interface as revealed by CLSM. Substratum colonization during different stages of biofilm development was calculated and plotted against incubation time in Fig 3.2 (g). The percent coverage increased steadily with time and reached the plateau by 12 h. At this stage, growth and dispersal of biofilms were balanced. At a cellular level, phase contrast microscopy revealed that both *P. aeruginosa* and *B. subtilis* exhibited a high degree of spatial organization during the development of A-L interface biofilms with well-aligned cells bound together, in a way similar to their S-L interface counterparts [3, 19]. The entire biofilm development was expedited by

the hanging droplet biofilm reactor presumably because of a facilitated exchange of oxygen and nutrients across the air-medium phase boundary. While the submerged biofilm usually take 3-5 days to form, this hanging droplet biofilm reactor is able to yield mature A-L interface biofilms in 12 h.

After approximately 29 hours incubation in microfluidic HDBR, *B. subtilis* could be observed to detach from the biofilm matrix (Supplementary video available at: http://youtu.be/JFXia0_DC0c). Fragments of biofilms shed off and recirculated inside the droplet. Biofilm dispersal is a process in which sessile biofilm cells undergo phenotypic modifications to convert to planktonic cells, often triggered by chemicals and mechanical cues from the local environment [29]. Active biofilm dispersal is influenced by nutrient availability attributed to local hydrolysis of the extracellular polysaccharide matrix. Hydrodynamic forces cause passive biofilm dispersal. There was not enough evidence to support whether this detachment process fell under active dispersal or passive dispersal. This dispersal could be due to local EPS hydrolysis or simply as a result of a physical detachment process. The dislodged fragments were carried by the intra-droplet circulation until they returned to the bulk biofilm matrix as the entire process was confined in a small droplet.

P. aeruginosa is conventionally used as a model strain in studying the dispersal phenomenon in submerged biofilms [28]. The dispersal behavior of *P. aeruginosa* A-L interface biofilm in this experiment coincided with that of their S-L interface biofilm counterpart. The underlying driving force for dispersal rests on nutrient availability, metabolic state and quorum sensing of the biofilm cells, which is beyond the scope of this study. Motile cells from the substrate-associated biofilms

differentiate into chains of cells aligned in a parallel fashion that cooperatively form aerial protrusions for the dispersal of cells. In this experiment, no such aerial structures were observed probably because the formation of the structure entail a hard substrate for anchorage, support, and spatial organization. Here, we first report on the *in vitro* detachment and dispersal behavior of *B. subtilis* A-L interface biofilm. *B. subtilis* vegetative cells at the air-liquid interface showed a lower degree of motility. The cells were bound together as early as 6 h after incubation. In future studies, surfactant might be added to the droplet to lower the surface tension as a potential strategy to encourage formation of *B. subtilis* A-L biofilms.

Role of surface tension and evaporation flow

A surface tension gradient is generated along the surface of an evaporating droplet by a temperature gradient or a composition variation induced by nonuniform evaporation of the droplet. As a consequence, changes in two parameters were observed. First, shape of the droplet is changed because surface profile of a droplet is determined by the surface tension and gravity [146]. For a small droplet, gravity can be ignored [145-147] resulting in a spherical-cap shaped droplet. So, droplet radius is only determined by the surface tension gradient. The other changed parameter is that a convective flow is generated by the surface tension gradient, known as Marangoni flow [158]. Marangoni flow affects the hydrodynamics in the droplet that, in turn, contributes to the composition variation and temperature gradient resulting in a change of the surface tension gradient [157]. In this experiment, formation of biofilms on the A-L interface contributes to the surface tension gradient. The profile of the hanging droplet and the flows inside the HDBR were changed by the biofilm colonization induced surface tension gradient.

In the biofilm-growing evaporating droplet in this experiment, the momentum, heat and mass transfer were modeled as quasi-steady processes. Our droplet analysis was based on image processing, particle velocimetry, and finite element analysis. The density of biomass near the air-liquid boundary interface affected the osmotic pressure, which subsequently affected the surface tension of the hanging droplet.

In Fig. 3.3, the droplet was visualized from the side with a portable microscope. An LED array was set up in a way to illuminate the plane parallel to the central axis of the droplet. Caution has to be taken because the bright glaring region shown in the supplementary movie (Supplementary video available at: http://youtu.be/JFXia0_DC0c) was an artifact of lens refraction.

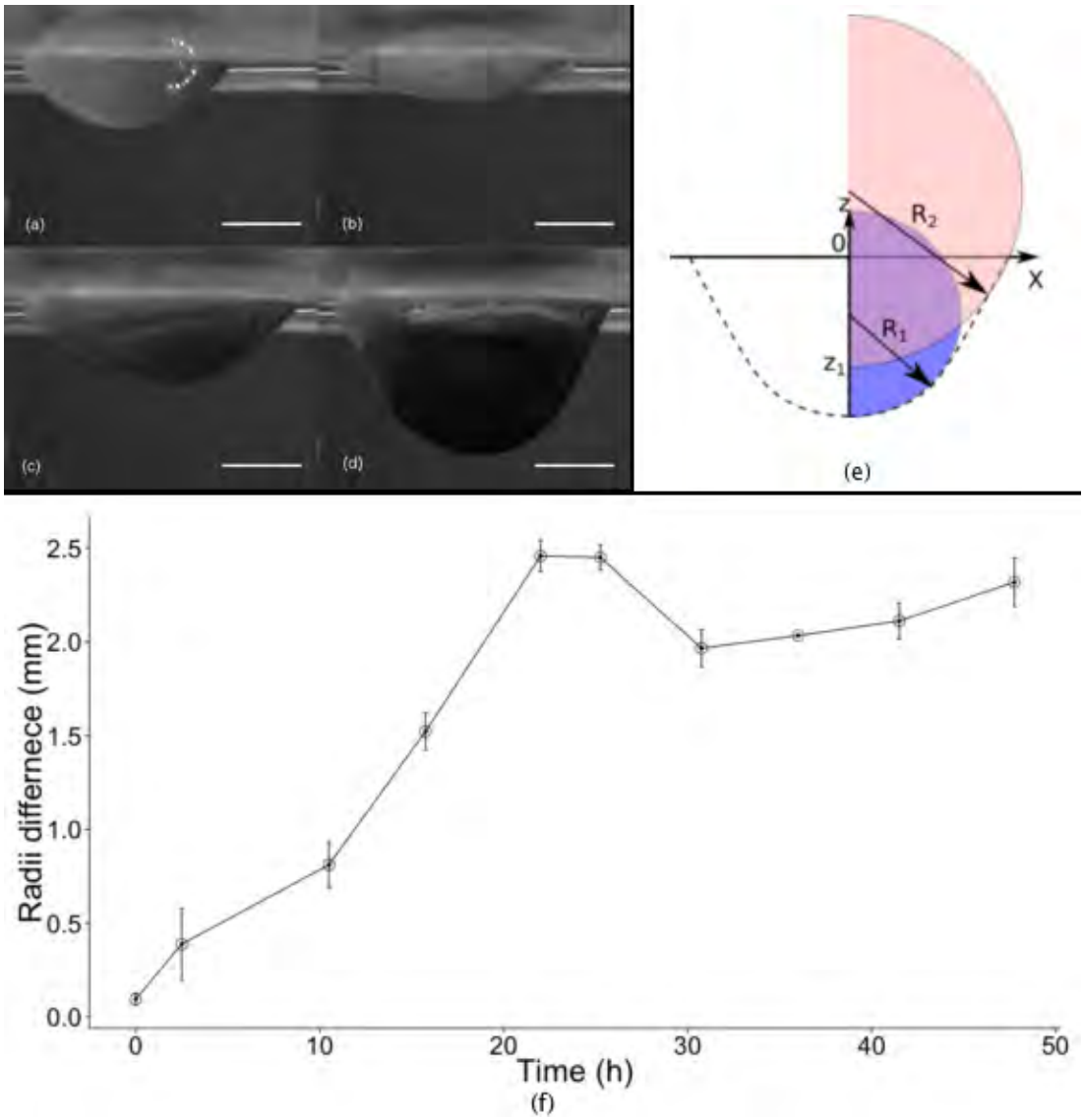

Figure 3.3 Changes of droplet profile over time. (a-d) A hanging droplet was suspended from the HDBR device. (a) Original droplet at time 0. (b) Droplet profile at 2.5 h. (c) Droplet profile at 20 h. (d) Droplet profile at 48 h. Scale bar, 1.5 mm. (e) The droplet profile was drawn in dashed line. The upper horizontal line at z = 0 is the contact line of hanging droplet with the microfluidic device. Lower profile was fitted with a circle with a radius of R_1. Upper part near the contact line was fitted using a circle with the radius of R_2. A virtual apex was at the intersection point of the upper circle and *z* axis. (f) Radius difference of the droplet apex and virtual apex (R_2 - R_1) was plotted as a function of incubation time. Error bars represent standard deviation (n = 3).

Fig. 3.3 and the supplementary movie described the shape profile of the droplet over the course of biofilm formation in a hanging droplet. The size, volume of the droplet varied as a function of incubation time. The evaporation and replenishment rates were made equal to each other. Therefore the droplet size and volume changes were due to the formation of A-L interface biofilms. Formation of the A-L biofilm was

found to be along the phase boundary. From phase contrast micrographs, biofilms were observed to colonize at the interface with a film of cells.

In Fig. 3.3 (e), two circles were used to model the droplet interface covered and uncovered by biofilms. Because the small size, the droplets have spherical-cap shapes. The droplet was modeled as two partially overlapped hanging spherical-cap shaped liquid: the liquid near the apex of the droplet was covered by biofilm and the liquid near the PDMS device was uncovered by biofilms. The circle radius indicated the curvatures of the surfaces covered and uncovered by biofilms. Radius difference variation of two circles over time is plotted in Fig. 3.3 (f). At the beginning, the radius difference was 0, indicating that the profile of the droplet was spherical. This difference increased till a peak was reached at about 22 hours. Afterwards, this difference leveled off. The results indicated the surface tension changed by biofilms.

The surface tension gradient generated by the coverage of biofilm changed the profile and the Marangoni flow of the hanging droplet. A numerical simulation was conducted in Comsol Multiphysics to verify the validity of the hypothesis that the presence of surface tension gradient caused changes in the droplet shape and Marangoni flow. The droplet governed by a uniform surface tension showed a spherical shape (result not shown), which is in accordance with findings reported by Hu [157]. When a surface tension difference was applied, the profile of the droplet was shown in Fig. 3.4. The droplet profile was similar to experimental observation in Fig. 3.3. The surface tension of the lower droplet was set as 0.85-fold of the surface tension of the upper part. This simulation result supported the hypothesis that presence of surface tension gradient caused changes in the droplet shape. Coverage

of the biofilms decreased the surface tension of the droplet. This observation may be used to monitor biofilms by observing the profile of the hanging droplets.

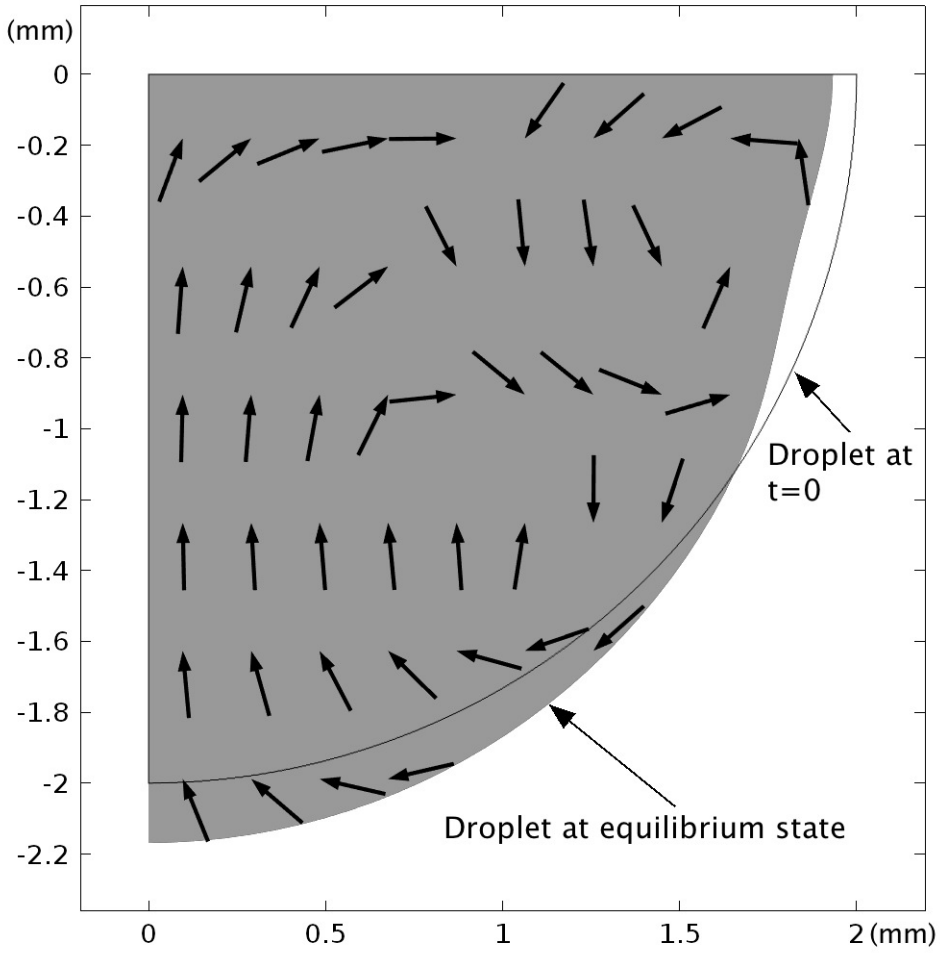

Figure 3.4 Simulation result of droplet deformation and Marangoni flow generation by a surface tension gradient. Axis of the hanging droplet was $x = 0$. The top of the droplet was connected with a PDMS solid surface placed at $z = 0$. A static semispherical droplet with the center at (0,0) and a radius of 2 *mm* was assumed at the beginning of the simulation. Arrows indicated the flow directions inside the hanging droplets at an equilibrium state.

Numerical study of an evaporating pure liquid droplet demonstrated a circulation flow in a symmetric droplet [157], which was also observed in this simulation with a uniform surface tension (results not shown). In this chapter, the flow was affected by the formation of biofilms. Velocity field indicated by the arrows in the simulation result showed two types of circulations, including a clockwise circulation near the

three phase contact line and a counterclockwise circulation close to the apex of the droplet (Fig. 3.4). Marangoni stress due to the surface tension gradient induced the flows in this simulation.

The Marangoni flows in sessile droplets in a hanging droplet biofilm reactor were analyzed by monitoring time-lapse images of biofilm as in Fig. 3.5. The combined effect of latent heat of evaporation and Marangoni stresses were modeled by an axisymmetric steady-study Navier-Stokes equations [174]. A nonuniform evaporation-flux distribution could be obtained, which shed light on the latent heat flux and velocity fields. In Fig. 3.5 (a), velocity fields were measured by particle image velocimetry analysis. Similar biofilm structures were reported in the 30-minute interval time frames and were used as markers for PIV analysis Flow vectors were of both vertical direction and radial directions.. PIV result indicated rotating biofilms inside the droplet. Flows were also observed by tracing the moving biofilms (Supplementary video available at: http://youtu.be/JFXia0_DC0c). At the early stage within 12 hours, small pieces of biofilm on the bottom were observed to rotate. Movement of the detached biofilms indicated the radial flow in the droplet (Fig. 3.5 (b)).

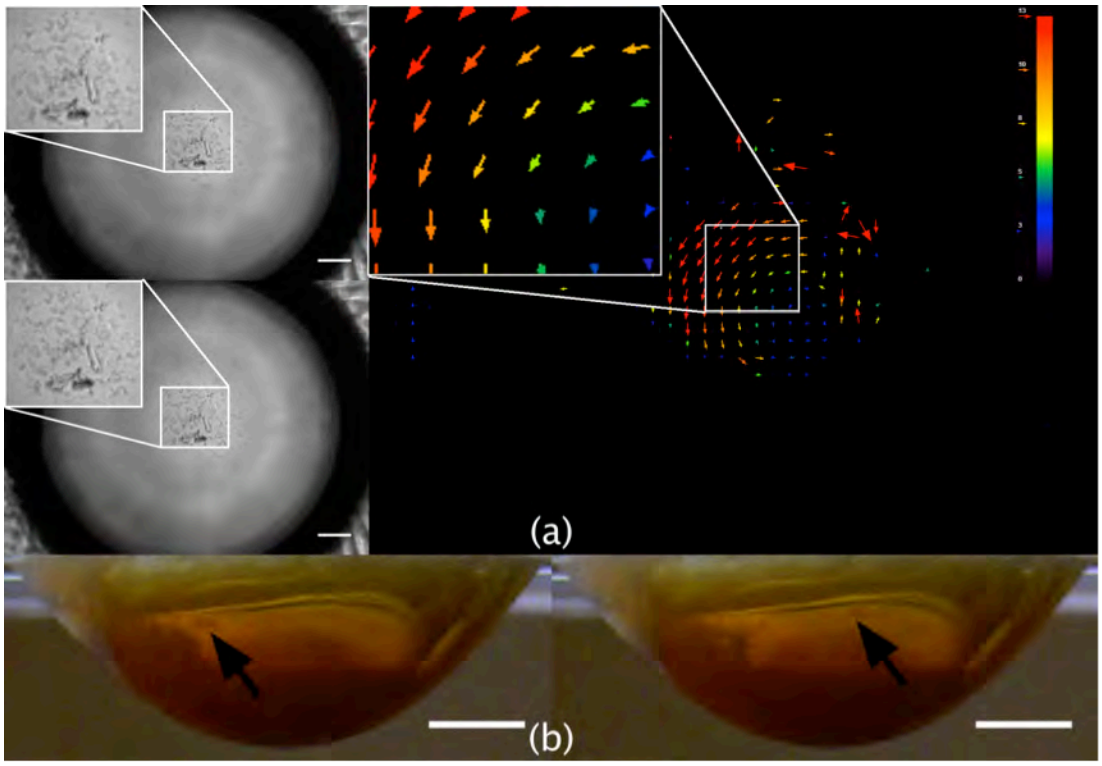

Figure 3.5 Flows inside a hanging droplet biofilm reactor. (a) Flow inside a hanging droplet biofilm reactor plate. Evaporation caused nonuniform temperature gradient along the air-liquid interface, which consequently led to a varying gradient of surface tension. This resultant Marangoni flow was manifested by a particle image velocimetry technique. In the color lookup table, red was assigned the highest magnitude and blue the lowest magnitude. Scale bar was 200 μm. (b) Flow inside the hanging droplet of a microfluidic version of hanging droplet biofilm reactor. The arrows pointed at a piece of detached biofilm flew inside the reactor. The detached biomass in this case has been received to move from left to right by the hydrodynamic forces and presumably Marangoni forces. Time interval between these two images was 1 min. Biofilms inside the droplets was formed by *B. subtilis*. Scale bar was 1 mm.

The evaporation flow in the microfluidic version of HDBR is faster than that in the HDBR plate as indicated by the PIV result and image processing. No radial flow has been observed in an evaporating water droplet [157]. In our simulation, the flows did not have radial component because the surface tension was assumed to be symmetrical. However, radial flows were observed in the results, which may be due to biofilm formation. It was well established that colonization of biofilms are inhomogeneous [175, 176], which is consistent with our observations (Supplementary video available at: http://youtu.be/JFXia0_DC0c). Biofilms aggregated on droplet surface is a surfactant, which changed the surface tension

gradient along the droplet surface. The partial coverage of the droplet surface by biofilms surfactant caused an abrupt surface tension change across the edge of the biofilm. Therefore, a Marangoni stress generated by this surface tension gradient at the edge of inhomogeneous biofilm is expected. Torque at the edge of the biofilm induced by Marangoni stress along the edge of the biofilm resulted in a radial movement of the biofilm. Experimental results are in good agreement with this theory.

Harvested biofilm

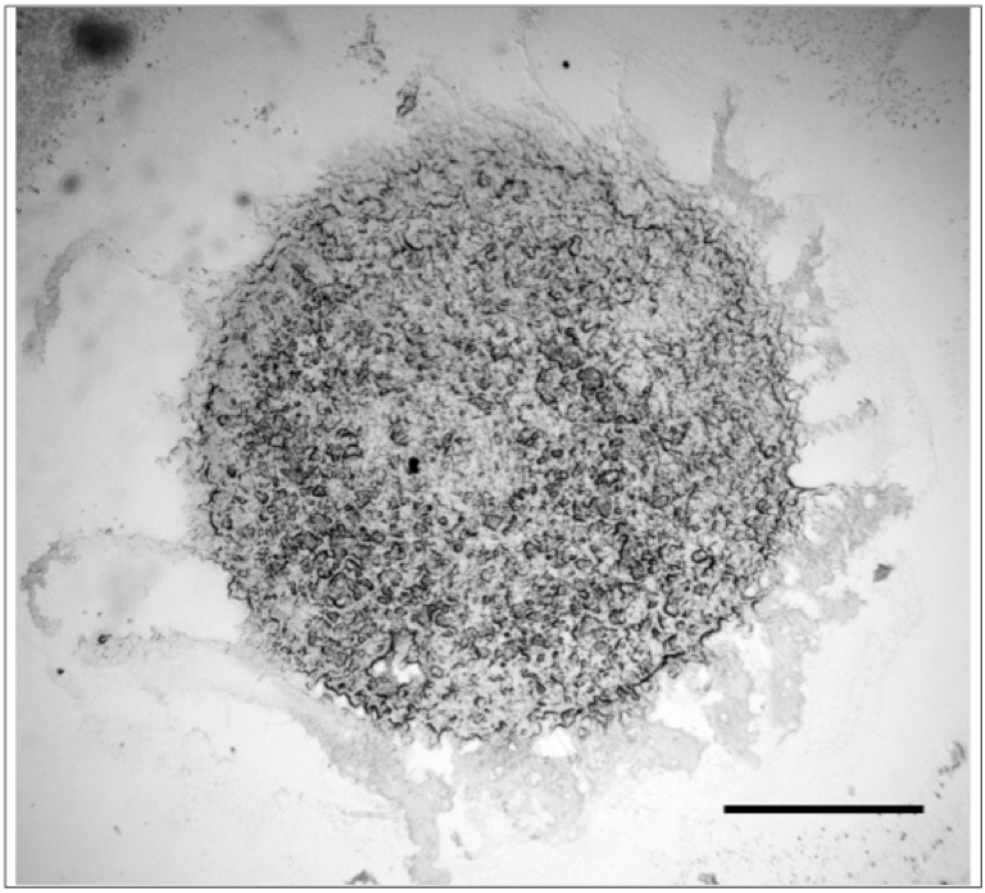

Figure 3.6 Deposition pattern from the drying of a 12-h *B. subtilis* biofilm-containing droplet obtained using light microscopy. The spherical-cap pattern was of a diameter of 2.8 mm taken 2 hours after deposition. Deposited patterns observed included circular mounds of biofilm mass, which was originally found at the air-liquid interface of the droplet. Scale bar was 1 mm.

The droplet phase boundary between air and liquid was employed as the surface for microbial initial attachment and facilitation of the growth and formation of A-L interface biofilms. The thus formed biofilms were then harvested by dripping and air-drying the droplet on a non-porous glass substrate horizontally placed for quantitative and qualitative assessment. Fig. 3.6 depicts the deposition pattern from the drying of a biofilm-containing droplet. The spherical-cap pattern was of a diameter of 2.8 ±.8 d *mm* taken 2 hours after deposition. Upon evaporation, biomass in the form of biofilm inside the droplet deposits on the non-porous surface. Solvent loss by evaporation along the edge of the droplet was replaced by solvent drawn from the center of the droplet. This evaporation flow resulted in the biofilms at the edge of the spherical-cap shaped biofilm deposited around the periphery.

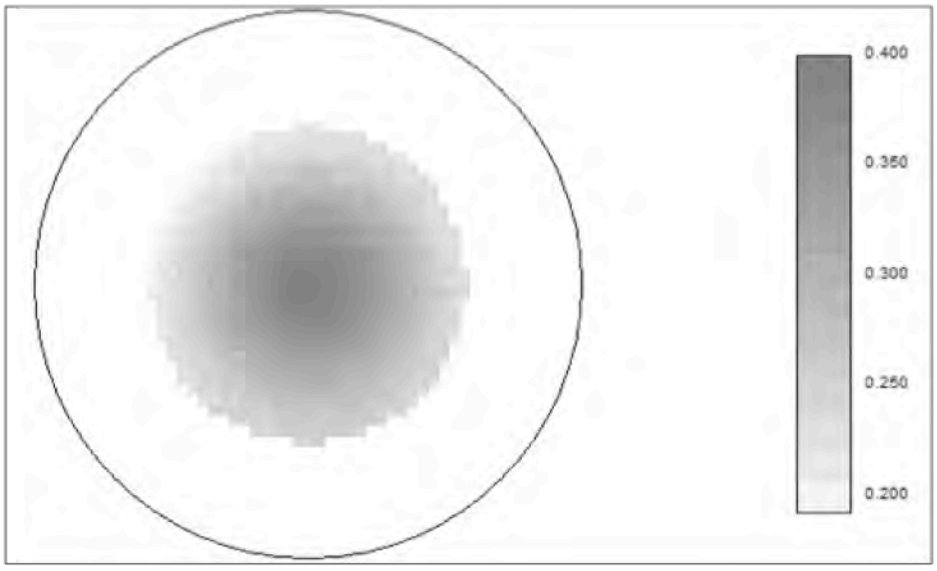

Figure 3.7 Optical density scan of a deposited *B. subtilis* biofilm. Quantitative profile of the biomass was analyzed by measuring the distribution of optical density at 600 nm. The grayscale level indicated the light density, with a higher intensity in the middle and lower intensity around the periphery. The gradient of the OD_{600} from middle to the edge showed a gradual change of thickness of the deposited biofilm.

Fig. 3.7 shows an optical density scan of a deposited biofilm. The intensity at the center of the image is higher than at the periphery, which means the optical density of biofilm in the center is higher than the periphery. The gradient of the OD_{600} from center to the edge shows the thickness gradient of the deposited biofilm. Transmittance decreased from 0.4 at the center to 0.2 at the edge indicating that the thickness of the biofilm decreased from the center to the periphery. The thickness profile was also observed by CLSM, where the thickness in the center was approximately 50 μm and 10 μm at the periphery. This evaporative deposition technique exhibits great potential in lots of applications, including deposition of biomass on microarrays, proteomics, genomics, and formation of self-assembly coatings for sensor and biotemplate development.

Biofilm viability

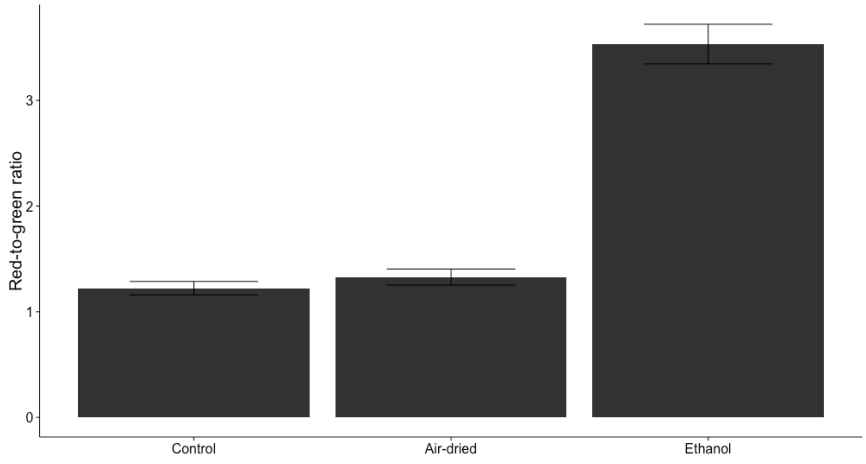

Figure 3.8 *B. subtilis* A-L interface biofilms possess an elevated degree of resistance to desiccation and ethanol disinfection. Bar graph of the red-to-green ratios of the biofilms before and after air-drying and ethanol disinfection treatment is shown. Using the BacLight viability stain, green bodies indicated the live cells and red bodies indicated the dead cells. Confocal laser scanning microscopy image of control biofilm without drying or disinfection were processed with COMSTAT. Without any inactivation treatment, the red-to-green ratio was about 1.2 ± 0.1. After air-drying for 2 hours, the red-to-green ratio increased to 1.3 ± 0.2. Small amount of cells were dead after air-dried. Biofilms were disinfected by immersing in 75% ethanol for 20 min. Red-to-green ratio increased to about 3.5 ± 0.4. For all samples three replicates were averaged and the standard deviation is shown. Error bars represent standard deviation (n = 3).

The effect of 70% ethanol on A-L interface biofilms was expressed using fluorescent dyes. More than 20% of the biofilm cells remained viable as revealed by fluorescence staining. There was no observable change in biofilm cell viability associated with the air drying procedure. Live cells were stained green and dead cells were stained red. The red-to-green ratio was 1.2 ± 0.1, 1.3 ± 0.2 and 3.5 ± 0.4 in the control, air-dried, and ethanol-treated biofilms, shown respectively in Fig. 3.8.

The elevated resistance of biofilms against disinfecting agents is still not well understood. Some explanations put forward in the literature include sacrificial protection provided by the biofilm matrix and the slower growth rate in biofilm cells [13]. It has been noted that cells associated with biofilms tend to grow at a much slower rate than their planktonic counterparts. The chemical disinfectant intake by cells is therefore slower. Evan *et al*. reported an inverse correlation between the grow rate of biofilm-associated cells and degree of resistance, as exemplified in a slow-growing strain of *E. coli* [177]. When planktonic cells and biofilm-associated cells exhibited similar growth rates, they were found to be equally susceptible to disinfectants. Submerged biofilms conventionally grow on metal coupons usually yielded an increase in resistance by two to three folds. In this experiment, A-L interface biofilms, with a much faster growth rate than S-L interface biofilms, only improved the resistance level by approximately 1-fold as revealed in the culture and viability stain observation.

Ultrastructure of biofilms

The ultrastructure of *B. subtilis* and *P. aeruginosa* A-L interface biofilm observed through scanning electron microscopy demonstrated bacteria in biofilms were held

together by nanotubes intertwined through thin films of a matrix materials (Fig. 3.9). The nanotubes structures reminiscent the fibrillar structures found in A-L interface biofilms, which was suggested as a morphological strategy to facilitate attachment [178]. Without a rigid substrate as in our suspended droplet case, these fibrils are thought to serve as scaffolding materials for the formation of floating biofilms at the air-liquid interface. The fibrillar structures, sometimes known as amyloid fibers and fimbriae depending on the context and proteins involved, have been well reported in copious amounts in *B. subtilis* and *P. aeruginosa* surface-associated biofilms [178].

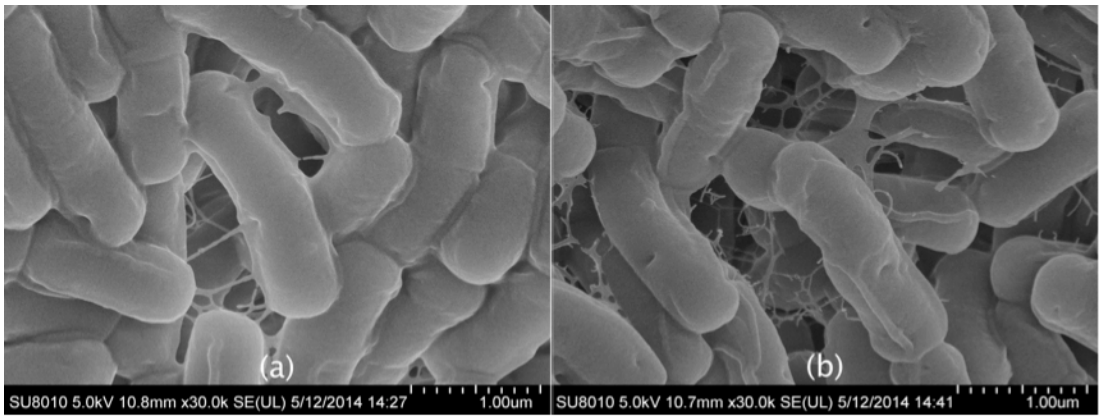

Figure 3.9 Scanning electron micrographs of A-L interface biofilms. Scanning electron micrographs of A-L interface biofilms of (a) *B. subtilis* after 22 hours of incubation, and (b) *P. aeruginosa* after 16 hours of incubation, all deposited on filter papers. Rod-shaped cells were observed in both images. No endospores were found in the *B. subtilis* case. Cells appeared to be held together by nanotubes intertwined through thin films of a fibrous casing.

Biofilm formation takes places in multiple stages with distinctive gene expression pattern different from planktonic cells [65]. An intricate network of intercellular signaling is involved. Establishment of biofilm community entails communication between constituent cells. Bacteria are kenned to communicate through the release of extracellular factors. Nanotubes conjugating between *B. subtilis* cells have been proposed as a new type of bacterial communication for the exchange of cellular molecules in 2011 [179]. Tubular protrusions were observed in *B. subtilis* culture

emanating from cell surface in a non-specific and non-uniform manner, bridging neighboring cells to form a mesh of network. Branching nanotubular structures were sometimes observed to link multiple cells together. The observation of these nanotubes by Dubey *et al.* [179] was only limited to cells grown on solid substrates, but not suspended in liquid medium. In this work, we noticed similar nanotubular structure in the case of *B. subtilis* biofilms growing along the air-liquid interface in Fig. 3.9. Further experiments would be carried out to investigate and characterize these intercellular nanotubes on both molecular and cellular levels. As far as we are aware, this is the first report on the formation of intercellular nanotubular structure on *B. subtilis* on air-liquid interface.

Role of EPS

Biofilm EPS is defined as the extracellular matrix between the environment and indwelling cells. The functions of EPS are multifaceted and are sometimes not well understood. Apart from structural support, EPS also serves as a functional interface for protection, nutrient transport and relay of external and physicochemical information [13]. Depending on the physical environment, biofilm EPS is likely to perform vastly different functions. For instance, S-L submerged biofilms are subjected to constant hydration and dehydration in arid terrestrial environments. The EPS should be equipped with the necessary structure to confer desiccation tolerance for the indwelling cells [16-18]. EPS has been reported to play major roles in the initial adherence and anchorage to solid substrate [14, 15]. This type of EPS from S-L interface biofilms has been widely studied and imaged. The air-liquid interface in this experiment, on the other hand, presents an utterly different scenario and set of challenges for the formation of pellicle biofilms. The air-exposed side will

experience a harsh dehydrating niche whilst the liquid submerged side will experience a nutrient-rich condition. Through this study, we aim to highlight a new structure-function relationship in A-L interface biofilms, as opposed to conventionally studied S-L interface biofilms, from a physiological and cellular perspective. The molecular and genetic underpinning will have to be scrutinized by other research endeavors. Caution has to be taken because the EPS was susceptible to the invasive dehydration process during SEM sample preparation, thereby compromising biofilm topography. Variable pressure scanning electron microscopy (VPSEM) will be a good option to preserve EPS integrity in future experiments.

We have applied an array of methods to observe the 3D structure, morphology, topography, attachment, cellular components, and resistance of the A-L interface biofilms cultured inside a hanging droplet under an open microfluidics platform.

Conclusion

Biofilms formed by *B. subtilis* and *P. aeruginosa* in laboratory hanging droplet bioreactors represent examples of surface-associated microbial communities, which display dynamic developmental patterns. The complex microenvironment formed by biofilms is hard to mimic by conventional technologies used for culturing biofilms because the conventional methods are of low throughput, labor-intensive, material consuming, and lack of reproducibility and precise control. Microfluidic tools used in this work are able to mimic the complexity of biofilm microenvironment by the better control of the environmental parameters in a high throughput way in microfluidics. Here we introduce a novel open microfluidic hanging drop biofilm reactor forming biofilm at the air-liquid interface under evaporating flow to

investigate the complex biology of biofilm in response to changes in local microenvironments. This work may help to understand the biology and cement the clinical and industrial potentials of biofilms.

Chapter 4 Segmented-flow microfluidic air-liquid-solid interface biofilm reactor

Abstract

Drip-flow biofilm reactors (DFBR) have been used to culture and study air-liquid-solid (A-L-S) interface biofilms, which are commonly seen as air-liquid (A-L) interface biofilms. Drip-flow reactors are however cumbersome to operate and not readily amenable for real-time monitoring. We designed and fabricated a segmented-flow microfluidic A-L-S interface biofilm reactor (SFMBR) to grow A-L-S interface biofilms on chip. A distinct A-L-S interface was made available by introducing a gas phase into successive nutrient flows with a T-junction design, forming a segmented gas-liquid flow (SGLF). Velocity fields along the interfacial flows were computed by numerical simulation, involving not only the hydrodynamic fields in the gaseous and aqueous phases, but also of the air-liquid and solid-liquid interfaces. Formation of A-L-S interface biofilms along microfluidic channels was observed and characterized by microscopy techniques non-destructively. The effect of hydrodynamics on A-L-S biofilm formation was simulated and tested. Liquid films trapping by monolayer bacterial colonies was fist reported in literature in this chapter. Interactions of biofilms with A-L interfaces of moving bubbles were studied with particle image velocimetry (PIV) methods and numerical simulation. This device is a low-cost on-chip biofilm reactor to culture A-L-S interface biofilms and to measure *in situ* biological and mechanical properties of the growing biofilm.

Introduction

Biofilms are highly complex sessile matrix-enclosed communities where the indwelling cells adhere to surfaces or phase boundaries with the aid of a network of

extracellular substances. Biofilms enjoy enhanced resistance against physical and chemical environmental assaults, higher resilience to host immune responses and nutritional limits [1]. Biofilms are implicated in food hygiene and medical sterility because of their ability to resist normal cleaning and disinfection processes, thus causing spoilage and diseases [36, 37, 44]. Formation of biofilm is a complex process involving genetic mechanisms and contributory factors from the substrate properties, cell type, interaction of cells, availability of nutrients, microenvironments, and many others [167, 180]. Over 90% of microorganisms have been estimated to exist in biofilms rather than in the planktonic state. Over the years, many chemical, physical and biological techniques have been used to characterize and understand this sessile form of cell communities adhered on surfaces and phase boundaries. Little do researcher understand the mechanism of biofilm formation because of the difficulty to form biofilms with reproducible and consistent properties in the laboratory. Most of the previous biofilm work has focused on biofilms formed at the solid-liquid (S–L) interfaces. In earlier chapters of this thesis, we have been looking into the formation, characteristics and bioreactor designs for biofilms formed at the air-liquid (A-L) interface. Another type of biofilm that has often been overlooked is the air-liquid-solid (A-L-S) interface one, which is of great ecological interest. The ability to colonize both the surface of liquids and solids has obvious advantages for biofilm formation. For instance, soil-borne microorganisms constantly undergo hydration-dehydration cycles to thrive under such a dynamic and ever-changing microcosm. It is important to study biofilms, rather than their planktonic counterparts, in the most natural and pathogenic ecosystems.

A-L-S interface biofilms are defined as A-L interface biofilms adhering to solid surface. A-L interface biofilms cultured in microtiter plates [100], tubes and beakers [90] were conventionally characterized by conducting crystal violet (CV) staining and CLSM on the cell aggregates adhered on the walls of containers [87]. These A-L-S interface biofilms grown at the three-phase (gas-liquid-solid) contact line were characterized by the CV staining method to represent the total biomass of A-L interface biofilms. However, the efficiency of these methods was low because of the small three-phase area compared to the A-L interface area of the container. Drip flow biofilm reactors are also widely used to culture A-L-S interface biofilms. Biofilms on coupons were cultivated by dripping and flowing media along coupons slanted at an inclination angle of 10° [86]. Biofilms have also been cultured on the bottom of microtiter plates by pumping dripped media across wells of 6-well microtiter plates [100]. The use of drip flow, rotating disk and slanted bioreactors are costly to build and do not readily render high-throughput operation, as well as precise and automated control. Microfluidics is a promising tool to solve the aforementioned problems due to its advantages of low material cost, precise gradient generation, *etc.* Microfluidics has been extensively utilized in a wide array of biofilm researches recently [168]. However, they are mostly flow cell biofilm reactors, which cultures only S-L interface biofilms in the microchannels [131, 142, 144] or chambers [132, 141, 143] with continuous flow of nutrients or bacterial suspensions. The existing microfluidic flow cell biofilm reactors are not amenable for culturing A-L-S interface biofilms.

Segmented air-liquid flow (SALF) is a type of multiphase flow realized on microfluidic platforms for facilitated mixing. Multiphase flow is conventionally

generated with immiscible liquid based on geometry such as T-junction, flow-focusing microchannels or based on electrohydrodynamic phenomena such as dielectrophoresis and electrowetting [122]. Air-liquid slug reactors take advantage of the “Taylor flow” to enhance fluid mixing and mass transfer along interfacial flows, specifically from the bubbles to the liquid and from the bubbles to the microchannels, and vice versa. Another important application of segmented flows is particle synthesis [181]. Trains of gas bubbles are commonly used as spacers between liquid plugs. Therefore, repeated microreactors spaced with air are generated in microfluidic channels. Owing to the ease of fabrication and operation [182], geometry-based multiphase flow generating devices are widely used to generate discrete air bubbles in SALF. When a train of air bubbles fills up channels, the continuous fluid plugs are divided into “segments”, constituting the basis of segmented-flow microfluidics [183, 184]. Fractions of the liquid and air (media droplet and bubble) in segmented flow depend on the flow rates of air and liquid [184, 185]. Many factors such as roughness, partial wetting and bending of the channels affect the segmented flow by increasing the mixing of solutions in the plugs (droplets) [184]. It was also reported that biomass transfer between the inner walls and outer walls is increased in the plugs in a curved channel [186]. Flow velocities inside the droplets of SALF are related to the radius ratio of the inner wall and outer wall of the meandering channels [187]. An interesting phenomenon in SALF is that there is a thin liquid film formed between the bubbles and the wall of the microchannels [186, 188]. Though SALF can be precisely controlled for biochemical reactions, applications of SALF have primarily been limited to chemical reactions [184, 189] and material synthesis [181]. There is no report on utilizing SALF mechanism to culture biofilms at the A-L-S interface.

Biofilm formation on solid substrata is affected by many factors, including bacterial strains, culture media, surface properties, *etc*. Biofilm formation inside microchannels is further affected by flow hydrodynamics, channel geometry and interfacial interactions [32]. In microfluidics, Reynolds number, ratio of inertial force to viscous force, is defined as $Re = \frac{\rho v d}{\mu}$ (where μ is the liquid viscosity, v is average velocity, ρ is liquid density and d is characteristic dimension of channel). It has been reported that a low Reynolds number and high flow rate of media encouraged biofilm growth; whilst a high Reynolds number with high nutrient flow rates suppressed biofilm growth in microchannels [138]. The exact role of Reynolds number on biofilm formation in microfluidic devices remains elusive. Reynolds number is positively correlated with shear force, which enhances microbial adhesion and anchorage to solid substrata by promoting the growth of fimbriae [190-192]. However, biofilm removal has been observed in the presence of fast-moving A-L interfaces due to high shear forces [193-195]. On another account, biofilm formation increases the resistance associated with microfluidic channels, which results in changes of nutrient flow rates [138].

A segmented-flow microfluidic A-L-S interface biofilm reactor (SFMBR) was designed and fabricated here to culture A-L-S interface biofilms on a microfluidic chip with SALF. Finite element numerical analysis and flow visualization experiments were carried out to characterize the generated SALF and biofilm formation. The air or liquid thread continued to grow until pinch-off when the force equilibrium and the threads reached a critical volume [196]. In SFMBR, A-L-S interface biofilms were cultured in a train of segmented flows of nutrient plugs and

air bubbles along a curved microchannel. The chip was designed to stabilize multiphase flows by geometrical features. Geometry of microchannels determined the hydrodynamics of the fluid resulting in special structures of biofilm inside the channels [139]. In this case, a change in the corners of turning microchannels was observed to trigger biofilm formation and accumulation. Low velocity SALF was generated using a T-junction geometry to culture A-L-S interface biofilms. The SFMBR enables high throughput automated cultivation using less volumes of reagents and cell culture, provides shear force of a larger dynamic range, and *in situ* real-time microscopic monitoring of A-L-S interface biofilms on chip.

Materials and methods

Chemicals

All chemicals were purchased from Sigma-Aldrich (St. Louis, MO, USA), and all biological supplies were purchased from Difco Laboratories (Detroit, MI, USA) unless otherwise stated.

Cell culture

Pseudomonas aeruginosa ATCC 15692 was obtained from American Type Culture Collection. *P. aeruginosa* culture was hydrated in nutrient broth and inoculated onto separate nutrient agar plates and incubated at 37 °C for 24 h. After incubation, stocks of the strains were stored at -80 °C in Luria–Bertani broth supplemented with 30% glycerol. Working cultures of *P. aeruginosa* were routinely grown in TSB at 37 °C under aerobic conditions with shaking for 24 h. Bacterial suspension was prepared by diluting the cells in freshly prepared TSB to a concentration of 5×10^7 *cells/mL*.

Device design

Microchannels were designed with dimensions of 100 μm (width) by 60 μm (height). A T-junction design based on cross-flowing rupture technique was composed of a horizontal channel with nutrient/cells inputs intercepted by a vertical air channel. A meander-shape channel was included to enhance mixing and encourage biofilm formation due to channel curvatures.

Device fabrication

The device was fabricated by soft-lithography techniques using replica molding [75, 140]. Briefly, a spin coated 60-µm thick layer of SU-8 (2035, Microchem, USA) photoresist was exposed to ultraviolet light through a mask to fabricate a SU-8 mold on a silicon wafer. The masks were printed at a resolution of 10,000 dpi using a high-resolution printer. PDMS (Sylgard 184, Dow Corning Corporation, USA) base and curing agent was mixed with a 10:1 weight ratio, degassed using a vacuum pump and cast onto the SU-8 mold in a Petri dish to replicate the patterns on PDMS. The PDMS was cured on a hot plate at 75 °C for 3 h. Then, the PDMS was peeled from the mold, and the inlets and outlets were punched subsequently with a puncher. The device was comprised of a layer of PDMS bonded onto a glass substrate using oxygen plasma (Fig. 4.1). The PDMS layer housed the biofilm culture channels and inputs and outputs channels. After bonding, silicone tubing was affixed with epoxy to surround the access holes.

Experimental setup

Silicon tubes were used to connect the syringes containing bacterial suspension, microfluidic device and waste bottle. A peristaltic pump (LLS, Kamoer, China)

pumped air into the device. A 0.2-µm sterile syringe membrane filter was placed at the inlet to ensure the sterility of air. Bacterial suspension was injected into the channels by a syringe pump (Harvard 2000, Holliston, MA, USA). The device was placed inside an incubator (Cu-109, Life Cell Instrument, Korea) incubated at 37 °C. The entire setup was mounted under a Nikon Eclipse Ti-U microscope (Nikon, Japan) (Fig. 4.1).

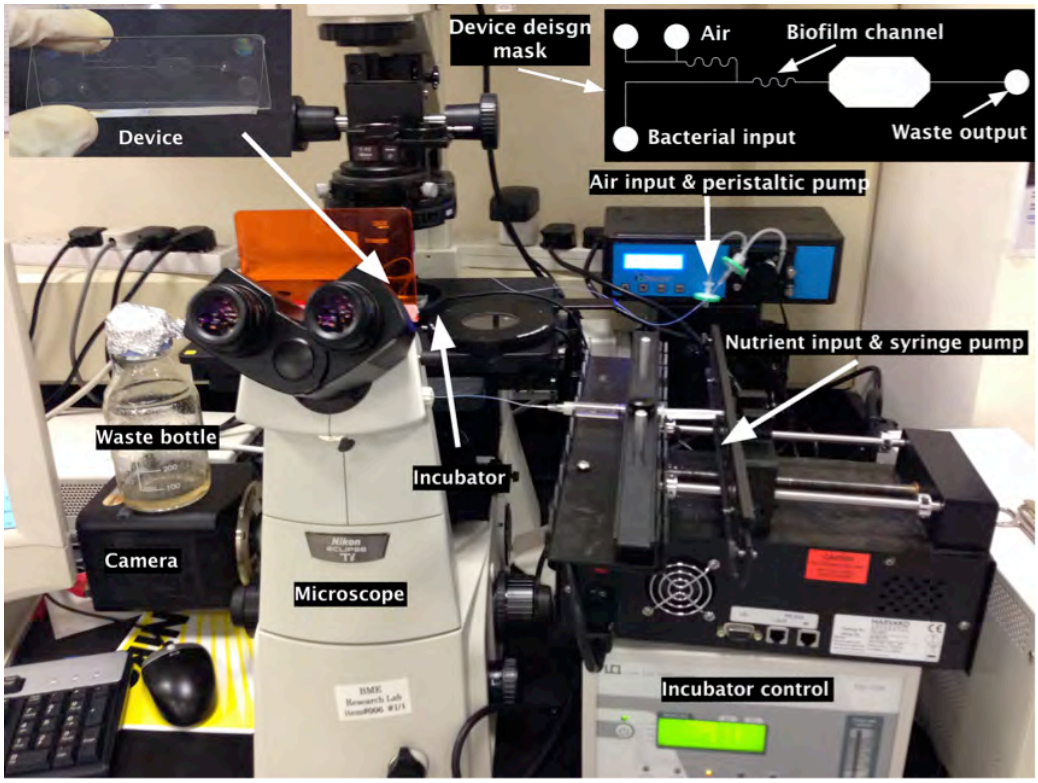

Figure 4.1 Experimental configuration of the segmented-flow microfluidic air-liquid-solid interface biofilm reactor. A peristaltic pump and a syringe pump were used to deliver the air and liquid into the microfluidic device. The air was pumped into the intersecting liquid channel. The multiphase flow was observed by a bright field microscope and recorded by a CCD camera at an image acquisition frequency of 10 *images/s*. Schematic of the PDMS-glass microfluidic device was shown in the top right. There were separate inlets for air and liquid to generate a segmented air-liquid flow. Bacterial sample and nutrient inlets, intercepted by a vertical air stream injected sideways, led way to a meander-shape biofilm cultivation channel with a total length of 5 *mm*, followed by a large reservoir of a dimension of 12 *mm* × 6 *mm* × 60 μm (length × width × height).

All the tubing and microfluidic device were autoclaved prior to culture. The prepared bacterial suspension was fed at the flow rate of 0.3 $\mu L/min$ for 2 hours for initial adherence. After the inoculation, sterile air was introduced at a rate of 15 $\mu L/min$ to

generate SALF with bacterial suspension flow for 24 h. The liquid and gas streams, introduced from the main channel and the side channel, respectively, met at the T-junction crossing (Fig. 4.2). For each flow rate, the system was run for at least 15 minutes to reach a steady state, verified through measuring the bubble formation frequency and the bubble size.

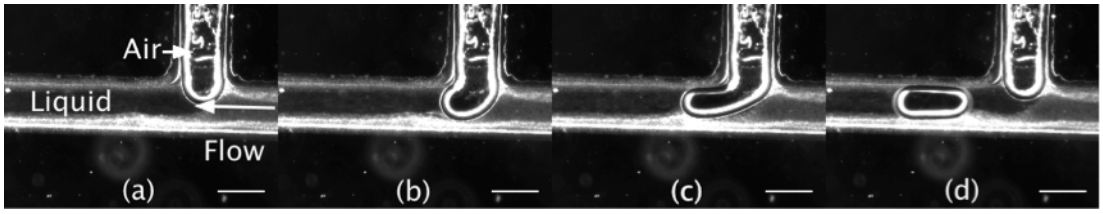

Figure 4.2 Sequential pictures showing the generation of segmented air-liquid flow in a T-junction. Air from the vertical channel was injected into the main flow of the horizontal channel. The air stream was inserted at a rate of 15 $\mu L/min$ to generate the segmented air-liquid flow. Flow direction was from right to left. The T-junction helped to stabilize the air pressure during the dispersion process. The horizontal liquid flow was cut into discrete plugs by the air phase and air-liquid dispersion, with a break-up rate determined by hydrodynamic conditions. The wall of the horizontal channel was covered by biofilms as verified by direct microscopy observation. Scale bars were 150 μm.

Particle image velocimetry (PIV)

Images were acquired by a Nikon Eclipse Ti-U microscope (Nikon Corp., Japan) equipped with a Spot Xplorer camera and Spot software (SPOT Imaging Solutions, MI, USA). PIV is a well-established optical flow measurement technique. Biofilms were translocated with the A-L interfaces of the bubbles. The movement of biofilm relaxation was measured and quantified by PIV. Time-lapse biofilms images acquired at an interval of 0.1 s were used to calculate the movement. Region of interest (ROI) was recorded along the channel turns in the meandering segment. Displacement of cells in biofilm between sequential images was determined from their cross-correlation. Velocity field could be calculated based on displacements of bacteria in the biofilm. The shift was calculated as $v = \frac{\Delta x}{\Delta t}$, where Δx was expressed in terms of micrometers converted from the measured number of pixels and Δt

represented the elapsed time between successive images. Optical flow was computed based on cross-correlation between successive image pairs. 16 × 16 pixels search size was used for the interactive calculation. PIV data processing was analyzed and computed using the PIV plugin-in of ImageJ. Calibration was done by applying a root-mean-squared mask, created by taking the average of the full set of images, to eliminate stagnant area and artifacts [197].

Image processing

Biofilms were observed to form at the bottom of the channel. Percentage of biofilm coverage was used to represent biofilm formation in the system. The biofilm-covered areas were measured using ImageJ.

Numerical simulation

In order to study the hydrodynamic conditions, fluid flow and shear rate field along the microfluidic channels were simulated using COMSOL 4.4 (Comsol Inc., Palo Alto, CA). The geometry was modeled according to the design. Fluid flow was simulated by a finite element analysis using the microfluidic module of COMSOL Multiphysics software. A constant contact angle assumption was made, which radius of the contact base between the bubbles and the non-porous S-L phase boundary substrate was assumed to stay constant throughput the biofilm formation process inside microchannels. Contact angle of liquid with respective to the channel wall was set to 67.5°. Flow rate of the liquid was set to 0.3 $\mu L/min$. Outlet pressure was set to be 0.

Numerical simulation was carried out under two simplified scenarios. One scenario was to simulate the liquid flow without considering bubbles inside the channels to shed light on the hydrodynamics. Another scenario was to simulate the bubble movement inside the channel filled with liquid for calculation of the shear rate on the biofilms during the passage of bubbles. In modeling the multiphase flow and droplet/bubble movement, the following assumptions were made: channel walls were of no-slip, constant velocity on the inlet, multiphase flow was to start from a stable initial position, and of a constant contact angle.

Results and discussion

Conventional biofilm reactors based on microtiter plates are widely used for studying biofilm formation in static conditions. Microorganisms are, however, living in a highly dynamic environment with sporadic exposure to a wide range of environmental assaults and perturbations. The use of microtiter plates provides a limited similar system for biofilms. This underlines the development of the SFMBR.

Operation of biofilm reactor

SFMBR cultured biofilms in a way similar to DFBR. In a widely used DFBR, biofilms were cultured by dripping nutrients on coupons placed in a slanted position [86]. SALF in channels and dripping droplets sliding on a coupon are illustrated in Fig. 4.3. Passage of nutrients across the surface of biofilms in the two reactors versus time shown in Fig. 4.3 indicates that liquid (droplet/plug) and air (bubble/slug) feed the biofilms alternatively in a similar fashion in both reactors. Similarities between the two cultivation microenvironments in a SFMBR are spotted. In SFMBR, the diffusion time of the nutrient and oxygen are controlled by the A-L fractions and

flow rate of the segmented flow. In DFBR, the diffusion time of nutrient and air are controlled by the moving speed of the drops on the coupon [86]. Horizontal angle and the material of the coupon determined the movement of the droplets in DFBR.

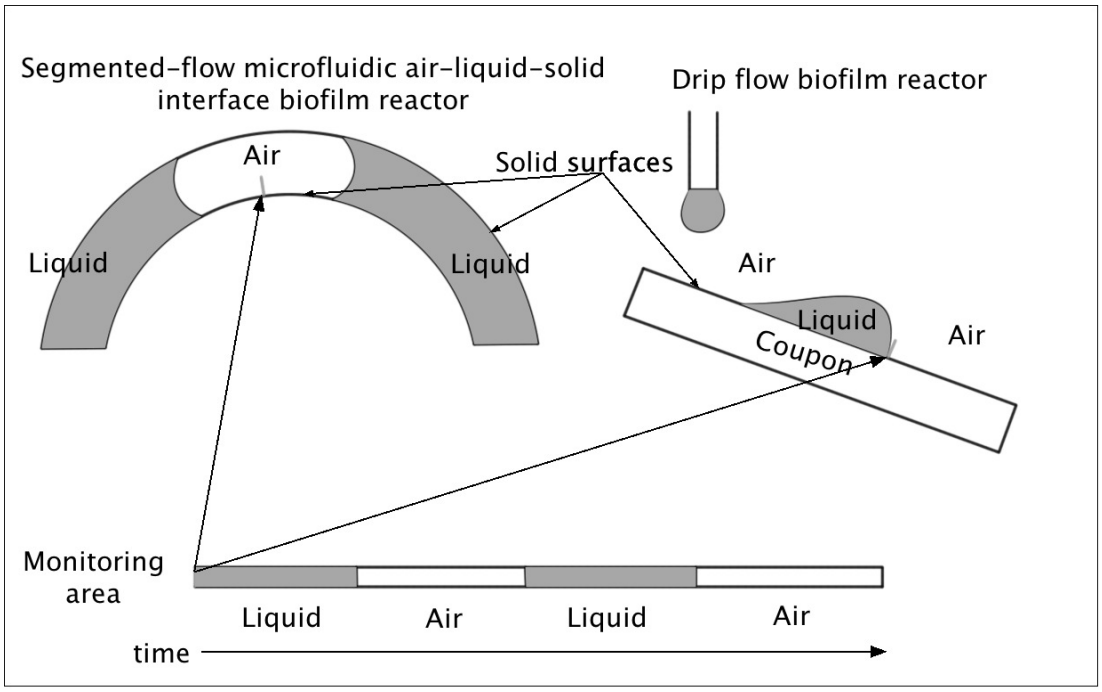

Figure 4.3 Similarity of the A-L-S biofilm cultivation environment between the segmented-flow microfluidic air-liquid-solid interface biofilm reactor and drip flow biofilm reactor. The channel surface and coupon surface were constantly being subjected to the passage of air-liquid interfaces.

Microflows in the liquid plugs of a SGLF (Taylor flow) have been reported to enhance mixing [181]. The flows in the plugs, which are spaced by bubbles, are affected by the length of the plugs. Meanwhile, the lengths of the bubbles and nutrients droplets were determined by the flow rates of the air and nutrients [185]. Flow rate of air (15 $\mu L/min$) was set as 50 times of the flow rate (0.3 $\mu L/min$) as the liquid in this experiment determined by adjusting the flow rate of air to get a steady SALF. However, air pumped with peristaltic pumps does not accumulate enough air pressure (1-3 *atm*) for the nutrient flow. A T-junction design was used to accumulate sufficient pressure to form SALF in the microfluidic device. According to our observation, at the beginning of the experiment, the bubbles were generated at a

frequency of 0.2 ± 0.1 *Hz*, and the length of the bubble was 3.1 ± 0.1 *mm.* The plugs in the channel were assumed to be of single-phase laminar flow because the low frequency of bubbles resulted in the channels were free of bubbles at times. The single-phase laminar flow model of microfluidics in COMSOL was used to compute the flows. For microbial cultivation, however, materials in liquid need to be mixed, which is a difficult task in a laminar flow. In microfluidics, mixing are traditionally achieved by using special geometries such as meandering channels and micro patterns in the channel [198]. Meandering channels were used here to enhance the mixing of nutrients for biofilm cultivation.

SGLF in microfluidics has long been used for gas-liquid reactions, gas-liquid-solid reactions, particles synthesis, *etc.* [181, 184, 189]. Plugs generated with SGLF used as microreactors are spaced with well-controlled bubbles. Here, droplets and bubbles generated with segmented flows were first used to offer biofilms with precisely controlled doses of nutrients. We first demonstrated the implementation of SALF in culturing A-L-S interface biofilms in this chapter. Advantages of using SALF in this reactor include offering precise controlled and repeated does of both nutrients and air, enhanced mixing and many other advantages offered by microfluidics [118]. Our design can also better mimic A-L-S biofilm formation environment than traditional methods by precisely control the nutrient and air. Traditional method mimicking A-L-S biofilms cultivation environment using microfluidic devices did not have direct air contact with the biofilms like in the nature. For example, the biofilm formation environment of interproximal space of teeth was mimicked with flow cell microfluidic devices [199], which can be improved by introducing air with this device.

A-L-S biofilm monitoring

A-L-S interface biofilms formed on the glass bottom of the biofilm cultivation channel was non-invasively monitored under microscopy and analyzed with image processing method (Fig. 4.4, 4.5). Bacteria adhered on the surface was scattered in the area after incubation. While the SALF was introduced, the biofilms began to form. A few colonies were formed on the glass bottom of the microchannel after incubated for 4 hours (Fig. 4.4 (a)). The coverage of the colonies increased till the glass bottom of the microchannel was mostly covered by biofilms from 8-24 hours (Fig. 4.4 (b-f)). The biofilms were single-layer on the glass bottom, which were verified by microscopy. Percentage of the biofilm-covered area increased continuously from 0% to approximately 93% representing the formation process of biofilms in the channel during the incubation (Fig. 4.5).

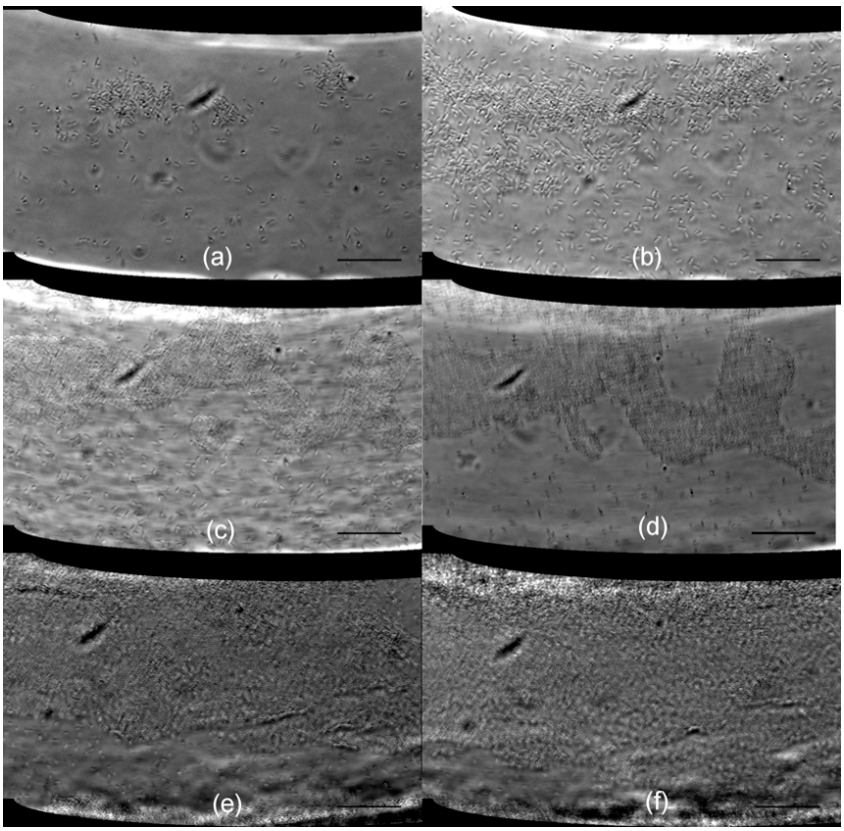

Figure 4.4 *P. aeruginosa* biofilm formation process on the glass bottom of microchannels. The images were taken at 4-24 h with a 4-h interval (a-f). Nutrients flew from the right to the left of the images. Bacteria gathered into monolayer colonies at the beginning. Then, the colonies covering areas expanded during the experiment. Scale bars were 25 μm.

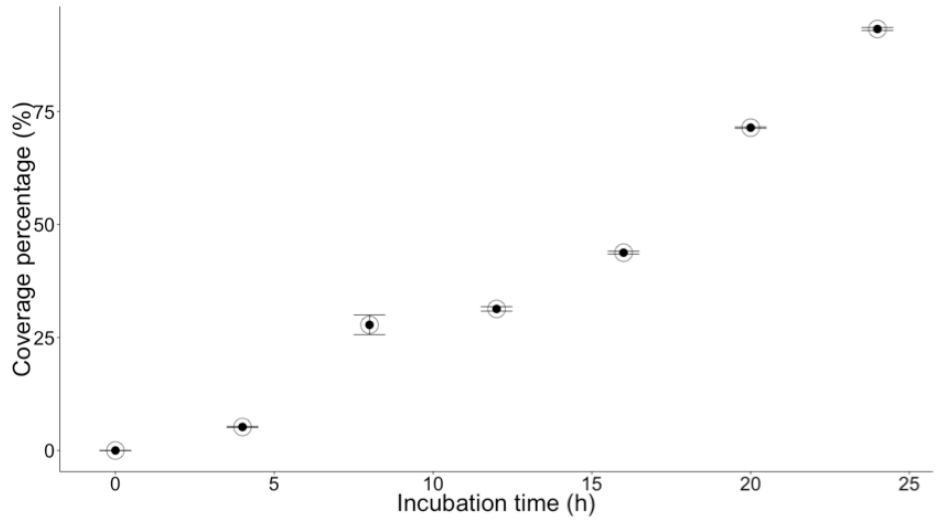

Figure 4.5 Percentage of *P. aeruginosa* biofilm coverage with respect to total channel area. The percentage increased from 0 to 93% in 24 h. Error bars represent the standard deviation (n = 3).

In conventional DFBR and other microfluidic biofilm reactors, bacteria are inoculated at first for the initial adherence in a static or mild flows environment and followed by flowing nutrients with a higher flow rate to grow biofilms under defined shear rate [132]. SFMBR follows the same strategy to culture A-L-S interface biofilms except SALF was used here instead of continuous nutrients flows at the cultivation stage. Hydrodynamics of flows and the geometry of the channels in microfluidics contribute to the formation of biofilms greatly [138]. Biofilm streamers found at the early images (Fig. 4.4 (b-d)), which were the biofilms with “streamline” patterns, were somewhat in agree with the results reported by Rusconi [139].

P. aeruginosa is a well sequenced biofilm positive species commonly found in lots of industrial and medical applications. *P. aeruginosa* biofilms develop in 5 stages including initial adherence, irreversible adherence, maturation I and maturation II and dispersal [3, 19]. However, under high shear force, experimental results suggested that *P. aeruginosa* tends to form dense monolayer biofilms [200]. The

monolayer biofilms formed on the glass bottom of SFMBR were consistent with the reported results from aforementioned investigations in the literature. The most significant difference between this experiment and literature is that the shear rate generated by liquid plugs in our experiment is low. However, our results suggest that a high shear were generated on the glass surface of the channel, which may be due to the moving A-L interface. Because of the monolayer property, expenditure of biofilm coverage area was analyzed to monitor the biofilm. However, accuracy of this method may be affected by the biofilms with multilayer structures. Biofilm monitoring accuracy of the method can be improved by using CLSM to inspect the multilayer biofilms.

Biofilm filamentous streamers, which the "length" of the biofilm along the downstream of the flow is larger than the "width", were reported to form under a high shear force [200-202]. Microfluidic corners also triggered biofilm streamers [139]. These streamers were also caused by the high shear rate induced by the flows around the corners in a microfluidic channel. Therefore, we propose that the streamer observed in our experiment were also caused by the high shear rate generated by the passages of A-L interfaces in the microfluidic channel.

Surface properties changed by biofilms

Wettability of the microfluidic channels changed during the A-L-S interface biofilm formation process. Contact angle of the plugs decreased from 63.2° ± 3.6° to 18.2° ± 0.4° (Fig. 4.6 (a) and (b)) after the formation of biofilms on the PDMS walls of the channel. A film of water remained trapped on the bacterial colonies during a bubble was passing by the area (Fig. 4.7, Supplementary video available at:

http://youtu.be/J9mhjmvNu4I).

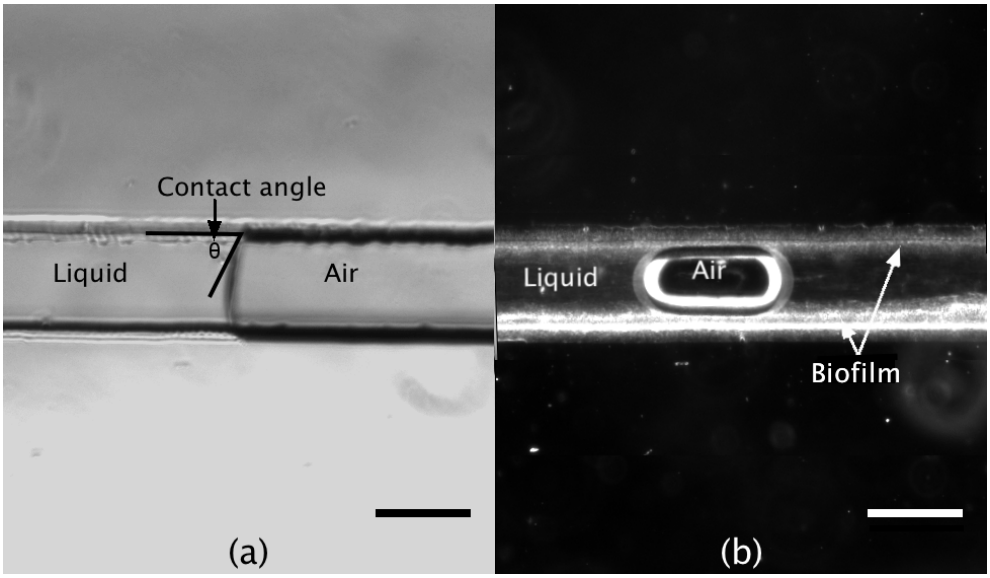

Figure 4.6 Contact angle pinned by the air-liquid interface inside microchannels before and after *P. aeruginosa* biofilm formation. Flow direction was from right to left in the images. Receeding contact angle of the upstream A-L interface was measured and reported. (a) Before formation of biofilm. (b) After formation of biofilms along the channel, as indicated by the arrow. Contact angles were measured to be 63.2° ± 3.6° and 18.2° ± 0.4° (standard derivation, n = 3), respectively. When an air-liquid interacts meets a solid substrate, the degree of wettability or hydrophobicity of the solid substrate is given by the equilibrium contact angle as computed by the Young's equation. Mass transfer could be observed when the liquid plug flowed along the microchannel. Scale bars were 150 μm.

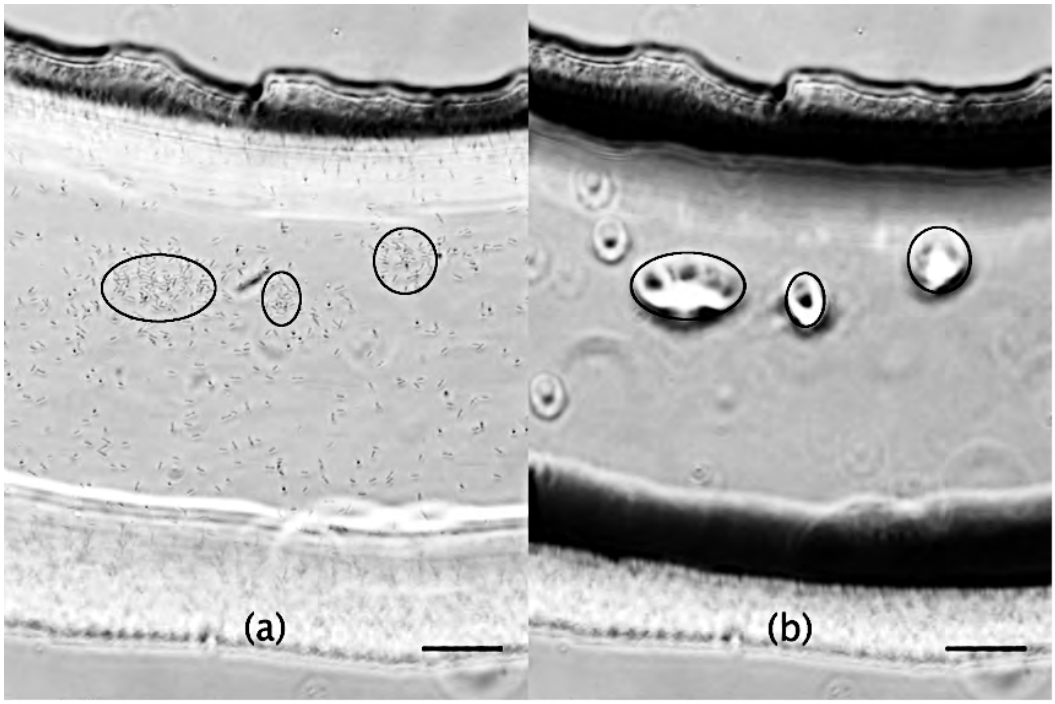

Figure 4.7 Formation of water films associated with *P. areugonisa* biofilm cell aggregates inside microchannels. (a) Bacterial aggregates were labeled with circles and bacterial suspension was flowing in the microchannel. (b) Films of water remained on the colonies of the bacterial aggregates at the same location labeled in (a) during an air bubble was passing the area. Scale bars were 25 μm.

Contact angle is affected by many factors, such roughness of the substrate, impurities of the liquids, environmental temperature and the dynamics of the liquid [203, 204]. The contact angle discussed in this experiment was under a movement of the liquid on a solid surface named dynamic contact angle [205]. Two terms are used to describe the contact angles: the contact angle at the contact line approaching to the liquid phase is called advancing contact angle; the other contact angle at the receding contact line is called receding contact angle [205]. Contact angle we measured at the front A-L interface of the flow is a receding contact angle. Dynamic contact angle was presumed to be a function of the movement velocity of the contact line. Because of the small scale, the dynamic contact angle can be expressed by the capillary number $Ca = \frac{\mu \bar{U}_r}{\gamma}$ where μ is liquid viscosity, $\bar{U}_r$ is average radial velocity, and γ is surface tension [206]. Biofilm formation in the channel increased the velocity of the flow because the biofilms narrowed the microchannel, which will be discussed later. Therefore, the contact angle should be increased according to the literature [206]. However, the contact angle was measured decreased in this experiment. So the measured contact angle was primarily a function of the surface property, called wettability or hydrophobicity in this experiment.

B. subtilis biofilms on agar were hydrophobic reported by the literature [207]. The hydrophobic property offered the biofilm a higher antibiotic resistance due to the reduced penetration of the antibiotics. But the hydrophobicity of biofilms in hydration-dehydration circling environment remains elusive. As far as we know, no literature discussed about the hydrophobicity of biofilms in this kind of environment. Results of this experiment suggested that wettability of the biofilms were higher than

PDMS because the contact angle of the liquid was greatly decreased after *P. aeruginosa* biofilms formed on the surface of PDMS wall. So the biofilms formed by different species or in different microenvironment may have different hydrophobicity properties.

Water preservation by the bacterial colonies may be because of the microstructures constructed by the bacteria. It is well known that microstructures enhance the hydrophobicity of surfaces [207]. For a hydrophobic surface with microstructures on it, the wetting can be fall into two stages [208]. One stage is Wenzel stage, while the droplet completely wet the microstructure by filling all the crevices. The other stage is Cassie stage, in which the droplet will sit on the microstructure with air trapped under the droplet. Droplets in the Cassie stage are repelled by the microstructure. In the Wenzel stage, the water was trapped with the contact line pinning on the microstructure [209]. The state can be easily transferred from Cassie stage to Wenzel stage by means of evaporation or by the passage of a small droplet [208]. In this study, the bacterial colony microstructures are composed of bacteria. When the superhydrophobic properties failed, the droplets were in Wenzel stage and films of water were trapped. The observation of the water films trapped on the bacterial colonies in this experiment is consistent with the results on water films on fabricated by microstructures reported Forsberg *et al.* [209].

S-L interface biofilms are subjected to repeated hydration and dehydration in natural environments such as in soil. Necessary structures could be constructed by EPS to confer desiccation tolerance for the cells [16-18]. However, before biofilms secrete EPS in the early stage of biofilm development, how the initial adhered bacteria

survive amidst repeated dehydration processes still remains unclear. Our result suggests that water can be preserved by the monolayer bacterial aggregations. The observation may shed light on answering this fundamental question.

Flow environment in the channels and biofilm morphology

Biomass of the biofilms adhered on the walls of the channels were affected by the hydrodynamics of the fluid flow. The velocity field of the flow in the channel was mapped by numerical simulation. The high shear represented by the red streamline was found off the middle of the channel (Fig. 4.8 (a)). Biofilms on the lower wall of the channel (24.9 ±24.9 μm) was thicker than the biofilm on the upper wall (21.2 ± 2.3 μm) at position 1 (Fig. 4.8 (b)(1)) while the high shear rate was located near the middle of the channel in the simulation result (Fig. 4.8 (a)). At position 2, more biofilm adhered on the right wall than on the left wall (Fig. 4.8 (b)(2)). Location of the high shear rate was close to the left wall in the simulation shown in Fig. 4.8 (a). In Fig. 4.8 (b)(3-5), flow channels, where fewer bacteria were aggregated, can be identified. They are in accordance with the shear rate distribution in the simulation (Fig. 4.8 (a)). Biofilms on the walls close to the high shear rate was thinner and smoother than the biofilms on the walls away from the high shear rate.

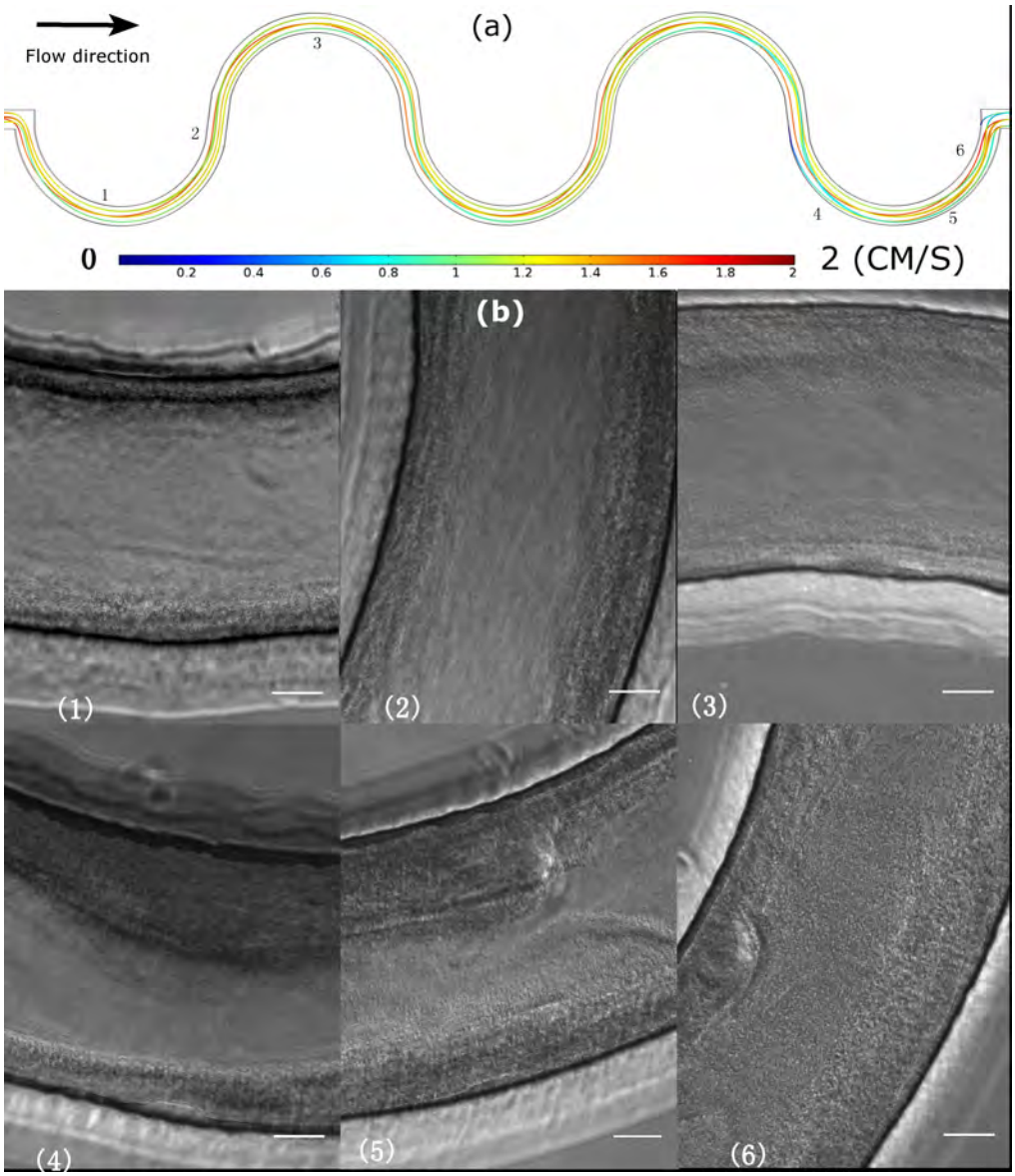

Figure 4.8 *P. aeruginosa* biofilm formation and morphology as affected by hydrodynamics. (a) Numerical simulations of the velocity field in a water-filled channel. Locations of the images in (b) were labeled with numbers. (b) Microscopic images of the biofilms formed in the channel at the different locations labeled in (a). Black lines were the walls of the channel. Biofilms were found adhered on the walls. Biofilm thickness on the walls was correlated to the flows shown in (a). Scale bars were 25 μm.

Morphologies of the biofilms are highly related to the hydrodynamics in microfluidics [138]. Under a higher shear generated by liquid flow, the biofilms are thinner and smoother [169], otherwise, the biofilm are thicker and rougher. Biofilms close to the higher shear rates experienced a higher shear forces and grown thinner. So, the biofilm development on the channel were mostly in agreed with the shear rate

field mapped by numerical simulation and the literature [169]. Liquid films form between the bubbles and the channel walls in a SGLF [186]. Thickness of the liquid films between bubbles and walls were different between on the inner and the outer walls in a meandering channel, which may also contribute the morphology difference of the biofilms.

Hydrodynamics of the channel were changed by the formation of biofilms reversely. Biofilms are heterogeneous 3-D structure [210]. In microfluidics especially in segmented gas-liquid flow, small changes of the geometry of channels will greatly change the hydrodynamics of the flow [184]. Covered by the biofilms, the microfluidic channel was narrowed by the biofilms, which increased the resistance of the channel and resulted in changes of the flow and shear in the channel [138]. Therefore, it is not surprising that the appearance of biofilms may not strictly depend on the simulation result. Because the simulation boundary conditions were simplified without considering the changes of the channels caused by the formation of biofilms resulting in a disagreement among the simulation results and the experimental results such as biofilm formation at location 1 (Fig. 4.8).

Bubble-biofilm interaction

Shear forces generated by the moving A-L interfaces of the bubbles stretched the biofilms. During the passage of the front A-L interface, the biofilms moved with the A-L interface downstream. Afterwards, the biofilms in air (bubble) relaxed (Supplementary video available at: http://youtu.be/3FuTowHxYaY). The biofilms close to the right of the image relaxed at a speed of about 6.4 $\mu m/s$ (Fig 4.9 (a)). The biofilms were also pressed to the wall of the channel by the moving A-L interface of

the bubble where the biofilms near the left of the image were thicker. Therefore, the biofilms relaxed to the upstream direction as well as to the middle of the channel resulting in the movement in this area appeared nonuniform. The highest relaxation speed at this area was 35.3 $\mu m/s$.

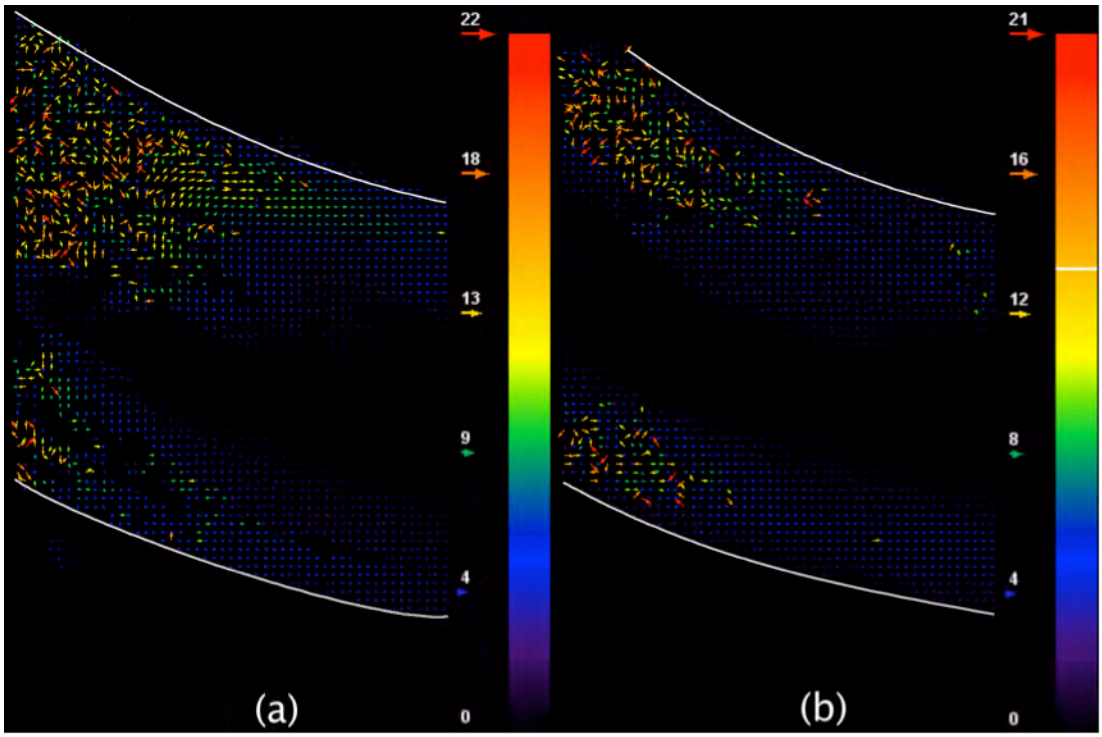

Figure 4.9 PIV results of *P. aeruginosa* biofilm relaxation inside microchannels after the passage of air-liquid interfaces as in an air bubble and in the liquid. A-L-S interface biofilms were first cultured in microfluidics by dosing nutrient and air with segmented air-liquid flow for 24 hours. The A-L interface and liquids flow from right to left in the images. Two images taken at the interval of 0.1s were used for the PIV measurement. Raw data outputs of PIV were visualized as a vector flow. Vectors represented displacements of individual cells in the biofilms between successive images. Directions and magnitude of the movements were labeled with arrows. Both color and length of the arrows represent the magnitude of the movements. (a) Relaxation of biofilm after the front A-L interface. The biofilms were in the bubble. (b) Relaxation of the biofilms after passage of a bubble. The biofilms were in the liquid during the relaxation. Unit of the legend is pixels (6.24 $pixel/\mu m$). The highest speeds were represented by the red arrows (35.3 $\mu m/s$).

While the other A-L interface of the bubble passed by the biofilms, the biofilms were stretched again to the downstream direction and relaxed afterward (Fig. 4.9 (b)). Numerical simulation result illustrated that a moving A-L interface generates the highest shear stress (about 0.66 Pa) at the three phase (A-L-S) contact line of the

moving A-L interface (Fig. 4.10). The biofilms interacted with the bubbles by moving along with the A-L interface of the bubbles.

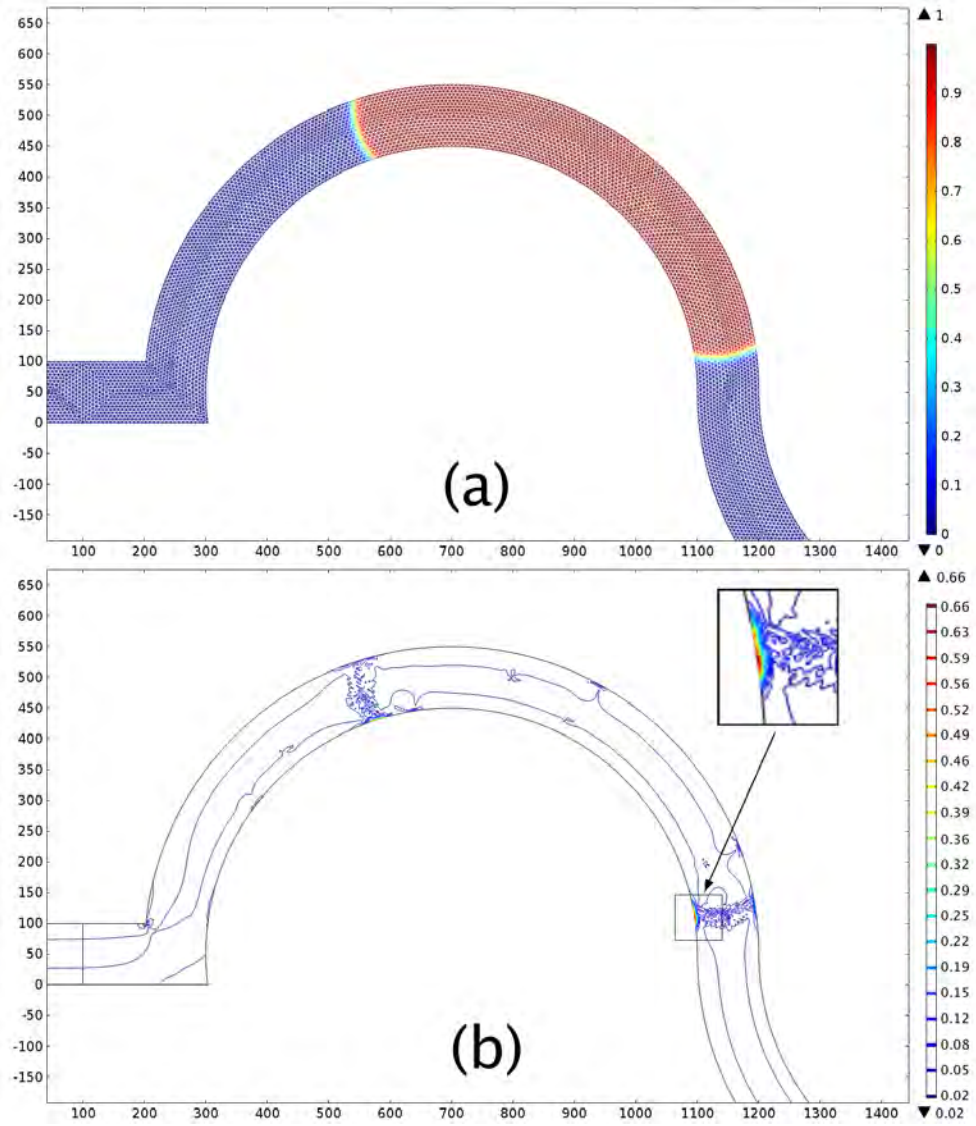

Figure 4.10 Numerical simulations of shear stresses during passage of a bubble along the meandering channel. (a) Fraction of air and liquid. Red area indicated air bubble and blue area represented liquid. (b) Contour of shear stresses in the channel at the same time and location with (a). Unit is Pa. The highest shear stress appeared at the three phase (air-liquid-solid) contact area.

Mechanical properties of biofilms such as Young's modulus and biofilm adherence can be measured using this device. By numerical simulation, the shear force of the moving A-L interface was determined in this experiment. Stretch and relaxation of the biofilm during and after the A-L interface passage can be measured by PIV. Mechanical properties measurements of material always include measuring and

recording the forces exerted on the boundary of the specimen and the displacements of the material generated by the forces [211]. However, because of the unique mechanical and structural properties of biofilms, special experimental designs have to be used to characterize mechanical properties of biofilms [211]. For example, a technology utilizing fluid shear to generated varies forces exerted on biofilms followed by analyzing the biofilms response was developed by P. Stoodley and his group as early as 1990s [212, 213]. The flow cell can achieve a various flow shears. However, continuous flows were used, which constrained the controllability of the shears forces. With microfluidic devices, some groups cultured the biofilms and measured the mechanical property, such as Yung's modulus and adherence by the deformations of a PDMS membrane of the device with biofilms [137] or measure the biofilm with AFM after disassemble the device [132]. With the share forces generated not only by the liquid, but also by the A-L interfaces, the device designed here can precisely control shear flows and the displacements of the biofilms. Moreover, superior to the microfluidic methods reported by literature, the measurements using the microfluidic biofilm reactor designed here were independent of the substrate Young's modulus [137] and do not need to deconstruct the device [132].

The flow rate of segmented air-liquid flow was set to be 0.3 $\mu L/min$ in the cultivation phase in order to simulate the low shear force and mild flow conditions found in the natural environment at which A-L-S biofilms conventionally thrive [86]. To retrieve biofilms from SFMBR, the obvious method is detachment. In the context of biofilm, detachment refers to the release of cells from the biofilm biomass into the environment. Factors contributing to detachment include microbial composition,

enzyme, environmental condition, hydrodynamic parameters, fluid shear stress and quorum-sensing signals. Mechanical shear stresses associated with fluid flow have long been established as a technique to detach biofilms from surfaces [29]. High-speed moving A-L interface have been reported to contribute to biofilm losses and dislodgment [190]. Therefore, high velocity bubbles and micro droplets were utilized for biofilm removal, particularly in the field of oral cavity hygiene [193-195]. The biofilm removal rate was reported to be related to the size, moving velocities and gas fractions of the moving bubbles [194]. These parameters can readily be controlled in microfluidics as a routine in the designed device to harvest the biofilms and study the detachment of the A-L-S interface biofilms.

In our experiment, we have demonstrated that the passage of bubbles or air slugs functioned as mechanical stresses over the surfaces of biofilm, during which the three-phase (air, liquid, and solid) contact line was in contact with the biofilm cells. It translated into a wall shear stress of about 0.66 *Pa*, exerted by the traveling air-liquid interfaces without removing the biofilms off the microchannels. SFMBR allows modulation of shear stresses by changing the fluid velocity. Our finding demonstrates that shear-based biofilm mechanical property studies can be realized in SFMBR.

Conclusion

Bacterial biofilm is a structurally and functionally dynamic and complex system of great importance in the research of biological and medical sciences. The formation of biofilms at the air, liquid and solid interface presents a unique niche for bacterial cells as a survival and dispersal mechanism. Development of biofilm entails an

elaborative interaction with environmental conditions and physical, chemical, and biological cues. Microfluidics techniques is an encompassing technology to address these factors by creating tailor-made hydrodynamic microenvironments for cells to adhere to surfaces, communicate with each other, secret extracellular matrices, undergo maturation and dispersal. Concurrent optical, electrochemical and genetic measurements are also made possible with the nifty, compact, and versatile microfluidic platform.

A SFMBR has been designed and fabricated to culture and monitor A-L-S interface biofilms in this work. An inexpensive on-chip drip flow biofilm reactor enabled real-time non-destructive monitoring of A-L-S interface biofilms. A-L-S interface biofilms were first cultured in microfluidics by providing doses of nutrient and air to precisely control the diffusion of nutrient and oxygen. Elastic relaxations of biofilms were first characterized by analyzing the movement of biofilms during and after interactions with an air bubble during passage. Biofilm removal by microdroplets or microbubbles can be studied in well-controlled environments offered by this device. SFMBR finds applications in biofilm research, drug resistance screening and material science. There are rooms of improvement in the SFMBR as revealed by empirical and simulation results. For instance, the channel geometry and flows dynamics needed to be better coordinated to improve performance. This work provides researchers with an increased understanding on the culture, characteristics and functionalities of A-L-S interface biofilms.

Chapter 5 Conclusion

Bacterial biofilm is a structurally and functionally dynamic and complex system of great importance in the research of biological and medical sciences. The formation of biofilms at the air, liquid and solid interface presents a unique niche for bacterial cells as a survival and dispersal mechanism. Biofilms formed by *Bacillus subtilis* and *Pseudomonas aeruginosa* in laboratory hanging droplet bioreactors in this thesis represent examples of surface-associated microbial communities, which display dynamic developmental patterns. Conventional technologies used to culture biofilms suffer from low throughput operation, labor-intensive and material consuming procedures, and a lack of reproducibility and precise control. These technologies often fail to mimic the complexity of the microenvironment in which biofilms are grown in nature. Microfluidic bioreactors, on the other hand, can mimic the biofilm microenvironment owing to a better control of the physical, chemical, and mechanical parameters in a high throughput way. Therefore, using microfluidic reactors may help with the understanding of biofilm physiology and reveal the clinical and industrial potential of biofilms.

In this thesis, we introduce a novel open microfluidic hanging droplet biofilm reactor forming biofilm at the air-liquid interface under evaporating flow to investigate the complex biology of biofilm in response to changes in local microenvironments. We novel utilized evaporation flow as an on-chip mixer and vertex for the first time. This new microfluidic component can find wide range of applications in microbiology. The special property of A-L interface biofilms formed in hanging droplet biofilm reactor, such as freely standing on the surface of the hanging bottom and fast

formation enables the ease of *in vitro* measurement and high efficiency formation and harvesting. We also first observed the nanotubes interconnecting the *B. subtilis* cells in A-L interface biofilms formed in broth. This observation may improve the understanding of the physiology of *B. subtilis* biofilms.

A segmented-flow microfluidic air-liquid-solid interface biofilm reactor has been designed, fabricated and validated to culture and monitor A-L-S interface biofilms in this work. An inexpensive on-chip drip flow biofilm reactor enabled real-time non-destructive monitoring of A-L-S interface biofilms. A-L-S interface biofilms were first cultured with precisely controlled doses of nutrient and air using segmented air-liquid flow on chip. Elastic relaxations of biofilms were first characterized on chip by experimentally and mathematically analyzing the deformation of biofilms during and after interactions with an air bubble. Biofilm removal by microdroplets or microbubbles can be studied in well-controlled environments offered by this device. SFMBR can be applied in biofilm research, drug resistance screening and material science. There are rooms of improvement in the SFMBR. For instance, the channel geometry and flows dynamics needed to be better coordinated to improve the performance. This work provides researchers with an increased understanding on the culture, characteristics and functionalities of biofilms on A-L-S interface.

Future work: Patterned printing of air-liquid interface biofilm arrays

High-throughput cultivation, manipulation and detection in multiarray patterns have been widely practiced in conventional microbiology, but only a few applications have been reported on biofilm arrays [140, 214, 215]. Many microbial arrays are

patterned by printing. However, biofilm cultured with the existing method cannot be used to pattern biofilms. Currently, the existing biofilm patterning methods are based on an initial patterning of bacterial arrays and subsequently growing the bacterial arrays into S-L interface biofilm arrays. S-L interface biofilms grown on substrates are highly affected by the surface properties. In this thesis, I have demonstrated a method to culture A-L interface biofilms on the surfaces of hanging droplets. The microfluidic devices are feasible to transfer biofilms by printing. I will develop a biofilm printing system to pattern biofilm arrays. The high-throughput, automatic 3D biomaterial printing system using 3D ink can find applications in (1) patterning biofilm arrays for high-throughput biofilm drug resistance screening, (2) coating surfaces with 3D biomaterials, (3) studying interactions of biofilms with different surfaces, (4) patterning 3D materials such as 3D tissue spheroidal for high throughput researches, (5) printing 3D structure such as organs with 3D materials.

Introduction

Microorganisms are ubiquitous in the environment and are often associated with solid surfaces or phase boundaries [216]. These interfacial microbial communities are termed 'biofilms' and are structurally and dynamically complex biological systems. The structures consist primarily of a matrix of extracellular polymeric substance (EPS) that the bacterial cells secrete and within which they are embedded [217]. The EPS matrix has several functionalities, such as protecting cells from threats, forming 3D structures to hold cells and many others [218]. Fully developed biofilms have complex architectures containing microcolonies encased in an EPS matrix and criss-crossed by interstitial water channels [219]. Their spatial heterogeneity harbors a range of microenvironments, providing niches for multiple

phenotypes and affects community structure and productivity [220]. Colonization of bacteria on surfaces is usually spatially heterogeneous scattered with hot spots, plausibly because of the heterogeneous distributions of hydrodynamic shear on surfaces and other environmental factors [221]. Therefore, it would be desirable to study properties (e.g., quorum sensing, detachment) of biofilms as a function of their spatial structure, and thus to be able to control and manipulate this spatial structure.

Many approaches to bacterial patterning have been reported, including dip-pen lithography [222], inkjet printing [223], photolithography [224], and spotting [225, 226]. Although spotting, photolithography, and inkjet printing can create micropatterns of cells and dip-pen lithography is suitable for fabricating nanopatterns, these methods depend heavily on specialized microfabrication facilities and, as a result, have been used very little to address fundamental questions about biofilm dynamics. Also, these robot-controlled printing methods are serial and require long processing that is undesirable to prepare single-use, disposable devices for flexible experimentation. Microbial arrays are promising tools in microbiology and molecular biology. For instance, DNA arrays are widely used [161], but they are not ideal to study activities on the cellular and physiological level such as quorum sensing, viability, and toxicity [162]. To fill this gap, cell based microbial arrays are developed, which can be utilized to study biofilms. However, only a paucity of biofilm array patterning methods has been reported due to the lack of methods to prepare biofilms suitable for array patterning.

Microcontact printing (μCP) provides us with an alternative method, which affords great flexibility to readily alter the size and shape of features that control cell

adhesion, density and geometry. Pioneering work in μCP was performed by Whitesides' group at Harvard University [227-229]. They patterning transferred thiols onto gold surfaces by means of a microstructured PDMS stamp. PDMS is the material most frequently used to make stamps, as a slab of polymer that bears a microscale relief pattern on one side, since it can be molded using a master. PDMS itself is a versatile polymer that provides sufficient mechanical stiffness in μCP in a wide range of surfaces with different roughness and topology. The successful application of μCP of chemicals from a micro-stamp onto a surface is dependent upon the time required to progress from drying the stamp to printing onto substrates, and upon the property of the immobilizing surfaces [230]. Insufficient pressure might result in poor printing and excessive pressure will induce sagging of the stamp, causing chemicals to print outside of the features.

μCP has also used to print biofilm arrays. An immiscible liquid was used to prevent evaporation for long-term cultivation. An array of "stamps" was brought into contact with bacterial colonies on agar plate [215]. Few other methods were also reported to print biofilm arrays. Stencils with an array of holes have been used as masks to pattern biofilms arrays [140]. Biofilms were cultured on a glass substrate covered by the stencil mask. An aqueous two-phase system has also been used to culture biofilms in an array of drops containing bacterial suspension [214]. Operations of biofilm array patterning utilizing stencils mask and aqueous two-phase system are complex and time-consuming. Although transferring biofilm array with stamps is straightforward, this technique is prone to contamination and non-specificity as the stamps may be in touch with other cells or extracellular substances in the local vicinity of the biofilm under study. To solve these problems, a biofilm printing

method is proposed here to print air-liquid interface biofilms from a HDBR to a patterned array on solid substrates.

Another motivation for this work is a lack of techniques for biofilm study. It is difficult to compare biofilms grown on different surfaces because biofilm properties are largely affected by substratum materials, surface roughness, and hydrophobicity [164, 165]. For example, *Legionella pneumophila* biofilms in plumbing systems have been reported to grow better on latex surfaces than ethylene-propylene, polyethylene, PVC, polypropylene, stainless steel, and glass [180]. Surface roughness is an important consideration in biofilm formation. For example, Tang *et al.* reported that biofilm preponderance was better on stainless steel with a relatively higher surface roughness than on sol-gel surfaces [167]. *Pseudomonas aeruginosa* and *Staphylococcus epidermidis* biofilms were reported to behave non-linearly with respect to surface roughness changes [231]. Other work has suggested that biofilm formation did not show observable correlation with surface roughness [22, 232]. Similarly, the effect of hydrophobicity of substrate on biofilm formation remains unclear. Adherence of *B. subtilis* biofilm was reported to be related to surface hydrophobicity [233]. In contrast, *Streptococcus sobrinus* biofilms show no preference to form on hydrophobic or hydrophilic surfaces [167, 231]. On the other hand, biofilm formation actively affects properties of a surface. For example, it was reported that *Streptococcus mutant* biofilms changed surface roughness of resin composites [234]. In a nutshell, surface and biofilm formation are intricately related. To thoroughly understand the actual properties of biofilms, there is a must to decouple biofilm from the surface-associated adherence and growth. In order to arrive at a common ground to better understand biofilms without consideration of

surface properties, printing of A-L interface biofilms on solid substrates presents an ideal candidate for further biofilm study.

Another reason to use A-L interface biofilm as the subject of this study is that surface-associated S-L interface biofilms are difficult to transport. To harvest S-L interface biofilms, one often needs scrapping with blades or tweezers. In the process of these invasive procedures, the resident biofilms topology will be compromised with possibilities of contamination, compounded with the added challenge of transferring biofilms from these tools. Harvesting and sub-culture of S-L interface biofilms are plagued with all sorts of problems. A-L interface biofilms are freely standing in an open space along the phase boundary of air and liquid. Atomization, printing, and μCP are all potential non-invasive methods to harvest these biofilms for further analysis and use. An A-L interface biofilm cultivation method based on hanging droplet biofilm reactor has been thoroughly introduced in previous chapters. In the case of A-L interface biofilms forming in a hanging droplet, a simple pinch-off and dripping mechanism can be practiced for non-invasive sampling and harvesting.

We herein propose an A-L interface biofilm printing methodology by evaporating biofilm-containing droplets on a solid substrate. As an evaporating droplet diminishes in mass, convection, and dispersion forms in the outer surface, gas medium transport the droplet mass far from the droplet. A vigorous interior flow, known as Marangoni flow, was generated during the course of evaporation due to drastic changes in surface tension gradient. The Marangoni number is $Ma = \Delta\sigma R/\rho\nu\alpha$, where $\Delta\sigma$ is the surface tension change along the air-liquid interface, ρ is density, ν is kinematic viscosity, α is thermal diffusivity, and R is the radius of the

droplet. An evaporation-induced pattern of biofilm structure is thus formed. In this work, we report the results of investigation of the A-L interface biofilms arrays patterned from deposited hanging droplets by evaporation. Objective of this study is to understand the structure and functionality of evaporation-induced pattern generated by biofilms.

Materials and methods

Chemicals

All chemicals were purchased from Sigma-Aldrich (St. Louis, MO, USA). All cell culture supplies were purchased from Difco Laboratories (Detroit, MI, USA) unless otherwise stated. Crystal violet was purchased from Molecular Probes (Invitrogen, Eugene, OR, USA).

Cell culture

Bacillus subtilis ATCC 6051 was obtained from American Type Culture Collection. *B. subtilis* cultured was maintained in buffer composed of 50 mM Tris-HCl, 1 mM $MgSO_4$, 4 mM $CaCl_2$, and 0.1 M NaCl at pH 7.2. Cultures were stored at 4 °C and transferred to fresh tryptic TSA or TSB incubated for 24 h at 37 °C in an orbital shaker at 160 rpm before use.

Hanging drop method

The hanging drop method in this study was adapted from the 3D spheroid production using a 384-well hanging droplet biofilm reactor (3D Biomatrix, MI, USA) developed by Kelm *et al*. [171]. Liquid culture media was firstly added via access holes on the topside of the plate. Hanging droplets were formed suspended on the

underside of the plate. An array of hanging droplets could be produced, sandwiched between a lid and bottom tray. The dispensing tip of pipettes was extended through the access hole to inoculate 25 μL of *B. subtilis* suspension into each hanging droplet. The bottom tray contained a water reservoir to reduce evaporation. The suspending droplets were incubated at 37 °C.

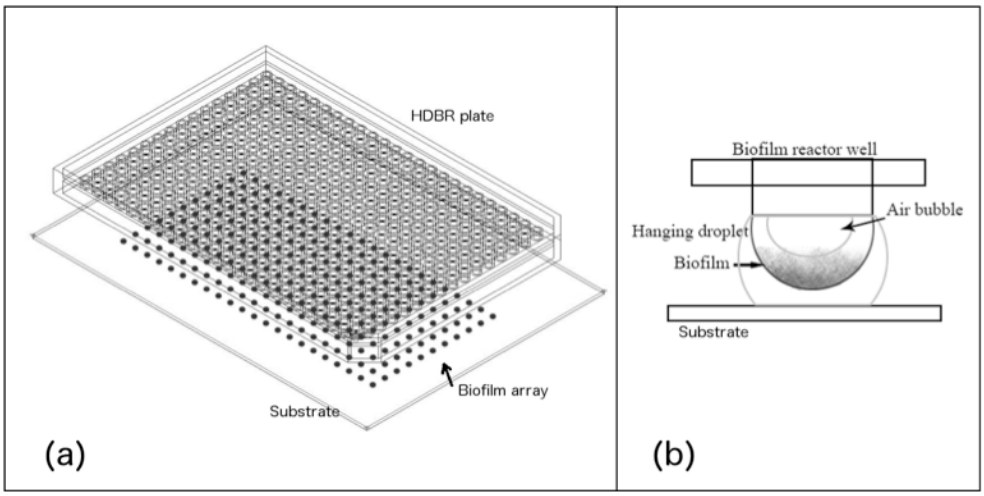

Figure 5.1 Schematic diagrams illustrating the biofilm array printing technique. (a) Biofilms grew in the form of droplets suspended from a handing drop biofilm reactor plate. Detailed operation is outlined in Chapter 3 of this thesis. An array of biofilms was formed underneath by direct printing and evaporative drying. (b). An injector pipette tip was inserted into the open neck region of an access hole where a meniscus was formed. Upon addition of air, the hanging droplet would start to grow. The elongated droplet would eventually pinch off forming droplet depositing on a collecting substrate placed at 1.5 mm form the bottom of the droplet.

Biofilm printing

An injector pipette tip was inserted into the open neck region of an access hole where a meniscus was formed. Upon addition of air, the hanging droplet would start to grow and get into contact with a collecting substrate placed at 1.5 mm form the bottom of the droplet. The elongated droplet would eventually pinch off forming a droplet containing the biofilm and deposit on the substrate. Substrates in this experiment included PDMS and glass slides, both were clean and free of any surfactants. Biofilms were printed onto substrates as a function of biomass concentration and time of cultivation. An array of biofilms was deposited on the

surface.

Microscopy

Biomass-containing droplets was allowed to dry at room conditions without controlling the relative humidity. The biofilm deposit morphology and spatial distribution were examined by light microcopy using a Nikon AZ100 stereomicroscope (Tokyo, Japan) equipped with a digital sight DS-Fi1C camera controlled by a standalone control unit DS-L2 (Tokyo, Japan).

Results and discussion

Biofilm deposition

Printing of A-L interface biofilms on solid substrates by evaporative drying can be viewed as a way to pattern biomaterials. Upon drying, the suspended A-L interface biofilm biomass was deposited in a well-defined macroscopic pattern based on the pinned contact line, evaporative rate, internal flow field, and interactions among the biomass. This phenomenon has found applications in the self assembly of nanoparticles [156, 235]. As the droplet evaporates, solvent flows toward the contact ring, carrying suspended biomass with it. Once the culture media has evaporated, a ring of biomass particles was left as residue.

The drying of an A-L interface biofilm water droplet gave rise to a “coffee-ring” type deposit pattern along the perimeter. Pinning of the A-L-S contact line of the drying droplet ensured that liquid evaporating from the edge was replenished by liquid from the interior, which resulted in an outward flow that carried planktonic cells and dispersed biomass to the periphery of the pattern. This concentration method has

long been used as a means of organizing suspended particles with dimensions ranging from nanometers and micrometers.

Biofilm arrays were deposited on different substrates including PDMS and glass slides (Fig. 5.2-5.4). On a PDMS substrate, *B. subtilis* biofilm microarray-based multiplex arrays incubated for 9 hours and 16 hours were printed into two 3×3 arrays (Fig.5.2). Fig. 5.3 shows the transmission light microscopy image of the macroscopic residual pattern of A-L interface biofilms deposited on a surfactant-free unmodified flat surface of PDMS. A highly organized network formed by the biofilm biomass left as residue after evaporative drying of the suspended droplet was complete. Biofilm clustered to form ridge-like surface topography, as revealed by the black regions (Fig 5.3). As the droplet evaporates, solvent flows toward the contact ring, carrying suspended biomass with it. Once the culture media has evaporated, pattern of biomass particles was left as residue. Therefore a higher density of biomass was observed in the middle region with a gradual decrease of cell mass towards the periphery based on the biomass separation by the evaporating flows.

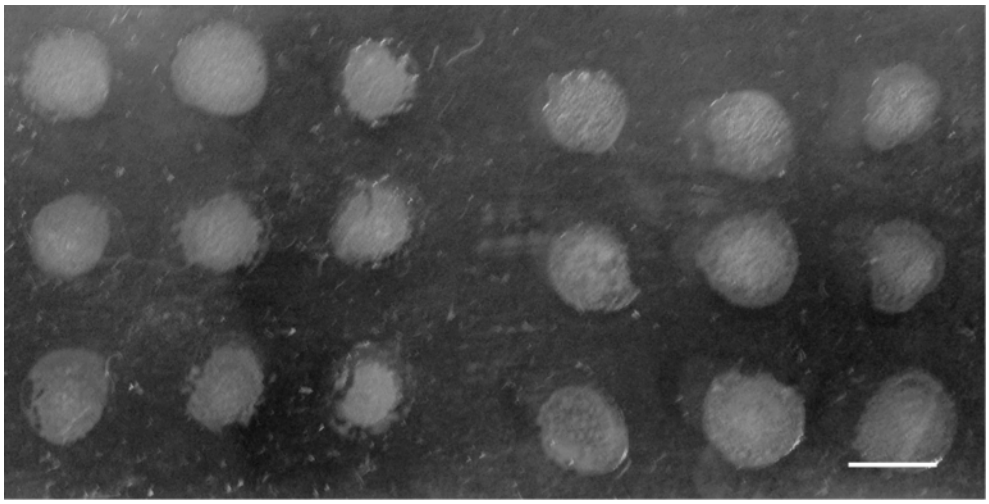

Figure 5.2 A *B. subtilis* biofilm microarray-based multiplex array on PDMS. (Left) A 9-hour biofilm array was patterned in a 3×3 matrix. (Right) A 16-hour biofilm array was patterned in a 3×3 matrix. Scale bar, 5 *mm*.

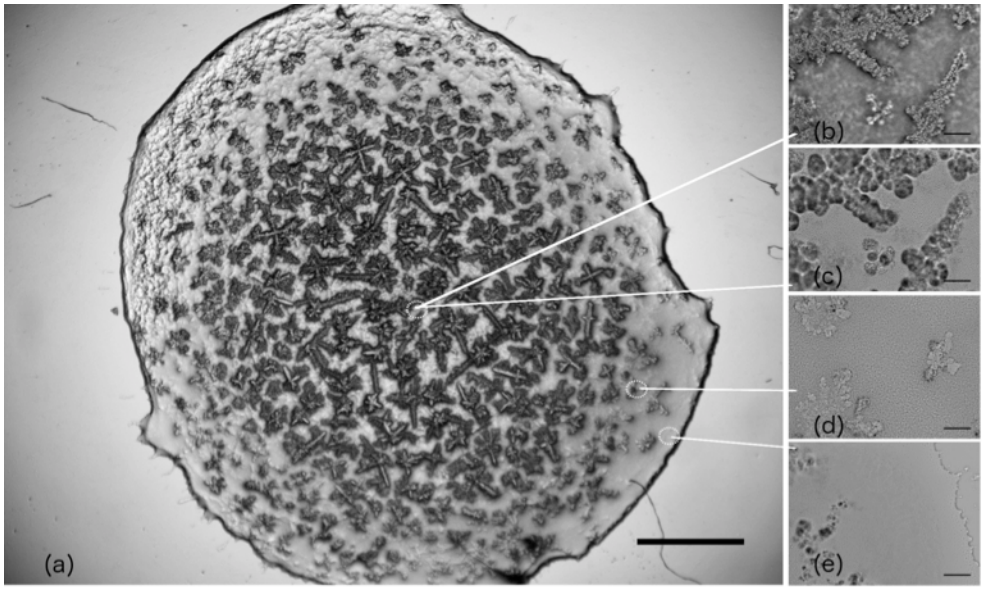

Figure 5.3 Light microscopy images of the macroscopic residual pattern of A-L interface *B. subtilis* biofilms deposited on a surfactant-free unmodified flat surface of PDMS. A highly organized network formed by the biofilm biomass left as residue after evaporative drying of the suspended droplet was complete. Biofilm clustered to form ridge-like surface topography, as revealed by the black regions. Scale bar, 1 *mm*. (b) – (e) Magnified views of specific zones in the biofilm pattern. Scale bar, 50 μm.

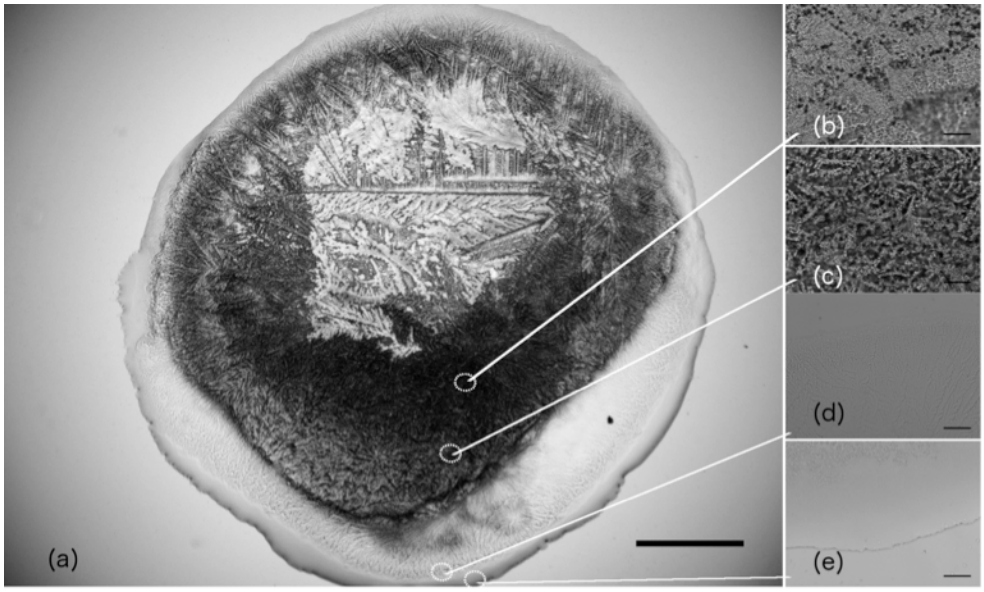

Figure 5.4 A *B. subtilis* biofilm pattern formed when the droplet on the glass substrate becomes pinned. Detailed structures of four different locations of the biofilms are shown in (b-e). Scale bar, 1 *mm* in (a) and 50 μm in (b-e).

While S-L interface biofilm typically needs 3 days for growth on solid substrates [140], biofilms cultured in the captioned hanging droplet biofilm reactor (detailed information found in chapter 3 of this thesis) has been observed to reach maturity in

12 hours. This is likely to be attributed by a combination of culture conditions, such as better mixing due to evaporating flow and more direct exposure to oxygen along the phase boundary. Another advantage of A-L interface biofilms is that biofilm properties do not depend on substrate morphology, which is difficult to achieve by traditional methods for S-L interface biofilms. Further more, surface-associated microorganisms such as biofilms also change substrate properties. All these explain the lack of an objective standard quantification and assessment technique for S-L interface biofilms.

Biofilm patterns differ greatly on PDMS and glass substrates as revealed in Fig. 5.3 and 5.4. This may be accounted by the vast difference in hydrophobicity between these two substrates. When an air-liquid interface meets a solid substrate, the degree of wettability (hydrophobicity) of the solid substrate is given by the equilibrium contact angle as computed by the Young's equation. The contact angle of biofilm droplet on PDMS measured around 90°, whilst it measured roughly 5° for glass. Droplets sitting on PDMS take a much longer time to evaporate because of a relatively smaller surface area comparing with droplets on glasses. Marangoni flow and evaporation flow are generated in droplets on PDMS by the evaporative cooling and nonuniform evaporation. Glass and PDMS present different droplet radius in the calculation of Marangoni flow, which also contributed to the different evaporation-induced pattern of biofilm structure following contact-line pinning. Consistent with that has been reported in the literature, when the contact angle of droplets on PDMS was larger than 14°, circulation flows were generated in the droplets [157]. On a glass slide where contact angle was smaller than 14°, liquid was observed to primarily flow to the edge of the droplet [236]. Biofilm structures on the PDMS may

therefore be interrupted by the evaporating flows, resulting in biofilm clusters eliciting ridge-like surface topography as seen in Fig. 5.3. The density and height of these ridge structures diminished as a function of distance away from the center. The pattern was relatively free of deposits along the perimeter. It was in accordance with the spherical cap shape biofilms that have been demonstrated in previous chapters. Planktonic cells did not form “coffee ring” patterns, which may be due to the flows in the evaporating droplet were affected by the biofilms. Another factor that contributes to this difference is the intrinsic hydrophobicity of the biofilm. *B. subtilis* has been reported to grow better on hydrophilic surfaces than hydrophobic surface due to its hydrophobic character [233]. If the same applies to *B. subtilis* biofilms, the glass substrate would have been much preferred over PDMS with a higher degree of adherence. As observed in the microscopy image, *B. subtilis* biofilms developed a more uniform spread (Fig. 5.4), whilst the PDMS substrate rendered hot spots and local high concentration of biomass. Caution has to be taken in interpreting the biofilm pattern because it is a function of a wide spectrum of factors, including pipetting technique, droplet formation kinetics and many others. This is the first study of the deposition of A-L interface biofilm. More studies have to be carried in the future to better characterize the surface morphology and biofilm hydrophobicity.

Layer-by-layer deposition of biofilms

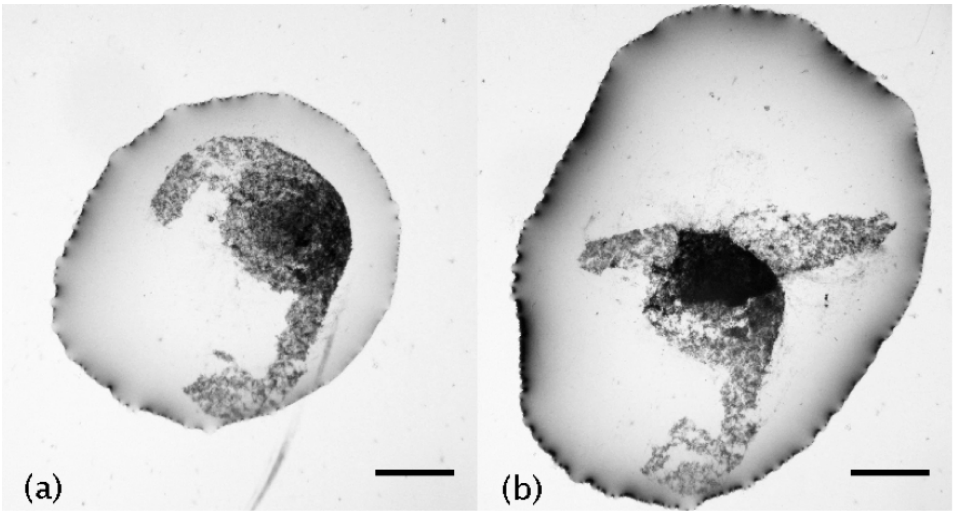

Figure 5.5 Multilayer 16-hour *B. subtilis* biofilm printed on a glass slide by evaporative drying with a sequential order. (a) Deposition pattern of the first layer of biofilm. Biofilm was evidently observed as the dark mass in the middle of the pattern. (b) A second layer of biofilm was deposited on the top of the first layer of biofilm in droplet to realize layer-by-layer deposition. An increase in biofilm layers was revealed by the dark biomass in the middle. Scale bars, 1.5 mm.

Fig. 5.5 shows the deposition of multiple laye/rs of biofilms on a glass substrate. Multilayer 16-hour *B. subtilis* biofilm was printed on a glass slide by evaporative drying sequentially. An increase in biofilm layers was revealed by the dark biomass in the middle. This is a proof-of-principle experiment showing the possibility of a layer-by-layer (LBL) biofilm deposition strategy. LBL assembly is described as oppositely charged polyelectrolytes sequentially self-assemble into layers by electrostatics to form multilayer films [237]. For example, artificial polypeptide biofilms were LBL assembled on $CaCO_3$ cores to produce nanoparticle vaccines, which induce protective T-cell and antibody responses [238]. This method is limited to the deposition of charged materials. To print 3D tissues using LBL method, thermo-reversible gel was used to adhere tissue layers [239].

Biofilm development process on a surface is a self-assembly process. LBL deposition method was used to print multilayer biofilm composed of *E. coli* strains

MG1655 and DH5α [214]. It takes days for multilayers of biofilms to be formed. The LBL deposition technique employs an aqueous two-phase microprinting system and S-L interface biofilm to grow biofilm layer after layer. With this proposed method, the 3D biofilm architecture formation could be greatly expedited with more flexibility on the number of species and biomaterials. Although biofilm layers were not adhered by electrostatics or chemical gluing agents conventionally used in LBL biomaterial deposition methods [238, 239], our proposed biofilm printing technique is good enough to study the interactions between different species and interactions between biofilm matrix and substrates in a multiplexed and high-throughput and rapid way.

This proposed LBL deposition can be used to build multilayers of cell–matrix on any substrates or inside microchannels with precise control on the thickness. This technology can re-create the *in vivo*-like 3D micro scale hierarchical architecture of biofilms for lots of potential applications. The composition and morphology of the deposited biofilm matrix can be customized by controlling the A-L interface biofilm properties. With a more precise deposition technique in the future, we envision this technique to provide micro-positioning and micro-patterning to reconstitute and fabricate biofilm matrix consisting of heterogeneous species. Future work will also provide us with better understanding of the fundamental process in multicellularity, cell co-culture and biofilm biology.

Future integration with microfluidics

The current experiment was based on manual operation. The suspended droplets may be susceptible to dropping, merging or contamination. While the current technology

is of a high-throughput, it entails trained personnel on the operation. Periodic media exchange and removal of waste products for long-term culture may prove to be challenging. To culture and print biofilm automatically, the microfluidic version of the hanging droplet biofilm reactor, as introduced in chapter 3 of this thesis, will be employed to print biofilms in future generations of this technology. Biofilms will be cultured in a 384-array device made of PDMS on a microfluidic platform. Channels and ports will be designed for inoculation, nutrient feeding, and removal of waste. A pneumatically-driven valving system will be set up for automatic operation, better control on the droplet dynamics, and to prevent back flow.

Future experiments

The following experiments will be performed to better characterize and validate this new biofilm printing technology. Biofilms will be cultured with a hanging droplet reactor of different sizes (*i.e.*, 3 μL, 5 μL, 7 μL, and 15 μL). Biofilms will be printed into arrays on a transparent substrate for microscopic observation. Dimension, size, surface topography and roughness of the biofilms will be measured and recorded. Ultrastructure of the indwelling cells and biofilm architecture will be characterized by SEM and CLSM. Multilayer biofilms will be printed with different patterns to shed light on biofilm formation and interaction with substrate.

One of the significant problems in biological cells printing is the cell viability after printing. In this bioprinting technique, cells in biofilm will undergo a desiccation process, which may compromise their viability. To determine cell viability in the deposited biofilm matrix, propidium iodide (PI) and SYTO 9 (BacLight Live/Dead Bacterial viability kit, Molecular Probes, United States) will be employed to study

the viability of the biofilms before and after printing. Live cells will be labeled with STYO 9 while dead cells will be labeled with PI. Stained biofilms will be observed with CLSM. Different antibiotics can be used to study biofilm resistance.

Resistance of multilayer biofilms will be tested. Adherence test will also be carried out accordingly. Glass slides printed with A-L interface biofilms will be positioned at an angle to be washed off by running water with different flow speeds. Biofilms before and after washing, as well as the washed off biofilms, will be quantified. Adherence of multilayer biofilms will be tested in a similar fashion. Elevated resistance to disinfection and antibiotics is an important property of biofilm [240]. Ethanol (75%) will be dripped on the cultured S-L interface biofilm and printed A-L interface biofilms with the previous mentioned methods for 20 minutes. BacLight live/dead bacterial viability kit and CLSM will be used to characterize the cell viability before and after the disinfection process. Images will be analyzed to measure the red-to-green ratio before and after disinfection.

Conclusion

We report the observation of specific pattern formation from the evaporation of aqueous droplets containing motile and nonmotile bacteria (biofilms). There are many limitations in the current biofilm arrays patterning methods as outlined in earlier text. I strive to develop a biofilm printing technique that does not rely on the substrate properties to enhance our understanding of the interaction between biofilms and solid surfaces. A manual biofilm printing technique has been developed and preliminarily characterized in this chapter. Multilayer biofilms have been formed on

substrates. Future work is needed to develop this technology into an automatic system with full integration with microfluidics and a pneumatic valving system.

Reference

[1] M. Ghannoum and G. A. O'Toole, *Microbial Biofilms*, ASM Press, 2004.

[2] L. Hall‐Stoodley and H. Lappin‐Scott, "Biofilm formation by the rapidly growing mycobacterial species *Mycobacterium fortuitum*," *FEMS Microbiology Letters*, vol. 168, pp. 77-84, 1998.

[3] P. Stoodley, K. Sauer, D. G. Davies, and J. W. Costerton, "Biofilms as complex differentiated communities," *Annual Reviews in Microbiology*, vol. 56, pp. 187-209, 2002.

[4] K. Sauer, A. K. Camper, G. D. Ehrlich, J. W. Costerton, and D. G. Davies, "*Pseudomonas aeruginosa* displays multiple phenotypes during development as a biofilm," *Journal of Bacteriology*, vol. 184, pp. 1140-1154, 2002.

[5] G. A. O'Toole, H. B. Kaplan, and R. Kolter, "Biofilm formation as microbial development," *Annual Reviews in Microbiology*, vol. 54, pp. 49-79, 2000.

[6] G. A. O'Toole and R. Kolter, "Flagellar and twitching motility are necessary for *Pseudomonas aeruginosa* biofilm development," *Molecular Microbiology*, vol. 30, pp. 295-304, 1998.

[7] R. M. Harshey, "Bacterial motility on a surface: Many ways to a common goal," *Annual Reviews in Microbiology*, vol. 57, pp. 249-273, 2003.

[8] T. F. Mah and G. A. O'Toole, "Mechanisms of biofilm resistance to antimicrobial agents," *Trends in Microbiology*, vol. 9, pp. 34-39, 2001.

[9] T. F. Mah, B. Pitts, B. Pellock, G. C. Walker, P. S. Stewart, and G. A. O'Toole, "A genetic basis for *Pseudomonas aeruginosa* biofilm antibiotic resistance," *Nature*, vol. 426, pp. 306-310, 2003.

[10] G. A. O'Toole, "Microtiter dish biofilm formation assay," *Journal of Visualized Experiments*, e2437, 2011.

[11] M. Morikawa, "Beneficial biofilm formation by industrial bacteria *Bacillus subtilis* and related species," *Journal of Bioscience and Bioengineering*, vol. 101, pp. 1-8, 2006.

[12] E. Karunakaran and C. A. Biggs, "Mechanisms of *Bacillus cereus* biofilm formation: an investigation of the physicochemical characteristics of cell surfaces and extracellular proteins," *Applied Microbiology and Biotechnology*, vol. 89, pp. 1161-1175, 2011.

[13] H. C. Flemming and J. Wingender, "The biofilm matrix," *Nature Reviews Microbiology*, vol. 8, pp. 623-633, 2010.

[14] S. S. Branda, S. Vik, L. Friedman, and R. Kolter, "Biofilms: The matrix revisited," *Trends in Microbiology*, vol. 13, pp. 20-26, 2005.

[15] S. J. Pamp, "The biofilm matrix: A sticky framework," in *The Biofilm Mode of Life: Mechanisms and Adaptations*, Horizon Bioscience, 2007, pp. 37-69.

[16] M. Hentzer, G. M. Teitzel, G. J. Balzer, A. Heydorn, S. Molin, M. Givskov, and M. R. Parsek, "Alginate overproduction affects *Pseudomonas aeruginosa* biofilm structure and function," *Journal of Bacteriology*, vol. 183, pp. 5395-5401, 2001.

[17] P. N. Danese, L. A. Pratt, and R. Kolter, "Exopolysaccharide production is required for development of *Escherichia coli* K-12 biofilm architecture," *Journal of Bacteriology*, vol. 182, pp. 3593-3596, 2000.

[18] P. I. Watnick, C. M. Lauriano, K. E. Klose, L. Croal, and R. Kolter, "The absence of a flagellum leads to altered colony morphology, biofilm

development and virulence in *Vibrio cholerae* O139," *Molecular Microbiology,* vol. 39, pp. 223-235, 2001.
[19] S. Kjelleberg and M. Givskov, *The Biofilm Mode of Life: Mechanisms and Adaptations*, Horizon Bioscience, 2007.
[20] R. M. Goulter, I. R. Gentle, and G. A. Dykes, "Issues in determining factors influencing bacterial attachment: A review using the attachment of *Escherichia coli* to abiotic surfaces as an example," *Letters in Applied Microbiology,* vol. 49, pp. 1-7, 2009.
[21] N. C. Caiazza and G. A. O'Toole, "Alpha-toxin is required for biofilm formation by *Staphylococcus aureus*," *Journal of Bacteriology,* vol. 185, pp. 3214-3217, 2003.
[22] R. A. N. Chmielewski and J. F. Frank, "Biofilm formation and control in food processing facilities," *Comprehensive Reviews in Food Science and Food Safety,* vol. 2, pp. 22-32, 2003.
[23] M. S. Aparna and S. Yadav, "Biofilms: Microbes and disease," *Brazilian Journal of Infectious Diseases,* vol. 12, pp. 526-530, 2008.
[24] M. F. DeFlaun, S. R. Oppenheimer, S. Streger, C. W. Condee, and M. Fletcher, "Alterations in adhesion, transport, and membrane characteristics in an adhesion-deficient pseudomonad," *Applied and Environmental Microbiology,* vol. 65, pp. 759-765, 1999.
[25] D. Davies and G. Geesey, "Regulation of the alginate biosynthesis gene algC in *Pseudomonas aeruginosa* during biofilm development in continuous culture," *Applied and Environmental Microbiology,* vol. 61, pp. 860-867, 1995.
[26] S. E. Cramton and F. Gotz, "Biofilm development in *Staphylococcus*," *Microbial Biofilms,* pp. 64-84, 2004.
[27] N. C. Caiazza and G. A. O'Toole, "SadB is required for the transition from reversible to irreversible attachment during biofilm formation by *Pseudomonas aeruginosa* PA14," *Journal of Bacteriology,* vol. 186, pp. 4476-4485, 2004.
[28] C. J. Southey-Pillig, D. G. Davies, and K. Sauer, "Characterization of temporal protein production in *Pseudomonas aeruginosa* biofilms," *Journal of Bacteriology,* vol. 187, pp. 8114-8126, 2005.
[29] J. B. Kaplan, "Biofilm dispersal: Mechanisms, clinical implications, and potential therapeutic uses," *Journal of Dental Research,* vol. 89, pp. 205-218, 2010.
[30] B. Purevdorj-Gage, W. J. Costerton, and P. Stoodley, "Phenotypic differentiation and seeding dispersal in non-mucoid and mucoid *Pseudomonas aeruginosa* biofilms," *Microbiology,* vol. 151, pp. 1569-1576, 2005.
[31] T. K. Wood, S. H. Hong, and Q. Ma, "Engineering biofilm formation and dispersal," *Trends in Biotechnology,* vol. 29, pp. 87-94, 2011.
[32] P. Stoodley, I. Dodds, J. Boyle, and H. Lappin‐Scott, "Influence of hydrodynamics and nutrients on biofilm structure," *Journal of Applied Microbiology,* vol. 85, 19S-28S, 1998.
[33] P. Stoodley, S. Wilson, L. Hall-Stoodley, J. D. Boyle, H. M. Lappin-Scott, and J. Costerton, "Growth and detachment of cell clusters from mature mixed-species biofilms," *Applied and Environmental Microbiology,* vol. 67, pp. 5608-5613, 2001.

[34] M. Wilson and D. Devine, *Medical Implications of Biofilms*, Cambridge University Press, 2003.
[35] J. D. Bryers, "Biofilms in disease," in *Microbial Biofilms: Current Research and Applications*, Horizon Scientific Press, 2012, pp. 25-42.
[36] J. P. O'Gara and H. Humphreys, "*Staphylococcus epidermidis* biofilms: Importance and implications," *Journal of Medical Microbiology*, vol. 50, pp. 582-587, 2001.
[37] J.-H. Lee, H. Wang, J. B. Kaplan, and W. Y. Lee, "Microfluidic approach to create three-dimensional tissue models for biofilm-related infection of orthopaedic implants," *Tissue Engineering Part C: Methods*, vol. 17, pp. 39-48, 2010.
[38] J. A. Berry, J. F. Biedlingmaier, and P. J. Whelan, "*In vitro* resistance to bacterial biofilm formation on coated fluoroplastic tympanostomy tubes," *Otolaryngology--Head and Neck Surgery*, vol. 123, pp. 246-251, 2000.
[39] J. Paredes, S. Becerro, F. Arizti, A. Aguinaga, J. L. Del Pozo, and S. Arana, "Real time monitoring of the impedance characteristics of *Staphylococcal* bacterial biofilm cultures with a modified CDC reactor system," *Biosensors & Bioelectronics*, vol. 38, pp. 226-232, 2012.
[40] G. M. Bruinsma, H. C. van der Mei, and H. J. Busscher, "Bacterial adhesion to surface hydrophilic and hydrophobic contact lenses," *Biomaterials*, vol. 22, pp. 3217-3224, 2001.
[41] J. E. G. Gonzalez, F. J. H. Santana, and J. C. Mirza-Rosca, "Effect of bacterial biofilm on 316 SS corrosion in natural seawater by EIS," *Corrosion Science*, vol. 40, pp. 2141-2154, 1998.
[42] E. Kuş, K. Nealson, and F. Mansfeld, "The effect of different exposure conditions on the biofilm/copper interface," *Corrosion Science*, vol. 49, pp. 3421-3427, 2007.
[43] S. Flint and G. Wolfaardt, "Corrosion and Fouling," in *Microbial Biofilms: Current Research and Applications*, Horizon Scientific Press, 2012, pp. 111-128.
[44] J. F. Frank, L. A. Jaykus, H. H. Wang, and L. S. Schlesinger, "Biofilms in the food environment," in *Food-Borne Microbes: Shaping the Host Ecosystem*, Wiley, 2009, pp. 95-115.
[45] A. Nakhamchik, C. Wilde, and D. A. Rowe-Magnus, "Cyclic-di-GMP regulates extracellular polysaccharide production, biofilm formation, and rugose colony development by *Vibrio vulnificus*," *Applied and Environmental Microbiology*, vol. 74, pp. 4199-4209, 2008.
[46] U. K. Gursoy, M. Gursoy, O. V. Gursoy, L. Cakmakci, E. Könönen, and V. J. Uitto, "Anti-biofilm properties of *Satureja hortensis* L. essential oil against periodontal pathogens," *Anaerobe*, vol. 15, pp. 164-167, 2009.
[47] T. Rudrappa, K. J. Czymmek, P. W. Paré, and H. P. Bais, "Root-secreted malic acid recruits beneficial soil bacteria," *Plant Physiology*, vol. 148, pp. 1547-1556, 2008.
[48] C. Nicolella, M. C. van Loosdrecht, and J. J. Heijnen, "Wastewater treatment with particulate biofilm reactors," *Journal of Biotechnology*, vol. 80, pp. 1-33, 2000.
[49] S. Andersson, G. Kuttuva Rajarao, C. J. Land, and G. Dalhammar, "Biofilm formation and interactions of bacterial strains found in wastewater treatment systems," *FEMS Microbiology Letters*, vol. 283, pp. 83-90, 2008.
[50] Water Environment Federation, *Biofilm Reactors*, McGraw-Hill., 2011.

[51] G. Pastorella, G. Gazzola, S. Guadarrama, and E. Marsili, "Biofilms: Applications in bioremediation," in *Microbial Biofilms: Current Research and Applications*, Horizon Scientific Press, 2012, pp. 73-98.
[52] S. Wuertz, P. L. Bishop, and P. A. Wilderer, *Biofilms in Wastewater Treatment: An Interdisciplinary Approach*, IWA Publishing, 2003.
[53] Y. Zhang and I. Angelidaki, "Submersible microbial fuel cell sensor for monitoring microbial activity and BOD in groundwater: Focusing on impact of anodic biofilm on sensor applicability," *Biotechnology and Bioengineering*, vol. 108, pp. 2339-2347, 2011.
[54] R. Singh, D. Paul, and R. K. Jain, "Biofilms: implications in bioremediation," *Trends in Microbiology*, vol. 14, pp. 389-397, 2006.
[55] G. M. Gadd, "Microbial influence on metal mobility and application for bioremediation," *Geoderma*, vol. 122, pp. 109-119, 2004.
[56] R. Gross, A. Schmid, and K. Buehler, "Catalytic biofilms: A powerful concept for future bioprocesses," in *Microbial Biofilms: Current Research and Applications*, Horizon Scientific Press, 2012, pp. 193-222.
[57] C. Picioreanu, I. M. Head, K. P. Katuri, M. van Loosdrecht, and K. Scott, "A computational model for biofilm-based microbial fuel cells," *Water Research*, vol. 41, pp. 2921-2940, 2007.
[58] R. P. Ramasamy, Z. Ren, M. M. Mench, and J. M. Regan, "Impact of initial biofilm growth on the anode impedance of microbial fuel cells," *Biotechnology and Bioengineering*, vol. 101, pp. 101-108, 2008.
[59] K. Nishio, A. Kouzuma, S. Kato, and K. Watanabe, "Energy from slime? Power from microbial fuel cells," in *Microbial Biofilms: Current Research and Applications*, Horizon Scientific Press, 2012, pp. 175-192.
[60] Z. W. Wang and S. Chen, "Potential of biofilm-based biofuel production," *Applied Microbiology and Biotechnology*, vol. 83, pp. 1-18, 2009.
[61] H. Vlamakis, Y. Chai, P. Beauregard, R. Losick, and R. Kolter, "Sticking together: Building a biofilm the *Bacillus subtilis* way," *Nature Reviews Microbiology*, vol. 11, pp. 157-168, 2013.
[62] H. P. Bais, R. Fall, and J. M. Vivanco, "Biocontrol of *Bacillus subtilis* against infection of arabidopsis roots by *Pseudomonas syringae* is facilitated by biofilm formation and surfactin," *Plant Physiology*, vol. 134, pp. 307-319, 2004.
[63] R. Fall, R. F. Kinsinger, and K. a. Wheeler, "A simple method to isolate biofilm-forming *Bacillus subtilis* and related species from plant roots," *Systematic and Applied Microbiology*, vol. 27, pp. 372-379, 2004.
[64] L. Nielsen, X. Li, and L. J. Halverson, "Cell-cell and cell-surface interactions mediated by cellulose and a novel exopolysaccharide contribute to *Pseudomonas putida* biofilm formation and fitness under water-limiting conditions," *Environmental Microbiology*, vol. 13, pp. 1342-1356, 2011.
[65] G. A. O'Toole, L. A. Pratt, P. I. Watnick, D. K. Newman, V. B. Weaver, and R. Kolter, "Genetic approaches to study of biofilms," *Methods in Enzymology*, vol. 310, pp. 91-109, 1999.
[66] S. L. Kuchma and G. A. O'Toole, "Surface-induced and biofilm-induced changes in gene expression," *Current Opinion in Biotechnology*, vol. 11, pp. 429-433, 2000.
[67] D. Ren, L. A. Bedzyk, R. W. Ye, S. M. Thomas, and T. K. Wood, "Differential gene expression shows natural brominated furanones interfere

with the autoinducer-2 bacterial signaling system of *Escherichia coli*," *Biotechnology and Bioengineering,* vol. 88, pp. 630-642, 2004.

[68] D. Ren, R. Zuo, A. F. Gonzalez Barrios, L. A. Bedzyk, G. R. Eldridge, M. E. Pasmore, and T. K. Wood, "Differential gene expression for investigation of *Escherichia coli* biofilm inhibition by plant extract ursolic acid," *Applied and Environmental Microbiology,* vol. 71, pp. 4022-4034, 2005.

[69] C. Solano, B. García, J. Valle, C. Berasain, J. M. Ghigo, C. Gamazo, and I. Lasa, "Genetic analysis of *Salmonella enteritidis* biofilm formation: Critical role of cellulose," *Molecular Microbiology,* vol. 43, pp. 793-808, 2002.

[70] D. Ren, L. A. Bedzyk, P. Setlow, S. M. Thomas, R. W. Ye, and T. K. Wood, "Gene expression in *Bacillus subtilis* surface biofilms with and without sporulation and the importance of yveR for biofilm maintenance," *Biotechnology and Bioengineering,* vol. 86, pp. 344-364, 2004.

[71] B. K. Hammer and B. L. Bassler, "Quorum sensing controls biofilm formation in *Vibrio cholerae*," *Molecular Microbiology,* vol. 50, pp. 101-104, 2003.

[72] J. P. Ward and J. R. King, "Thin-film modelling of biofilm growth and quorum sensing," *Journal of Engineering Mathematics,* vol. 73, pp. 71-92, 2011.

[73] S. H. Hong, M. Hegde, J. Kim, X. Wang, A. Jayaraman, and T. K. Wood, "Synthetic quorum-sensing circuit to control consortial biofilm formation and dispersal in a microfluidic device," *Nature Communications,* vol. 3, 613, 2012.

[74] D. J. Hassett, J. Cuppoletti, B. Trapnell, S. V. Lymar, J. J. Rowe, S. S. Yoon, G. M. Hilliard, K. Parvatiyar, M. C. Kamani, D. J. Wozniak, S. H. Hwang, T. R. McDermott, and U. A. Ochsner, "Anaerobic metabolism and quorum sensing by *Pseudomonas aeruginosa* biofilms in chronically infected cystic fibrosis airways: Rethinking antibiotic treatment strategies and drug targets," *Advanced Drug Delivery Reviews,* vol. 54, pp. 1425-1443, 2002.

[75] V. Janakiraman, D. Englert, A. Jayaraman, and H. Baskaran, "Modeling growth and quorum sensing in biofilms grown in microfluidic chambers," *Annals of Biomedical Engineering,* vol. 37, pp. 1206-1216, 2009.

[76] M. R. Frederick, C. Kuttler, B. A. Hense, and H. J. Eberl, "A mathematical model of quorum sensing regulated EPS production in biofilm communities," *Theoretical Biology & Medical Modelling,* vol. 8, pp. 1-29, 2011.

[77] R. M. Donlan, "Role of biofilms in antimicrobial resistance," *ASAIO Journal,* vol. 46, pp. 47-52, 2000.

[78] J. W. Costerton, *The Biofilm Primer* vol. 1, Springer, 2007.

[79] J. B. Xavier, C. Picioreanu, and M. C. M. van Loosdrecht, "A framework for multidimensional modelling of activity and structure of multispecies biofilms," *Environmental Microbiology,* vol. 7, pp. 1085-1103, 2005.

[80] J. B. Xavier, D. C. White, and J. S. Almeida, "Automated biofilm morphology quantification from confocal laser scanning microscopy imaging," *Water Science & Technology* vol. 47, pp. 31-37, 2003.

[81] M. E. Davey and G. A. O'toole, "Microbial biofilms: From ecology to molecular genetics," *Microbiology and Molecular Biology Reviews,* vol. 64, pp. 847-867, 2000.

[82] O. E. Constantin, "Air-liquid interface biofilms of *Bacillus cereus*, *Bacillus subtilis* and *Pseudomonas fluorescens*," *Journal of Agroalimentary Processes and Technologies,* vol. 3, pp. 317-320, 2010.

[83] J. G. E. Wijman, P. P. L. A. de Leeuw, R. Moezelaar, M. H. Zwietering, and T. Abee, "Air-liquid interface biofilms of *Bacillus cereus*: formation, sporulation, and dispersion," *Applied and Environmental Microbiology,* vol. 73, pp. 1481-1488, 2007.

[84] A. Koza, P. D. Hallett, C. D. Moon, and A. J. Spiers, "Characterization of a novel air-liquid interface biofilm of *Pseudomonas fluorescens* SBW25," *Microbiology* vol. 155, pp. 1397-1406, 2009.

[85] A. J. Spiers, J. Bohannon, S. M. Gehrig, and P. B. Rainey, "Biofilm formation at the air-liquid interface by the *Pseudomonas fluorescens* SBW25 wrinkly spreader requires an acetylated form of cellulose," *Molecular Microbiology*, vol. 50, pp. 15-27, 2003.

[86] D. M. Goeres, M. A. Hamilton, N. A. Beck, K. Buckingham-Meyer, J. D. Hilyard, L. R. Loetterle, L. A. Lorenz, D. K. Walker, and P. S. Stewart, "A method for growing a biofilm under low shear at the air-liquid interface using the drip flow biofilm reactor," *Nature Protocols,* vol. 4, pp. 783-788, 2009.

[87] M. Robertson, S. M. Hapca, O. Moshynets, and A. J. Spiers, "Air-liquid interface biofilm formation by psychrotrophic pseudomonads recovered from spoilt meat," *Antonie van Leeuwenhoek,* vol. 103, pp. 251-259, 2013.

[88] J. E. Król, H. D. Nguyen, L. M. Rogers, H. Beyenal, S. M. Krone, and E. M. Top, "Increased transfer of a multidrug resistance plasmid in *Escherichia coli* biofilms at the air-liquid interface," *Applied and Environmental Microbiology*, vol. 77, pp. 5079-5088, 2011.

[89] C. Wu, J. Y. Lim, G. G. Fuller, and L. Cegelski, "Disruption of *Escherichia coli* amyloid-integrated biofilm formation at the air-liquid interface by a polysorbate surfactant," *Langmuir,* vol. 29, pp. 920-926, 2013.

[90] A. J. Spiers, D. Arnold, C. Moon, and T. Timms-Wilson, "A survey of A-L biofilm formation and cellulose expression amongst soil and plant-associated *Pseudomonas* isolates," in *Microbial Ecology of Aerial Plant Surfaces*, CABI, 2006, pp. 121-132.

[91] M. Van Loosdrecht, J. Lyklema, W. Norde, and A. Zehnder, "Influence of interfaces on microbial activity," *Microbiological Reviews,* vol. 54, pp. 75-87, 1990.

[92] K. P. Lemon, a. M. Earl, H. C. Vlamakis, C. Aguilar, and R. Kolter, "Biofilm development with an emphasis on *Bacillus subtilis*," in *Bacterial Biofilms*, Springer Berlin Heidelberg, 2008, pp. 1-16.

[93] A. J. Spiers, S. G. Kahn, J. Bohannon, M. Travisano, and P. B. Rainey, "Adaptive divergence in experimental populations of *Pseudomonas fluorescens*. I. Genetic and phenotypic bases of wrinkly spreader fitness," *Genetics*, vol. 161, pp. 33-46, 2002.

[94] K. Scher, U. Romling, and S. Yaron, "Effect of heat, acidification, and chlorination on *Salmonella enterica* serovar Typhimurium cells in a biofilm formed at the air-liquid interface," *Applied and Environmental Microbiology,* vol. 71, pp. 1163-1168, 2005.

[95] A. T. Henrici, "Studies of freshwater bacteria: I. A direct microscopic technique," *Journal of Bacteriology,* vol. 25, pp. 277-287, 1933.

[96] R. J. C. McLean, C. L. Bates, M. B. Barnes, C. L. McGowin, and G. M. Aron, "Methods of studying biofilms," in *Microbial Biofilms*, ASM Press, 2004, pp. 379-413.

[97] N. Narisawa, S. Furukawa, H. Ogihara, and M. Yamasaki, "Estimation of the biofilm formation of *Escherichia coli* K-12 by the cell number," *Journal of Bioscience and Bioengineering*, vol. 99, pp. 78-80, 2005.

[98] J. J. Harrison, C. A. Stremick, R. J. Turner, N. D. Allan, M. E. Olson, and H. Ceri, "Microtiter susceptibility testing of microbes growing on peg lids: A miniaturized biofilm model for high-throughput screening," *Nature Protocols*, vol. 5, pp. 1236-1254, 2010.

[99] H. Jin, R. Zhou, M. Kang, R. Luo, X. Cai, and H. Chen, "Biofilm formation by field isolates and reference strains of *Haemophilus parasuis*," *Veterinary Microbiology*, vol. 118, pp. 117-123, 2006.

[100] J. H. Merritt, D. E. Kadouri, and G. A. O'Toole, "Growing and analyzing static biofilms," *Current Protocols in Microbiology*, vol. 22, 1B.1.1–1B.1.18, 2011.

[101] A. J. McBain, "*In vitro* biofilm models: An overview," in *Advances in Applied Microbiology*. vol. 69, ed, 2009, pp. 99-132.

[102] N. Yurt, H. Beyenal, J. Sears, and Z. Lewandowski, "Quantifying selected growth parameters of *Leptothrix discophora* SP-6 in biofilms from oxygen concentration profiles," *Chemical Engineering Science*, vol. 58, pp. 4557-4566, 2003.

[103] M. Asally, M. Kittisopikul, P. Rue, Y. Du, Z. Hu, T. Cagatay, A. B. Robinson, H. Lu, J. Garcia-Ojalvo, and G. M. Suel, "Localized cell death focuses mechanical forces during 3D patterning in a biofilm," *Proceedings of the National Academy of Sciences*, vol. 109, pp. 18891-18896, 2012.

[104] E. D. Giaouris and G. J. E. Nychas, "The adherence of *Salmonella Enteritidis* PT4 to stainless steel: The importance of the air-liquid interface and nutrient availability," *Food Microbiology*, vol. 23, pp. 747-752, 2006.

[105] O. E. Constantin, "Bacterial biofilms formation at air liquid interfaces," *Innovative Romanian Food Biotechnology*, vol. 5, pp. 18-22, 2009.

[106] S. B. Peterson, Y. Irie, B. R. Borlee, K. Murakami, J. J. Harrison, K. M. Colvin, and M. R. Parsek, "Different methods for culturing biofilms *in vitro*," in *Biofilm Infections*, Springer, 2011, pp. 251-266.

[107] M. Weiss Nielsen, C. Sternberg, S. Molin, and B. Regenberg, "*Pseudomonas aeruginosa* and *Saccharomyces cerevisiae* biofilm in flow cells," *Journal of Visualized Experiments*, e2383, 2011.

[108] J. C. Garcia-Betancur, A. Yepes, J. Schneider, and D. Lopez, "Single-cell analysis of *Bacillus subtilis* biofilms using fluorescence microscopy and flow cytometry," *Journal of Visualized Experiments*, e3796, 2012.

[109] V. Jones, "Disinfection tests with intact biofilms: Combined use of the Modified Robbins Device with impedance detection," *Journal of Microbiological Methods*, vol. 21, pp. 15-26, 1995.

[110] M. Jacob, "Biofilms, a new approach to the microbiology of dental plaque," *Odontology*, vol. 94, pp. 1-9, 2006.

[111] Z. N. Pierre, "Acoustically-levitated drop reactor (ldr) employable for kinetics measurements of biochemical networks," Ph.D., Chemistry, University of Illinois at Urbana-Champaign, 2011.

[112] S. Kakaç, B. Kosoy, D. Li, and A. Pramuanjaroenkij, *Microfluidics Based microsystems: Fundamentals and Applications*, Springer, 2010.

[113] T. Das and S. Chakraborty, *Microfluidics and Microfabrication*, Springer US, 2010.

[114] D. N. Breslauer, P. J. Lee, and L. P. Lee, "Microfluidics-based systems biology," *Molecular Biosystems,* vol. 2, pp. 97-112, 2006.
[115] D. J. Beebe, G. A. Mensing, and G. M. Walker, "Physics and applications of microfluidics in biology," *Annual Review of Biomedical Engineering,* vol. 4, pp. 261-286, 2002.
[116] S. Ishii, K. Tago, and K. Senoo, "Single-cell analysis and isolation for microbiology and biotechnology: Methods and applications," *Applied Microbiology and Biotechnology,* vol. 86, pp. 1281-1292, 2010.
[117] Y. Marcy, C. Ouverney, E. M. Bik, T. Lösekann, N. Ivanova, H. G. Martin, E. Szeto, D. Platt, P. Hugenholtz, D. A. Relman, and S. R. Quake, "Dissecting biological "dark matter" with single-cell genetic analysis of rare and uncultivated TM7 microbes from the human mouth," *Proceedings of the National Academy of Sciences,* vol. 104, pp. 11889-11894, 2007.
[118] S. Saleh-Lakha and J. T. Trevors, "Perspective: Microfluidic applications in microbiology," *Journal of Microbiological Methods,* vol. 82, pp. 108-111, 2010.
[119] A. B. Theberge, F. Courtois, Y. Schaerli, M. Fischlechner, C. Abell, F. Hollfelder, and W. T. S. Huck, "Microdroplets in microfluidics: An evolving platform for discoveries in chemistry and biology," *Angewandte Chemie (International ed. in English),* vol. 49, pp. 5846-5868, 2010.
[120] A. Torkkeli, *Droplet Microfluidics On A Planar Surface,* VTT publications, 2003.
[121] R. Seemann, M. Brinkmann, T. Pfohl, and S. Herminghaus, "Droplet based microfluidics," *Reports on Progress in Physics* vol. 75, 016601, 2012.
[122] S. Y. Teh, R. Lin, L. H. Hung, and A. P. Lee, "Droplet microfluidics," *Lab on a Chip,* vol. 8, pp. 198-220, 2008.
[123] P. Garstecki, M. J. Fuerstman, H. A. Stone, and G. M. Whitesides, "Formation of droplets and bubbles in a microfluidic T-junction-scaling and mechanism of break-up," *Lab on a Chip,* vol. 6, pp. 437-446, 2006.
[124] J. Berthier and K. Brakke, *The Physics of Microdroplets,* Wiley. com, 2012.
[125] C. Zhang and D. Xing, "Decreasing microfluidic evaporation loss using the HMDL method: Open systems for nucleic acid amplification and analysis," *Microfluidics and Nanofluidics,* vol. 9, pp. 17-30, 2009.
[126] M. Zimmermann, S. Bentley, H. Schmid, P. Hunziker, and E. Delamarche, "Continuous flow in open microfluidics using controlled evaporation," *Lab on a Chip,* vol. 5, pp. 1355-1359, 2005.
[127] H. Y. N. Holman, R. Miles, Z. Hao, E. Wozei, L. M. Anderson, and H. Yang, "Real-time chemical imaging of bacterial activity in biofilms using open-channel microfluidics and synchrotron FTIR spectromicroscopy," *Analytical Chemistry,* vol. 81, pp. 8564-8570, 2009.
[128] G. V. Kaigala, R. D. Lovchik, and E. Delamarche, "Microfluidics in the "open space" for performing localized chemistry on biological interfaces," *Angewandte Chemie (International ed. in English),* vol. 51, pp. 11224-11240, 2012.
[129] M. A. M. A. Qasaimeh, S. G. S. G. Ricoult, and D. Juncker, "Microfluidic probes for use in life sciences and medicine," *Lab on a Chip,* vol. 13, pp. 40-50, 2013.
[130] S. Semenov, V. M. Starov, M. G. Velarde, and R. G. Rubio, "Droplets evaporation: Problems and solutions," *The European Physical Journal Special Topics,* vol. 197, pp. 265-278, 2011.

[131] J. Kim, M. Hegde, S. H. Kim, T. K. Wood, and A. Jayaraman, "A microfluidic device for high throughput bacterial biofilm studies," *Lab on a Chip*, vol. 12, pp. 1157-1163, 2012.
[132] A. P. Mosier, A. E. Kaloyeros, and N. C. Cady, "A novel microfluidic device for the *in situ* optical and mechanical analysis of bacterial biofilms," *Journal of Microbiological Methods*, vol. 91, pp. 198-204, 2012.
[133] K. Matsuura, Y. Asano, A. Yamada, and K. Naruse, "Detection of *Micrococcus luteus* biofilm formation in microfluidic environments by pH measurement using an ion-sensitive field-effect transistor," *Sensors (Basel, Switzerland)*, vol. 13, pp. 2484-2493, 2013.
[134] M. R. Benoit, C. G. Conant, C. Ionescu-Zanetti, M. Schwartz, and A. Matin, "New device for high-throughput viability screening of flow biofilms," *Applied and Environmental Microbiology*, vol. 76, pp. 4136-4142, 2010.
[135] M. Skolimowski, M. W. Nielsen, J. Emnéus, S. Molin, R. Taboryski, C. Sternberg, M. Dufva, and O. Geschke, "Microfluidic dissolved oxygen gradient generator biochip as a useful tool in bacterial biofilm studies," *Lab on a Chip*, vol. 10, pp. 2162-2169, 2010.
[136] K. P. Kim, Y. G. Kim, C. H. Choi, H. E. Kim, S. H. Lee, W. S. Chang, and C. S. Lee, "*In situ* monitoring of antibiotic susceptibility of bacterial biofilms in a microfluidic device," *Lab on a Chip*, vol. 10, pp. 3296-3299, 2010.
[137] D. N. Hohne, J. G. Younger, and M. J. Solomon, "Flexible microfluidic device for mechanical property characterization of soft viscoelastic solids such as bacterial biofilms," *Langmuir*, vol. 25, pp. 7743-7751, 2009.
[138] J. Kim, H. S. Kim, S. Han, J. Y. Lee, J. E. Oh, S. Chung, and H. D. Park, "Hydrodynamic effects on bacterial biofilm development in a microfluidic environment," *Lab on a Chip*, vol. 13, pp. 1846-1849, 2013.
[139] R. Rusconi, S. Lecuyer, L. Guglielmini, and H. A. Stone, "Laminar flow around corners triggers the formation of biofilm streamers," *Journal of the Royal Society Interface*, vol. 7, pp. 1293-1299, 2010.
[140] Y. J. Eun and D. B. Weibel, "Fabrication of microbial biofilm arrays by geometric control of cell adhesion," *Langmuir*, vol. 25, pp. 4643-4654, 2009.
[141] Y. Yawata, K. Toda, E. Setoyama, J. Fukuda, H. Suzuki, H. Uchiyama, and N. Nomura, "Monitoring biofilm development in a microfluidic device using modified confocal reflection microscopy," *Journal of Bioscience and Bioengineering*, vol. 110, pp. 377-380, 2010.
[142] M. T. Meyer, V. Roy, W. E. Bentley, and R. Ghodssi, "Development and validation of a microfluidic reactor for biofilm monitoring via optical methods," *Journal of Micromechanics and Microengineering*, vol. 21, 054023, 2011.
[143] J. Gottschamel, L. Richter, A. Mak, C. Jungreuthmayer, G. Birnbaumer, M. Milnera, H. Brückl, and P. Ertl, "Development of a disposable microfluidic biochip for multiparameter cell population measurements," *Analytical Chemistry*, vol. 81, pp. 8503-8512, 2009.
[144] L. Pires, K. Sachsenheimer, T. Kleintschek, A. Waldbaur, T. Schwartz, and B. E. Rapp, "Online monitoring of biofilm growth and activity using a combined multi-channel impedimetric and amperometric sensor," *Biosensors & Bioelectronics*, vol. 47, pp. 157-163, 2013.
[145] M. Hoorfar, M. A. Kurz, and A. W. Neumann, "Evaluation of the surface tension measurement of axisymmetric drop shape analysis (ADSA) using a

shape parameter," *Colloids and Surfaces A: Physicochemical and Engineering Aspects,* vol. 260, pp. 277-285, 2005.
[146] M. Hoorfar and A. W Neumann, "Recent progress in axisymmetric drop shape analysis (ADSA)," *Advances in Colloid and Interface Science,* vol. 121, pp. 25-49, 2006.
[147] A. Kalantarian, R. David, and A. W. Neumann, "Methodology for high accuracy contact angle measurement," *Langmuir,* vol. 25, pp. 14146-14154, 2009.
[148] T. T. Nellimoottil, P. N. Rao, S. S. Ghosh, and A. Chattopadhyay, "Evaporation-induced patterns from droplets containing motile and nonmotile bacteria," *Langmuir,* vol. 23, pp. 8655-8658, 2007.
[149] S. T. Chang and O. D. Velev, "Evaporation-induced particle microseparations inside droplets floating on a chip," *Langmuir,* vol. 22, pp. 1459-1468, 2006.
[150] Y. Cai and B. M. Zhang Newby, "Marangoni flow-induced self-assembly of hexagonal and stripelike nanoparticle patterns," *Journal of the American Chemical Society,* vol. 130, pp. 6076-6077, 2008.
[151] K. Birdi, D. Vu, and A. Winter, "A study of the evaporation rates of small water drops placed on a solid surface," *The Journal of Physical Chemistry,* vol. 93, pp. 3702-3703, 1989.
[152] H. Hu and R. G. Larson, "Evaporation of a sessile droplet on a substrate," *The Journal of Physical Chemistry B,* vol. 106, pp. 1334-1344, 2002.
[153] H. Y. Erbil, "Evaporation of pure liquid sessile and spherical suspended drops: A review," *Advances in Colloid and Interface Science,* vol. 170, pp. 67-86, 2012.
[154] H. Y. Erbil, G. McHale, and M. I. Newton, "Drop evaporation on solid surfaces: Constant contact angle mode," *Langmuir,* vol. 18, pp. 2636-2641, 2002.
[155] H. Hu and R. G. Larson, "Microflow in an evaporating sessile droplet," *Langmuir,* vol. 21, pp. 8271-8279, 2005.
[156] R. D. Deegan, O. Bakajin, T. F. Dupont, G. Huber, S. R. Nagel, T. A. Witten, and S. E. Ave, "Capillary flow as the cause of ring stains from dried liquid drops," *Nature,* vol. 389, pp. 827-829, 1997.
[157] H. Hu and R. G. Larson, "Analysis of the effects of Marangoni stresses on the microflow in an evaporating sessile droplet," *Langmuir,* vol. 21, pp. 3972-3980, 2005.
[158] X. Xu and J. Luo, "Marangoni flow in an evaporating water droplet," *Applied Physics Letters,* vol. 91, 124102, 2007.
[159] S. G. Yiantsios and B. G. Higgins, "Marangoni flows during drying of colloidal films," *Physics of Fluids,* vol. 18, 082103, 2006.
[160] P. J. Yunker, T. Still, M. A. Lohr, and A. G. Yodh, "Suppression of the coffee-ring effect by shape-dependent capillary interactions," *Nature,* vol. 476, pp. 308-311, 2011.
[161] K. L. Maki and S. Kumar, "Fast evaporation of spreading droplets of colloidal suspensions," *Langmuir,* vol. 27, pp. 11347-11363, 2011.
[162] X. Shen, C. M. Ho, and T. S. Wong, "Minimal size of coffee ring structure," *The Journal of Physical Chemistry B,* vol. 114, pp. 5269-5274, 2010.
[163] L. Hall-Stoodley, J. W. Costerton, and P. Stoodley, "Bacterial biofilms: From the natural environment to infectious diseases," *Nature Reviews Microbiology,* vol. 2, pp. 95-108, 2004.

[164] B. Meyer, "Approaches to prevention, removal and killing of biofilms," *International Biodeterioration & Biodegradation,* vol. 51, pp. 249-253, 2003.
[165] V. Hancock, I. L. Witsø, and P. Klemm, "Biofilm formation as a function of adhesin, growth medium, substratum and strain type," *International Journal of Medical Microbiology,* vol. 301, pp. 570-576, 2011.
[166] K. A. Whitehead and J. Verran, "The effect of surface properties and application method on the retention of *Pseudomonas aeruginosa* on uncoated and titanium-coated stainless steel," *International Biodeterioration & Biodegradation,* vol. 60, pp. 74-80, 2007.
[167] L. Tang, S. Pillai, N. P. Revsbech, A. Schramm, C. Bischoff, and R. L. Meyer, "Biofilm retention on surfaces with variable roughness and hydrophobicity," *Biofouling,* vol. 27, pp. 111-121, 2011.
[168] J. Kim, H. D. Park, and S. Chung, "Microfluidic approaches to bacterial biofilm formation," *Molecules,* vol. 17, pp. 9818-9834, 2012.
[169] J. H. Lee, J. B. Kaplan, and W. Y. Lee, "Microfluidic devices for studying growth and detachment of *Staphylococcus epidermidis* biofilms," *Biomedical Microdevices,* vol. 10, pp. 489-498, 2008.
[170] A. Y. Hsiao, Y. C. Tung, X. Qu, L. R. Patel, K. J. Pienta, and S. Takayama, "384 hanging drop arrays give excellent Z-factors and allow versatile formation of co-culture spheroids," *Biotechnology and Bioengineering,* vol. 109, pp. 1293-1304, 2012.
[171] Y. C. Tung, A. Y. Hsiao, S. G. Allen, Y. S. Torisawa, M. Ho, and S. Takayama, "High-throughput 3D spheroid culture and drug testing using a 384 hanging drop array," *The Analyst,* vol. 136, pp. 473-478, 2011.
[172] X. Wang and P. Yang, "*In vitro* differentiation of mouse embryonic stem (mES) cells using the hanging drop method," *Journal of Visualized Experiments,* e825, 2008.
[173] A. Heydorn, A. T. Nielsen, M. Hentzer, C. Sternberg, M. Givskov, B. K. Ersbøll, and S. Molin, "Quantification of biofilm structures by the novel computer program COMSTAT," *Microbiology,* vol. 146, pp. 2395-2407, 2000.
[174] R. Savino, D. Paterna, and N. Favaloro, "Buoyancy and Marangoni effects in an evaporating drop," *Journal of Thermophysics and Heat Transfer,* vol. 16, pp. 562-574, 2002.
[175] M. Klausen, A. Aaes‐Jørgensen, S. Molin, and T. Tolker‐Nielsen, "Involvement of bacterial migration in the development of complex multicellular structures in *Pseudomonas aeruginosa* biofilms," *Molecular Microbiology,* vol. 50, pp. 61-68, 2003.
[176] H. M. Dalton, L. K. Poulsen, P. Halasz, M. L. Angles, A. E. Goodman, and K. C. Marshall, "Substratum-induced morphological changes in a marine bacterium and their relevance to biofilm structure," *Journal of Bacteriology,* vol. 176, pp. 6900-6906, 1994.
[177] D. Evans, D. Allison, M. Brown, and P. Gilbert, "Effect of growth-rate on resistance of Gram-negative biofilms to cetrimide," *Journal of Antimicrobial Chemotherapy,* vol. 26, pp. 473-478, 1990.
[178] D. Romero, C. Aguilar, R. Losick, and R. Kolter, "Amyloid fibers provide structural integrity to *Bacillus subtilis* biofilms," *Proceedings of the National Academy of Sciences,* vol. 107, pp. 2230-2234, 2010.
[179] G. P. Dubey and S. Ben-Yehuda, "Intercellular nanotubes mediate bacterial communication," *Cell,* vol. 144, pp. 590-600, 2011.

[180] J. Rogers, A. Dowsett, P. Dennis, J. Lee, and C. Keevil, "Influence of plumbing materials on biofilm formation and growth of *Legionella pneumophila* in potable water systems," *Applied and Environmental Microbiology*, vol. 60, pp. 1842-1851, 1994.
[181] B. K. Yen, A. Günther, M. A. Schmidt, K. F. Jensen, and M. G. Bawendi, "A microfabricated gas–liquid segmented flow reactor for high–temperature synthesis: The case of CdSe quantum dots," *Angewandte Chemie*, vol. 117, pp. 5583-5587, 2005.
[182] C. N. Baroud, F. Gallaire, and R. Dangla, "Dynamics of microfluidic droplets," *Lab on a Chip*, vol. 10, pp. 2032-2045, 2010.
[183] P. Garstecki, A. Ganan-Calvo, and G. Whitesides, "Formation of bubbles and droplets in microfluidic systems," *Technical Sciences*, vol. 53, pp. 361-372, 2005.
[184] A. Günther, S. A. Khan, M. Thalmann, F. Trachsel, and K. F. Jensen, "Transport and reaction in microscale segmented gas-liquid flow," *Lab on a Chip*, vol. 4, pp. 278-286, 2004.
[185] T. Cubaud, M. Tatineni, X. Zhong, and C. M. Ho, "Bubble dispenser in microfluidic devices," *Physical Review E*, vol. 72, 037302, 2005.
[186] M. Muradoglu and H. A. Stone, "Motion of large bubbles in curved channels," *Journal of Fluid Mechanics*, vol. 570, pp. 455-466, 2007.
[187] Z. Che, T. N. Wong, and N. T. Nguyen, "An analytical model for a liquid plug moving in curved microchannels," *International Journal of Heat and Mass Transfer*, vol. 53, pp. 1977-1985, 2010.
[188] D. M. Fries and P. R. von Rohr, "Liquid mixing in gas-liquid two-phase flow by meandering microchannels," *Chemical Engineering Science*, vol. 64, pp. 1326-1335, 2009.
[189] S. A. K. Oskooei and D. Sinton, "Partial wetting gas-liquid segmented flow microreactor," *Lab on a Chip*, vol. 10, pp. 1732-1734, 2010.
[190] B. E. Rittman, "The effect of shear stress on biofilm loss rate," *Biotechnology and Bioengineering*, vol. 24, pp. 501-506, 1982.
[191] W. E. Thomas, L. M. Nilsson, M. Forero, E. V. Sokurenko, and V. Vogel, "Shear-dependent 'stick-and-roll' adhesion of type 1 fimbriated *Escherichia coli*," *Molecular Microbiology*, vol. 53, pp. 1545-1557, 2004.
[192] W. E. Thomas, E. Trintchina, M. Forero, V. Vogel, and E. V. Sokurenko, "Bacterial adhesion to target cells enhanced by shear force," *Cell*, vol. 109, pp. 913-923, 2002.
[193] A. Rmaile, D. Carugo, L. Capretto, M. Aspiras, M. De Jager, M. Ward, and P. Stoodley, "Removal of interproximal dental biofilms by high-velocity water microdrops," *Journal of Dental Research*, vol. 93, pp. 68-73, 2014.
[194] M. R. Parini, D. L. Eggett, and W. G. Pitt, "Removal of *Streptococcus mutans* biofilm by bubbles," *Journal of Clinical Periodontology*, vol. 32, pp. 1151-1156, 2005.
[195] M. R. Parini and W. G. Pitt, "Dynamic removal of oral biofilms by bubbles," *Colloids and Surfaces B: Biointerfaces*, vol. 52, pp. 39-46, 2006.
[196] S. Van der Graaf, T. Nisisako, C. Schroen, R. Van Der Sman, and R. Boom, "Lattice Boltzmann simulations of droplet formation in a T-shaped microchannel," *Langmuir*, vol. 22, pp. 4144-4152, 2006.
[197] S. Kefayati, D. W. Holdsworth, and T. L. Poepping, "Turbulence intensity measurements using particle image velocimetry in diseased carotid artery

models: Effect of stenosis severity, plaque eccentricity, and ulceration," *Journal of Biomechanics,* vol. 47, pp. 253-263, 2014.

[198] C. Y. Lee, C. L. Chang, Y. N. Wang, and L. M. Fu, "Microfluidic mixing: A review," *International Journal of Molecular Sciences,* vol. 12, pp. 3263-3287, 2011.

[199] W. Shumi, J. Lim, S. W. Nam, K. Lee, S. H. Kim, M. H. Kim, K. S. Cho, and S. Park, "Environmental factors that affect *Streptococcus mutans* biofilm formation in a microfluidic device mimicking teeth," *BioChip Journal,* vol. 4, pp. 257-263, 2010.

[200] M. Kuehn, M. Hausner, H. J. Bungartz, M. Wagner, P. A. Wilderer, and S. Wuertz, "Automated confocal laser scanning microscopy and semiautomated image processing for analysis of biofilms," *Applied and Environmental Microbiology,* vol. 64, pp. 4115-4127, 1998.

[201] B. Dunsmore, A. Jacobsen, L. Hall-Stoodley, C. Bass, H. Lappin-Scott, and P. Stoodley, "The influence of fluid shear on the structure and material properties of sulphate-reducing bacterial biofilms," *Journal of Industrial Microbiology and Biotechnology,* vol. 29, pp. 347-353, 2002.

[202] P. Stoodley, R. Cargo, C. J. Rupp, S. Wilson, and I. Klapper, "Biofilm material properties as related to shear-induced deformation and detachment phenomena," *Journal of Industrial Microbiology and Biotechnology,* vol. 29, pp. 361-367, 2002.

[203] S. Kuhn, R. L. Hartman, M. Sultana, K. D. Nagy, S. Marre, and K. F. Jensen, "Teflon-coated silicon microreactors: Impact on segmented liquid-liquid multiphase flows," *Langmuir,* vol. 27, pp. 6519-6527, 2011.

[204] T. D. Blake, M. Bracke, and Y. D. Shikhmurzaev, "Experimental evidence of nonlocal hydrodynamic influence on the dynamic contact angle," *Physics of Fluids,* vol. 11, pp. 1995-2007, 1999.

[205] K. Sefiane, J. Skilling, and J. MacGillivray, "Contact line motion and dynamic wetting of nanofluid solutions," *Advances in Colloid and Interface Science,* vol. 138, pp. 101-120, 2008.

[206] I. V. Roisman, L. Opfer, C. Tropea, M. Raessi, J. Mostaghimi, and S. Chandra, "Drop impact onto a dry surface: Role of the dynamic contact angle," *Colloids and Surfaces A: Physicochemical and Engineering Aspects,* vol. 322, pp. 183-191, 2008.

[207] A. K. Epstein, B. Pokroy, A. Seminara, and J. Aizenberg, "Bacterial biofilm shows persistent resistance to liquid wetting and gas penetration," *Proceedings of the National Academy of Sciences,* vol. 108, pp. 995-1000, 2011.

[208] A. Lafuma and D. Quéré, "Superhydrophobic states," *Nature Materials,* vol. 2, pp. 457-460, 2003.

[209] P. S. H. Forsberg, C. Priest, M. Brinkmann, R. Sedev, and J. Ralston, "Contact line pinning on microstructured surfaces for liquids in the Wenzel state," *Langmuir,* vol. 26, pp. 860-865, 2009.

[210] P. S. Stewart and M. J. Franklin, "Physiological heterogeneity in biofilms," *Nature Reviews Microbiology,* vol. 6, pp. 199-210, 2008.

[211] M. Böl, A. E. Ehret, A. Bolea Albero, J. Hellriegel, and R. Krull, "Recent advances in mechanical characterisation of biofilm and their significance for material modelling," *Critical Reviews in Biotechnology,* vol. 33, pp. 145-171, 2013.

[212] P. Stoodley, Z. Lewandowski, J. D. Boyle, and H. M. Lappin-Scott, "Structural deformation of bacterial biofilms caused by short-term fluctuations in fluid shear: An in situ investigation of biofilm rheology," *Biotechnology and Bioengineering,* vol. 65, pp. 83-92, 1999.
[213] P. Stoodley, Z. Lewandowski, J. D. Boyle, and H. M. Lappin-Scott, "Oscillation characteristics of biofilm streamers in turbulent flowing water as related to drag and pressure drop," *Biotechnology and Bioengineering,* vol. 57, pp. 536-544, 1998.
[214] T. Yaguchi, M. Dwidar, C. K. Byun, B. Leung, S. Lee, Y. K. Cho, R. J. Mitchell, and S. Takayama, "Aqueous two-phase system-derived biofilms for bacterial interaction studies," *Biomacromolecules,* vol. 13, pp. 2655-2661, 2012.
[215] J. Merrin, S. Leibler, and J. S. Chuang, "Printing multistrain bacterial patterns with a piezoelectric inkjet printer," *PLoS One,* vol. 2, e663, 2007.
[216] W. B. Whitman, D. C. Coleman, and W. J. Wiebe, "Prokaryotes: The unseen majority," *Proceedings of the National Academy of Sciences,* vol. 95, pp. 6578-6583, 1998.
[217] J. W. Costerton, Z. Lewandowski, D. E. Caldwell, D. R. Korber, and H. M. Lappin-Scott, "Microbial biofilms," *Annual Reviews in Microbiology,* vol. 49, pp. 711-745, 1995.
[218] H. C. Flemming, T. R. Neu, and D. J. Wozniak, "The EPS matrix: The “house of biofilm cells”," *Journal of Bacteriology,* vol. 189, pp. 7945-7947, 2007.
[219] P. Stewart, B. Peyton, W. Drury, and R. Murga, "Quantitative observations of heterogeneities in *Pseudomonas aeruginosa* biofilms," *Applied and Environmental Microbiology,* vol. 59, pp. 327-329, 1993.
[220] C. Fux, J. Costerton, P. Stewart, and P. Stoodley, "Survival strategies of infectious biofilms," *Trends in Microbiology,* vol. 13, pp. 34-40, 2005.
[221] G. Singer, K. Besemer, P. Schmitt-Kopplin, I. Hödl, and T. J. Battin, "Physical heterogeneity increases biofilm resource use and its molecular diversity in stream mesocosms," *PLoS One,* vol. 5, e9988, 2010.
[222] D. S. Ginger, H. Zhang, and C. A. Mirkin, "The evolution of dip-pen nanolithography," *Angewandte Chemie International Edition,* vol. 43, pp. 30-45, 2004.
[223] A. Doraiswamy, T. M. Dunaway, J. J. Wilker, and R. J. Narayan, "Inkjet printing of bioadhesives," *Journal of Biomedical Materials Research Part B: Applied Biomaterials,* vol. 89, pp. 28-35, 2009.
[224] D. S. Shin, K. N. Lee, K. H. Jang, J. K. Kim, W. J. Chung, Y. K. Kim, and Y. S. Lee, "Protein patterning by maskless photolithography on hydrophilic polymer-grafted surface," *Biosensors and Bioelectronics,* vol. 19, pp. 485-494, 2003.
[225] E. W. Olle, J. Messamore, M. P. Deogracias, S. D. McClintock, T. D. Anderson, and K. J. Johnson, "Comparison of antibody array substrates and the use of glycerol to normalize spot morphology," *Experimental and Molecular Pathology,* vol. 79, pp. 206-209, 2005.
[226] H. Zhu and M. Snyder, "Protein arrays and microarrays," *Current Opinion in Chemical Biology,* vol. 5, pp. 40-45, 2001.
[227] A. Kumar and G. M. Whitesides, "Features of gold having micrometer to centimeter dimensions can be formed through a combination of stamping

with an elastomeric stamp and an alkanethiol ‘‘ink’’ followed by chemical etching," *Applied Physics Letters,* vol. 63, pp. 2002-2004, 1993.
[228] A. Kumar, H. A. Biebuyck, and G. M. Whitesides, "Patterning self-assembled monolayers: Applications in materials science," *Langmuir,* vol. 10, pp. 1498-1511, 1994.
[229] A. Kumar and G. M. Whitesides, "Patterned condensation figures as optical diffraction gratings," *Science-AAAS-Weekly Paper Edition-including Guide to Scientific Information,* vol. 263, pp. 60-61, 1994.
[230] J. L. Tan, J. Tien, and C. S. Chen, "Microcontact printing of proteins on mixed self-assembled monolayers," *Langmuir,* vol. 18, pp. 519-523, 2002.
[231] R. Bos, H. Mei, J. Gold, and H. Busscher, "Retention of bacteria on a substratum surface with micro-patterned hydrophobicity," *FEMS Microbiology Letters,* vol. 189, pp. 311-315, 2000.
[232] L. R. Hilbert, D. Bagge-Ravn, J. Kold, and L. Gram, "Influence of surface roughness of stainless steel on microbial adhesion and corrosion resistance," *International Biodeterioration & Biodegradation,* vol. 52, pp. 175-185, 2003.
[233] E. A. Soumya, H. Fatima, L. Hassan, H. Abdellatif, and I. K. Saad, "Quantification of *Bacillus subtilis* and *Bacillus sp.* adhesion on Fez medina cedar wood," *Journal of Adhesion Science and Technology,* vol. 25, pp. 1506-1512, 2011.
[234] N. Beyth, R. Bahir, S. Matalon, A. J. Domb, and E. I. Weiss, "*Streptococcus mutans* biofilm changes surface-topography of resin composites," *Dental Materials,* vol. 24, pp. 732-736, 2008.
[235] C. B. Murray, C. Kagan, and M. Bawendi, "Synthesis and characterization of monodisperse nanocrystals and close-packed nanocrystal assemblies," *Annual Review of Materials Science,* vol. 30, pp. 545-610, 2000.
[236] H. Hu and R. G. Larson, "Analysis of the microfluid flow in an evaporating sessile droplet," *Langmuir,* vol. 21, pp. 3963-3971, 2005.
[237] F. Hua and Y. M. Lvov, "Layer-by-layer assembly," in *The New Frontiers of Organic and Composite Nanotechnology,* Elsevier: Amsterdam, 2007, pp. 1-44.
[238] T. J. Powell, N. Palath, M. E. DeRome, J. Tang, A. Jacobs, and J. G. Boyd, "Synthetic nanoparticle vaccines produced by layer-by-layer assembly of artificial biofilms induce potent protective T-cell and antibody responses *in vivo*," *Vaccine,* vol. 29, pp. 558-569, 2011.
[239] V. Mironov, T. Boland, T. Trusk, G. Forgacs, and R. R. Markwald, "Organ printing: Computer-aided jet-based 3D tissue engineering," *Trends in Biotechnology,* vol. 21, pp. 157-161, 2003.
[240] B. D. Hoyle and J. W. Costerton, "Bacterial resistance to antibiotics: The role of biofilms," in *Progress in Drug Research/Fortschritte der Arzneimittelforschung/Progrès des recherches pharmaceutiques,* Birkhäuser Basel, 1991, pp. 91-105.

Publication list

Songlin Liu & Pun To Yung. (Accepted by PNAS) Droplet biofilms at the air-liquid interface.

Songlin Liu & Pun To Yung. (In prepare) Segmented-flow microfluidic air-liquid-solid interface biofilm reactor.

Songlin Liu & Pun To Yung. (In prepare) Printing based air-liquid interface bacterial biofilm array patterning.

Songlin Liu & Pun To Yung. (2011) Inkjet printing of *Bacillus cereus* biofilms using 2-D nozzle focusing microfluidic arrays. Proceedings of the IEEE International Conference on Nano/Molecular Medicine and Engineering. Jeju, Korea.

Songlin Liu, Si Li Liu, Hio Teng Cheong and Pun To Yung. (2013) Study of cannibalism behavior in *Bacillus* and *Clostridium* biofilm formation. Proceedings of the 113th General Meeting of American Society for Microbiology.

Songlin Liu, Sau Kam Liliana Law, Dawei Hu, Hio Teng Cheong and Pun To Yung. (2012) Analysis of biofilm formation at the air-liquid interface using electrochemical impedance spectroscopy. World Congress on Medical Physics and Biomedical Engineering (WC2012). Beijing, China.